# Fine-Tuning of Organotypic Skin Equivalents for Preclinical Research and Their Utilization to Study Epidermal-Dermal Crosstalk

Inaugural-Dissertation

to obtain the academic degree

Doctor rerum naturalium (Dr. rer. nat.)

submitted to the Department of Biology, Chemistry, Pharmacy

of Freie Universität Berlin

by

**Marijana Jevtić**

from Belgrade

Berlin

**2020**

This thesis and all associated experiments were prepared and performed from July 2016 to July 2019 under the supervision of Prof. Dr. Sarah Hedtrich at the Institute of Pharmacy – Pharmacology and Toxicology, Freie Universität Berlin, Germany.


1st Reviewer Prof. Dr. Sarah Hedtrich
Current address: University of British Columbia
Faculty of Pharmaceutical Sciences
2405 Wesbrook Mall
Vancouver, BC V6T 1Z3 Canada

2nd Reviewer Prof. Dr. Matthias Melzig
Freie Universität Berlin
Institut für Pharmazie
Königin-Luise-Str. 2+4
14195 Berlin



Date of disputation: 09.02.2021

If you don’t know how, observe the phenomenon of nature, they will give you clear answers and inspiration.

Nikola Tesla (1856-1943)

## ACKNOWLEDGMENT

First and foremost, I would like to express my deep gratitude to Prof. Dr. Sarah Hedtrich for the opportunity to work on this interesting and challenging topic and her ongoing trust in me. Also, I am grateful for her scientific support and expert guidelines that helped me to develop as a scientist.

I would also like to thank Prof. Dr. Matthias Melzig for taking time and effort to evaluate this thesis as a second reviewer.

Furthermore, I am grateful to all my colleagues who accompanied me during my doctorate – the groups of Prof. Dr. Sarah Hedtrich, Prof. Dr. Monika Schäfer-Korting and Prof. Dr. Günther Weindl from the Department of Pharmacology and Toxicology at the Institute of Pharmacy of Freie Universität Berlin. I want to thank my more senior lab mates Dr. Stefan Hönzke, Dr. Leonie Verheyen, Dr. Katharina Hörst and Dr. Anna Löwa. Special thanks goes to Dr. Guy Yealland for his great scientific input and professional support, bur also a linguistic remarks. I am deeply grateful to my dear Anne Eichhorst, Dr. Nan Zhang and Patrick Graff. Thank you for the long and inspiring conversations, and for your open and warm hearts. I am thankful for the continuous cell supply and the shared expertise from Carola Kapfer. Petra Schmidt deserves thanks in particular for her support in administration.

I would like to thank all cooperation partners for great collaboration and valuable scientific discussions. Namely, Prof. Dr. Kateřina Vávrová and her group from the Faculty of Pharmacy Hrádéc Kralove, Charles University Prague, and Dr. Sabine Käßmeyer, Ilka Slosarek and Franziska Ermisch from the Institute of Veterinary Anatomy, Department of Veterinary Medicine at Freie Universität Berlin.

I am grateful to the DFG – Deutsche Forschungsgemeinschaft, for the financial supporting of my doctoral project.

I thank the Women's Representative (Frauenförderung des Fachbereichs BCP) of Freie Universität Berlin for financial support of international conference meetings.

Special thanks to all my friends for their support, especially Nina for all fun days in discovering Berlin.

Finally, my parents, my sister and my husband deserve words of thank for their ongoing and unconditional support, encouragement and their trust in me.

Part of this thesis has already been published:

| | |
|---|---|
| Authors: | Marijana Jevtić, Anna Löwa, Anna Nováčková, Andrej Kováčik, Sabine Kaessmeyer, Gerrit Erdmann, Kateřina Vávrová, Sarah Hedtrich |
| Authorship: | First author |
| Year: | 2020 |
| Journal: | Biochimica et Biophysica Acta (BBA) - Molecular Cell Research |
| Source: | Marijana Jevtić, Anna Löwa, Anna Nováčková, Andrej Kováčik, Sabine Kaessmeyer, Gerrit Erdmann, Kateřina Vávrová, Sarah Hedtrich. Impact of intercellular crosstalk between epidermal keratinocytes and dermal fibroblasts on skin homeostasis. BBA - Molecular Cell Research 1867(8):118722 (2020), which has been published in final form at https://doi.org/10.1016/j.bbamcr.2020.118722 |

All figures and text passages based on this publication were marked with the specific source.

Experimental work and other contributions of co-authors were also clearly indicated.

## SUMMARY

With the studies performed for realization of this thesis, more insights into the complex intercellular crosstalk between epidermal keratinocytes and dermal fibroblasts were gained. These data demonstrated that dermal fibroblasts are critical for adequate epidermal differentiation and maturation and provided new insights into signalling pathways involved in these processes. When fibroblasts were lacking, consistently an impaired differentiation and dysregulated expression of skin barrier and tight junction proteins, increased skin permeability, and a decreased skin lipid/protein ratio have been shown. Most interestingly, impaired Ras/Raf/ERK/MEK signalling was evident when fibroblasts were not present in the skin equivalents, meaning that fibroblasts orchestrate epidermal differentiation processes. Furthermore, this project, utilised and confirmed the methods for EVs isolation and characterization from cell culture medium which is still under development. Here, it has been proved that fibroblasts-derived EVs – exosomes, which were present in fibroblasts condition medium. A more detailed analysis of these EVs should be of importance for further detailed understanding of the role EVs play in intercellular communication between fibroblasts and keratinocytes.

The results described in this thesis demonstrated development of completely human-based skin equivalents with dermal equivalent based on primary human fibroblasts-derived ECM with included endothelial cells. These skin equivalents showed features of excessive epidermal differentiation and maturation potentially conditioned by growth factors produced by fibroblasts and endothelial cells from dermal compartment that have direct impact on keratinocytes and/or the keratinocytes themselves as a result of their cellular interactions in the co-culture. New insights about the effect of endothelial cells on epidermal differentiation and their interactions with keratinocytes and fibroblasts have been noticed. Although the authentic fibroblast-derived ECM and endothelial cells have impact on epidermal morphogenesis, they have also shown a key role in the development of complex dermo-epidermal junction in the skin equivalents leading to their resemblance to native human skin. Due to the better understanding of the influence of endothelial cells on keratinocyte differentiation, this study could be helpful for the development of fully vascularised skin equivalents.

## ZUSAMMENFASSUNG

Mit der Umsetzung der durchgeführten Studien für diese Dissertation wurden weitere Erkenntnisse über die komplexe interzelluläre Kommunikation zwischen epidermalen Keratinozyten und dermalen Fibroblasten gewonnen. Diese Daten zeigen, dass dermale Fibroblasten für eine adequate Differenzierung und Reifung der Epidermis entscheidend sind und ermöglichen neue Einblicke in die Signalwege, die an diesen Prozessen beteiligt sind. Durch das Fehlen von Fibroblasten wurde stets eine beeinträchtigte Differenzierung und dysregulierte Expression von Hautbarriere- und Tight Junction-Proteinen, eine erhöhte Hautpermeabilität und ein verringertes Hautlipid/Protein-Verhältnis festgestellt. Hochinteressant ist, dass eine gestörte Ras/Raf /ERK/MEK-Signalübertragung offensichtlich vorliegt, wenn keine Fibroblasten in den Hautäquivalenten vorhanden sind, das lässt vermuten, dass Fibroblasten epidermale Differenzierungsprozesse verantworten. Darüber hinaus wurden in diesem Projekt, Methoden zur Isolierung und Charakterisierung von extrazelluären Vesikel (EVs) aus Zellkulturmedium verwendet und getestet, die sich noch in der Entwicklung befinden. Dazu haben wir bewiesen, dass von Fibroblasten abgeleitete EVs - Exosomen - in Fibroblasten-Zustandsmedium vorhanden waren. Eine ausführliche Analyse dieser EVs scheint für ein detaillierteres Verständnis für die Rolle von EVs bei der interzellulären Kommunikation zwischen Fibroblasten und Keratinozyten von Bedeutung zu sein.

Die Ergebnisse dieser Arbeit beschreiben die Entwicklung von einem human basierten Hautäquivalent, mit einem Dermis Kompartiment, auf der Basis von selbst produzierter ECM aus primären humanen Fibroblasten mit eingeschlossenen Endothelzellen. Die Hautäquivalente zeigen Merkmale einer übermäßigen epidermalen Differenzierung und Reifung, die möglicherweise durch Wachstumsfaktoren bedingt ist, die von Fibroblasten und Endothelzellen aus dem Dermis Kompartiment erzeugt werden und die aufgrund ihrer zellulären Wechselwirkungen in der Co-Kultur direkten Einfluss auf Keratinozyten und / oder die Keratinozyten selbst haben. Wir haben auch neue Erkenntnisse über die Wirkung von Endothelzellen auf die epidermale Differenzierung und ihre Wechselwirkungen mit Keratinozyten und Fibroblasten erhalten. Obwohl die authentischen Fibroblasten, die selbst produzierte ECM- und die Endothelzellen einen Einfluss auf die epidermale Morphogenese haben, haben sie auch eine Schlüsselfunktion bei der Entwicklung eines komplexen dermo-epidermalen Übergangs in den Hautäquivalenten aufgezeigt, was zu einer Ähnlichkeit mit nativer menschlicher Haut führt. Aufgrund des besseren Verständnisses über den Einfluss

von Endothelzellen auf die Keratinozyten-Differenzierung könnte diese Studie für die Entwicklung vollständig vaskularisierter Hautäquivalente hilfreich sein.

## LIST OF ABBREVIATIONS

| | |
|---|---|
| 2D | two-dimensional |
| 3D | three-dimensional |
| CLDN-1 | claudin-1 |
| CLE | cornified lipid envelope |
| CD31 | cluster of differentiation 31 |
| DAPI | 4′,6-diamidin-2-phenylindol |
| DEJ | dermal-epidermal junction |
| DED | de-epidermized dermis |
| DETC | dendritic epidermal T cells |
| DMEM | Dulbecco's modified eagle's medium |
| EC | endothelial cells |
| ECM | extracellular matrix |
| EU | European Union |
| EVs | extracellular vesicles |
| FFA | free fatty acid |
| FBS | fetal bovine serum |
| FLG | filaggrin |
| FGF | fibroblast growth factors |
| GAGs | glycosaminoglycans |
| HUVEC | human umbilical vein cord endothelial cells |
| HDMEC | human dermal microvascular endothelial cells |
| H&E | hematoxylin and eosin |
| HPTLC | high-performance thin layer chromatography |
| IF | immunofluorescence |
| KDM | keratinocyte differentiation medium |
| KGF-1 | keratinocyte growth factor-1 |
| LOR | loricrin |
| MVs | microvesicles |
| MVBs | multivesicular bodies |
| miRNA | microRNA |
| mRNA | messenger RNA |
| NTA | nanoparticle tracking analysis |
| OECD | Organization for Economic Co-Operation and Development |
| OCLD | occludin |
| PBS | phosphate buffered saline |
| PGs | proteoglycans |
| PDGF | platelet-derived growth factors |
| PI | propidium Iodide |
| PCR | polymerase chain reaction |
| RHS | reconstructed human epidermis |
| SDS-PAGE | sodium dodecyl sulfate polyacrylamide gel electrophoresis |
| SG | stratum granulosum |
| SEM | standard error of the mean |
| SS | stratum spinosum |
| TJ | tight junction |
| TGF | transforming growth factors |
| TEM | transmission electron microscopy |
| VEGF | vascular endothelial growth factor |
| vWF | von Willebrand factor |
| UV | ultraviolet |
| WB | western blot |

# TABLE OF CONTENTS

# 1. INTRODUCTION

## 1.1. Anatomy and Physiology of Human Skin

Human skin is a continuously self-renewing organ that covers the surface of the body and separates it from the outside world, while communicating with it in a dynamic manner (Baroni et al., 2012). The primary function of the skin is protection of the human body from external threats such as mechanical, physical, chemical and/or biological insults, as well as prevention of the excessive water loss and electrolytes, thereby protecting the body from dehydration (Simpson et al., 2011, Jansen van Rensburg et al., 2019). In addition to barrier function, skin also has important immune and sensory function (Roosterman et al., 2006, Vidal Yucha et al., 2019), and it plays a role in absorption and pigmentation (d'Ischia et al., 2015). Furthermore, the skin has complex appendages, such as hair follicles, sebaceous glands, sweat glands and nails (Sriram et al., 2015). So far, the anatomy of human skin is well characterised, and there is a clear relationship between its structure and function. From apical to basal, human skin is organized in a highly sophisticated composition and structural arrangement into three morphologically distinct structural compartments: the epidermis, the dermis and the hypodermis (Menon et al., 2012, Baroni et al., 2012). These compartments communicate in various ways and at different levels to establish, maintain, and/or restore skin homeostasis (Breitkreutz et al., 2013).

### 1.1.1. Epidermis

The epidermis is outermost skin layer. Primarily composed of keratinocytes, this keratinized stratified squamous epithelium is characterized by continuously renewing cells that ensure the maintenance of a functional barrier (Bataillon et al., 2019). Although keratinocytes comprise the majority of the cells in the epidermis, other cells are present such as melanocytes, Langerhans cells, tissue resident T cells and Merkel cells (Kolarsick et al., 2011). The epidermis consists of four layers according to keratinocyte morphology and position as they migrate from the epidermal-dermal basement membrane to the surface, and differentiate into horny cells including: i) the basal cell layer - *stratum basale*, ii) the squamous cell layer - *stratum spinosum*, iii) the granular cell layer - *stratum granulosum*, and iv) the cornified or horny cell layer - *stratum corneum* (James et al., 2006). The *stratum lucidum* is the fifth epidermal layer present in between *stratum granulosum* and *stratum corneum*, but it is only found in thicker skin, such as in the palms of hands and soles of feet (Yousef et al., 2017).

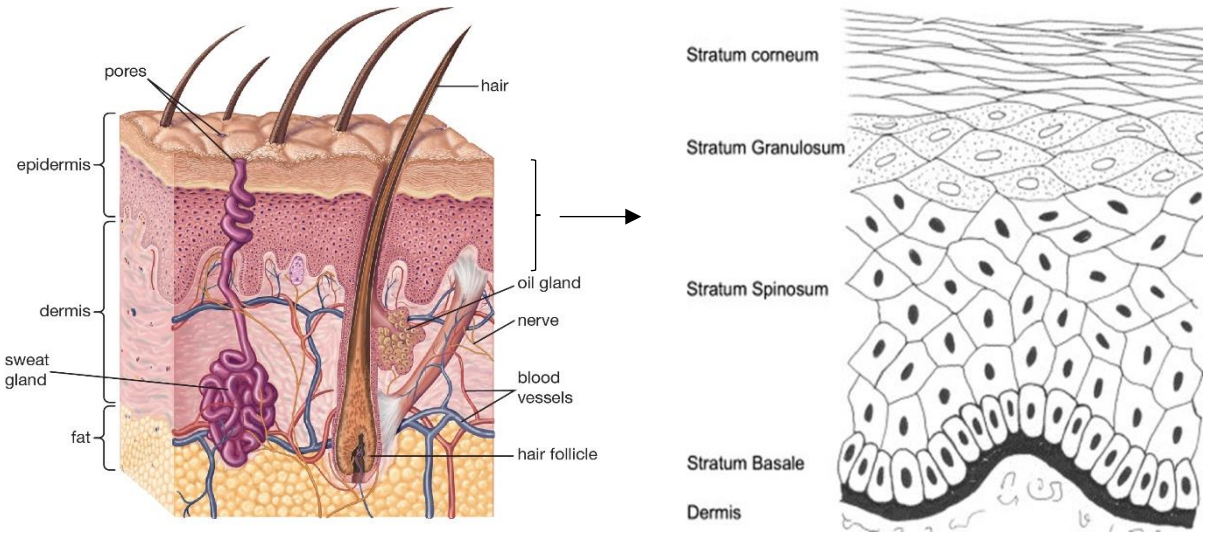


**Figure 1.** A cross section of human skin and its underlying structures (reproduced from Encyclopedia Britannica Inc., 2013). The three main layers of the skin: epidermis, dermis and hypodermis with appendages are represent (left arm). Diagram representing the main layers of epidermis: *stratum basale*, *stratum spinosum*, *stratum granulosum* and *stratum corneum* (right arm). Reprinted by permission from Elsevier (Wickett and Visscher, 2006).

The basal layer consists of a single layer of undifferentiated, mitotically active keratinocytes attached to the epidermal basement membrane by hemidesmosomes (Brandner and Schulzke, 2015). Columnar-shaped basal keratinocytes proliferate, migrate superficially, and sequentially differentiate to form the stratified epidermis thanks to expression of keratins 5 and 14, which form a cytoskeleton that has sufficient flexibility to permit cell division and migration upward to create the remaining layers (Haake et al., 2001, Roger et al., 2019). Some of these proliferative basal keratinocytes stay attached to the basal lamina as stem cells, while others differentiate to the *stratum spinosum* and push the overlying cells toward the surface (Arda et al., 2014). The *stratum basale* contains melanocytes, dendritically shaped cells, that synthesize melanin packaged in subcellular organelles, melanosomes, which are then transported to neighbouring basal keratinocytes. The melanosomes form a “melanin cap” that protects the basal keratinocyte nuclei from damage caused by ultraviolet radiation and determine skin colour (d'Ischia et al., 2015). Merkel cells, also found in the *stratum basale*, transmit sensory information from the skin to the sensory nerves (Lai-Cheong and McGrath, 2017).

The suprabasal spinous layer is characterized by prominent desmosomes, which are intercellular structures that allow cells to remain tightly bound to one another and resemble “spines” architecturally (Agarwal and Krishnamurthy, 2019). As the keratinocyte daughter cells move from *stratum basale* to the *stratum spinosum*, they become rounder in shape, synthesize

differentiation-specific keratins 1 and 10 and other early differentiation markers (e.g. involucrin) (Yagi and Yonei, 2018). In the upper *stratum spinosum*, keratinocytes start to produce lipid-enriched lamellar bodies, which are ovoid secretory organelles (Feingold et al., 2007). Langerhans cells, also found in the *stratum spinosum*, are immune cells that recognize and process antigens found in epidermal tissue and transport them to lymph nodes (Jaitley and Saraswathi, 2012).

The granulosum layer is characterized by flattened cells containing the keratohyalin granules; cytoplasmic organelles packed with electron dense proteins, such as pro-filaggrin, loricrin and keratin intermediate filaments (Griffiths et al., 2016). Tight junction proteins are also localized in the *stratum granulosum* and provide mechanical barrier function to ions and solutes of different molecular sizes (Bergmann et al., 2020). The cytoplasm of the upper-, spinous- and granular- layer contains the lamellar bodies; secretory organelles packed with precursor lipids that cluster together and fuse with the cell membrane and discharge their lipid components into the extracellular space (Griffiths et al., 2016). At the interface of the *stratum granulosum* and *stratum corneum*, keratinocytes initiate their terminal differentiation process, becoming flattened and ultimately losing their nuclei (Candi et al., 2005).

Lastly, the *stratum corneum*, the outmost layer, is made up of tightly packed intracellular aggregation of keratins, involucrin (IVL) and filaggrin (FLG) found within corneocytes surrounded by a complex hydrophobic extracellular lipid matrix composed of an approximately equimolar ratio of ceramides, free fatty acids and cholesterol (Mojumdar et al., 2016). Corneocytes are described as large, flattened, and terminally differentiated keratinocytes, that have typically lost their nuclei and other cell organelles. Extracellular lipid matrix is largely formed by the contents of lamellar bodies packed with precursor lipids found in the *stratum corneum* (Feingold, 2012). All together, these complex and fundamental processes lead to the development of a functional skin barrier. Disturbances in any of these can cause the skin barrier disruptions often seen in skin diseases.

The basal layer of the epidermis is intimately related to the underlying dermis and connected to it through a complex acellular basement membrane called dermal-epidermal junction (Benítez and Montáns, 2017). The basement membrane can be divided into a *lamina lucida* and *lamina densa*, so called for their appearance in transmission electron micrographs. It is a highly dynamic and specialized adhesive structure that serves as a selective barrier that functions as an exchange zone between epidermal keratinocytes and dermal fibroblasts whilst anchoring the basal epithelial cells to the dermis with hemidesmosomes, providing a mechanical support. The basement membrane provides autocrine and paracrine signalling that controls the growth and differentiation of the germinating basal layer of keratinocytes above. The proteins that form the basement membrane – collagen type IV and VII, nidogen

and laminins 5 and 10 – are synthesized by the dermal fibroblasts under keratinocytes exerted influence (Marionnet et al., 2006, Breitkreutz et al., 2013, Varkey et al., 2014).

### 1.1.2. Dermis

The dermis is a supportive connective tissue that both nourishes the skin and greatly contributes to elastic properties and flexibility. The dermis is mainly composed of the extracellular matrix (ECM) in which specialized cells – mainly fibroblasts – are embedded (Bataillon et al., 2019). The dermis is divided into two layers: a papillary dermis and a reticular dermis. The papillary dermis, as shown in Figure 2, is a relatively thin zone just beneath the dermal-epidermal junction. The papillary dermis is a loose connective tissue that forms extensions that reach out to the epidermis and provides soluble molecules, nutrients and oxygenation through the vasculature. In contrast, the reticular dermis is much thicker and runs in various directions (Woodley, 2017). The reticular dermis is a dense connective tissue that contains an extensive vascular plexus and lymphatics (Brown and Krishnamurthy, 2018). Furthermore, it is innervated by a variety of sensory neurons providing tactile sensations of pain, pressure, touch and temperature (Murphree, 2017) and also contains functional structures and appendages: hair follicles and endocrine-, eccrine- and sebaceous- glands (Sriram et al., 2015). Besides fibroblasts, macrophages, mast cells, T and B cells are common cellular components within the dermis responsible for the immune response (Nguyen and Soulika, 2019).

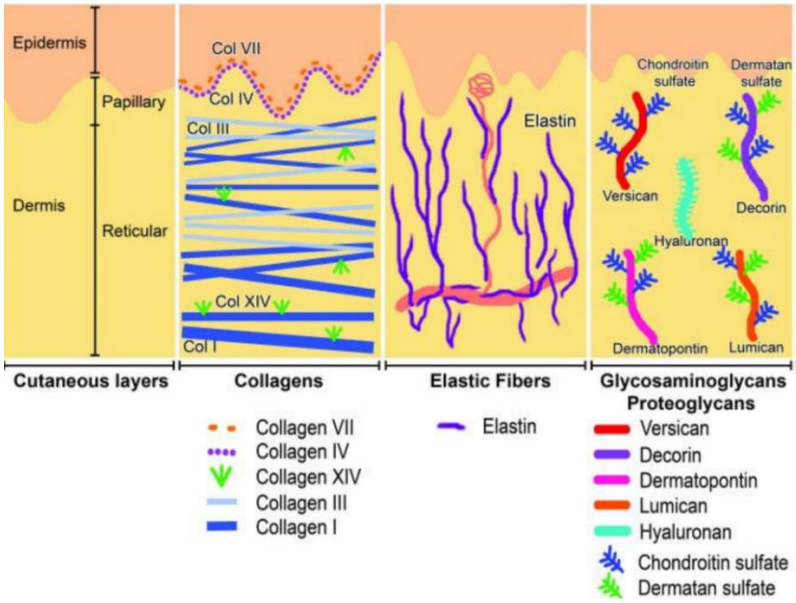


**Figure 2.** Shema representing that the dermis is divided into two layers: a papillary dermis and a reticular dermis. The extracellular matrix (ECM) of normal skin with selected components depicted – collagens, elastic fibers as well as glycoproteins and proteoglycans. Reproduced from (Tracy et al., 2016).

ECM as the main component in the dermis is a complex and dynamic network that surrounds fibroblasts, providing structural and mechanical support, and mediating diverse biological processes that are crucial for supporting tissue formation and function (Muiznieks and Keeley, 2013). Dermal tensile strength and elasticity are defined by its ECM (Sorrell and Caplan, 2004). ECM composition varies depending on the site in the skin. Papillary fibroblasts in the upper dermis secrete ECM, which is constituted of thin, poorly organized collagen fibre bundles, whereas thick, well-organized collagen bundles are characteristic within the lower dermis, which is produced by resident reticular fibroblasts (Sorrell and Caplan, 2009).

ECM components can be divided into fibrous and non-fibrous components. The fibrous connective tissue of the dermis consists mainly of type I and III collagen which create a complex three-dimensional (3D) framework of rigid proteins, as well as fibrin, fibronectin, vitronectin, elastin, and fibrillin which create elastic connective tissue (Tracy et al., 2016, Chermnykh et al., 2018). The non-fibrous component is composed of fine filamentous glycoproteins (GPs), proteoglycans (PGs), and glycosaminoglycans (GAGs) that fill the majority of the tissue's interstitial space and create a charged, dynamic, and osmotically active space (Tracy et al., 2016, Chermnykh et al., 2018). Their negatively charged and hydrophilic nature enable PGs and GAGs to function in hydration, buffering, and force dispersion within tissues. The most abundant PGs in the skin include hyaluronan, decorin, versican, and dermatopontin (Tracy et al., 2016). The papillary dermis has a higher ratio of collagen type I to III, higher levels of the dermatan sulfate PG decorin, yet lower levels of the chondroitin sulfate PG versican compared to the reticular dermis (Ghetti et al., 2018).

### 1.1.3. Hypodermis

Beneath the dermis lies the subcutis, also known as the hypodermis. The hypodermis functions as a support for the dermal layer, providing padding against pressure and shear forces. Next to fibroblasts, adipocytes are the most prominent cell type in this compartment – these store excess energy as fat that also provides acting thermal insulation (Mathes et al., 2014). In addition to fibroblasts and adipocytes, the hypodermis also contains blood and lymphatic vessels, nerve endings and mast cells (Murphree, 2017).

## 1.2. Role of Dermal Fibroblasts in Skin Homeostasis

Dermal fibroblasts are an essential component of the skin and represent a heterogeneous population of cells defined by their location within the dermis and according to whether fibroblasts reside in the papillary or reticular dermis, as described previously. Importantly,

dermal fibroblasts are considered key players for adequate skin differentiation and tissue homeostasis with distinct effects on the regulation of keratinocyte proliferation, differentiation, re-epithelization and cutaneous wound healing. Moreover, fibroblasts are not only responsible for the extracellular matrix (ECM) synthesis, remodelling and deposition, but also, they communicate with each other and other cell types including keratinocytes, endothelial cells and neural cells, playing a crucial role in skin physiology (El Ghalbzouri et al., 2004, Sorrell and Caplan, 2004, Spiekstra et al., 2007). The components of the ECM, the structural framework for the dermis, possess specific 3D arrangements of sequences orchestrating the crosstalk among different cell populations comprising the skin. Ultimately, such crosstalk affects the attachment, migration, differentiation and morphology (Urciuolo et al., 2019).

Most of the published data regarding crosstalk between cells is derived from experiments performed in 2D cell culture (Hoarau-Véchot et al., 2018, Joseph et al., 2018). Although, fibroblasts in monolayer culture exhibit significant metabolic differences from *in vivo* fibroblasts (Sorrell and Caplan, 2004), previous attempts to study the interactions between fibroblasts and keratinocytes in more detail have been mainly used fibroblasts and keratinocytes monolayers. These studies demonstrated that fibroblasts co-cultured with keratinocytes enhanced the release of soluble factors such as keratinocyte growth factor-1 (KGF-1) and interleukin-6 (IL-6) which play a significant role in wound repair by modulating the activity of keratinocytes (Smola et al., 1993). Furthermore, it was shown that double paracrine signalling loops between keratinocytes and fibroblasts, a key to their actions in restoring normal skin tissue homeostasis after wounding, was maintained through soluble factors IL-1, IL-6, and KGF-1. In response to disruption of the skin barrier, fibroblasts produce KGF that stimulates keratinocyte proliferation and migration. On the other hand, KGF secretion in fibroblasts is stimulated by IL-1 derived from keratinocytes. Thus, a paracrine loop was established (Maas-Szabowski and Fusenig, 1996, Maas-Szabowski et al., 1999). Further study has shown that keratinocytes cultured in monolayer alone produced only a thin epidermal layer and, without fibroblasts support, undergo apoptosis after about 2 weeks in culture (Wong et al., 2007).

More recent data indicate that fibroblasts may also drive skin diseases such as atopic dermatitis as demonstrated in 3D skin equivalents consisting of normal primary keratinocytes and fibroblast derived from the atopic dermatitis patients (Berroth et al., 2013, Löwa et al., 2020). In these studies, atopic dermatitis fibroblasts induced an atopic phenotype in skin equivalents, characterized by hyperproliferation, irregular epidermal stratification and inflammation, underlining their impact in healthy and diseased states of human skin.

Epidermal keratinocytes can interact with dermal fibroblasts either via soluble mediators (Smola et al., 1993, Sorrell and Caplan, 2004) or via secreted extracellular vesicles (EVs) that can carry signalling molecules to transfer information between the two cell types (Huang et

al., 2015). However, it is not well known, how fibroblasts-derived EVs regulate keratinocytes function and how keratinocytes-derived EVs regulate fibroblasts function. Therefore, before we try to answer these questions, we should first understand the role and function of EVs, as described in more details in the following chapter.

### 1.2.1. Extracellular vesicles (EVs)

Over the past few decades, extracellular vesicles (EVs) have received tremendous attention and much progress has been made in understanding the basic biology of EVs. EVs are a heterogenous group of small membrane-enclosed lipid bilayer vesicles, usually spherical in shape that cannot replicate. Hence, EVs are not only naturally released from all cell types into the extracellular environment, but they are also found in body fluids – from blood, urine, breast milk, saliva, malignant ascites, bile, to amniotic, semen and synovial fluid – as well as in the cell culture supernatant. Current understanding of EVs classify them according to their size, cargoes and their distinct mechanism of biogenesis. Thus, three classes of EVs are considered: exosomes, microvesicles (MVs) and apoptotic bodies (Vlassov et al., 2012, Rutter and Innes, 2017, Van Niel et al., 2018, Théry et al., 2018).

When examined under an electron microscope, exosomes show characteristic cup-shaped morphology with diameter ranging from 30 to 150 nm. Exosomes are vesicles generated by reverse intraluminal budding of the cell membrane and creation of an early endosome. Endosomes can bud again to form multivesicular bodies (MVBs) which undergo successive inward budding events which create multiple intraluminal vesicles. MVBs fuse with the plasma membrane, leading to the release of their contents – the exosomes – into the extracellular space. MVs are large vesicles 100-1000 nm diameter generated, contrary to exosomes, by the outward budding and direct fusion of the plasma membrane, thus resemble the plasma membrane composition of the parent cell. Lastly, apoptotic bodies measure approximately 1-5 µm and are released by cells undergoing apoptosis (Harding et al., 2013, Crescitelli et al., 2013, Lobb et al., 2015, Flamant and Tamarat, 2016, Rutter and Innes, 2017, Gangadaran et al., 2017, Van Niel et al., 2018).

Over the last decade, research on EVs has flourished and has progressed dramatically from the initial notion of “garbage bags” for cellular waste disposal to an emerging consensus that they operate as a highly-regulated mode of communication between and among cells and tissues in all multicellular organisms (Kalra et al., 2016). Emerging data indicate that EVs play key roles in many physiological and pathological processes as essential intercellular messengers by shuttling their functional cargo – proteins, lipids, nucleic acids, including RNA sequences (non-coding RNAs like messenger RNA (mRNA) and microRNA (miRNA)) and

DNA sequences – to recipient cells (Valadi et al., 2007, Raposo and Stoorvogel, 2013, Cicero et al., 2015, Yáñez-Mó et al., 2015, Iraci et al., 2016, Van Niel et al., 2018).

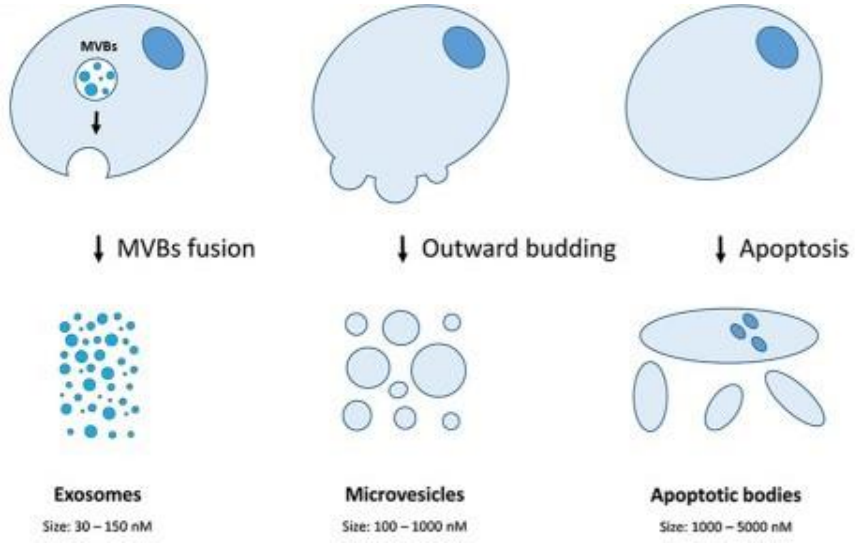


**Figure 3.** Schematic representation of EVs: exosomes, microvesicles and apoptotic bodies with mechanisms of generation, size range and specific protein markers of different EVs types. Reproduced from (Turchinovich et al., 2019).

However, despite many basic biological questions regarding their biogenesis, loading, secretion, and uptake and many promising uses for exosomes still remain unanswered (Rutter and Innes, 2017). Most EVs studies have been conducted in cell culture due to the ability to obtain purified EVs samples from defined cell types as well as better control over experimental conditions. Moving into the future, this will serve as an important platform for understanding their role in cell-to-cell communication *in vivo* (Pitt et al., 2016).

## 1.3. Established Models for Biomedical Skin Research

Models of epithelial barriers – namely the skin, the intestine and the lung – are currently enjoying increasing interest from various groups, including scientists in academia, product developers in industry, regulatory authorities and, last but not least, society in general as important alternatives to animal testing (Gordon et al., 2015). A variety of approaches to model skin barriers are currently employed in such fields, ranging from the utilization of *ex vivo* skin approaches to reconstructed *in vitro* models, and further to chip-based technologies (Gordon et al., 2015). Traditionally, skin care products, cosmetics and other topical agents were tested using *in vivo* (animal) and *ex vivo* skin approaches (Robinson et al., 2002, Abd et al., 2016). Consequently, there was increasing ethical pressure to improve the rights and welfare of

research animals that, within the European Union (EU), was pushing the development of valid alternative test systems (Löwa et al., 2018). For example, since 2009 the use of animals for the testing of cosmetic ingredients is prohibited and since March 2013 the general ban on the sale of cosmetic products tested in animals that came into effect across Europe (Pfuhler et al., 2014). Nevertheless, alternative methods are needed to derive data that are reproducible and reliable and which provide a meaningful prediction of the *in vivo* human situation (Franz et al., 2009).

Therefore, excised human skin mostly obtained from breast reductions or abdominoplastic surgeries or cadavers, is used in research with an appropriate ethical approval (Küchler et al., 2013). For instance, excised human skin is acknowledge as the gold standard for dermal absorption studies and accepted by many authorities, since the barrier properties are well preserved after excision (Gordon et al., 2015, Weinhart et al., 2019). Preservation is possible up to 6 months at -20°C, that does not impair the skin barrier properties (Schreiber et al., 2005). However, the storage of such samples sub 0°C can influence other properties of the skin tissue such as metabolic activity of CYP450 isoenzyme. Therefore, fresh skin is required (Henkler et al., 2012). Additionally, due to the growing need and the limited sources, it is not possible to cover the demand (Küchler et al., 2013).

Consequently, animal models have been used in research. The use of animal models have been for a long period of time the main model in the basic and preclinical research in medical and pharmacological science (Semlin et al., 2011, Osuchowski et al., 2014). Animal models have the great advantage over excised human skin by manifesting the complexity of entire organ, including systemic circulation, an immune system and full metabolic capacity and the presence of other interacting organs (Dellambra et al., 2019). To date, mouse models remain the most popular animal model in skin research. However, their use is questionable in the face of ethical considerations, major anatomical and physiological disparities with human skin, and reportedly poor translatability of results to human skin (Garcia et al., 2007, Seok et al., 2013).

Major differences were detected in genes associated with skin morphogenesis, growth and immunology between the skin of mice and men (Löwa et al., 2018). Indeed, mouse epidermis is much thinner than human epidermis – < 25 µm compared to > 100 µm for human skin, with only three layers in the adult murine epidermis compared with 16-18 layers in human epidermis. Mouse skin is also densely packed with hair follicles, whereas human epidermis possesses larger interfollicular regions. Furthermore, mouse melanocytes reside mainly in dermal hair follicles, while human melanocytes are located in the *stratum basale* of the epidermis. Finally, an additional cutaneous muscle layer, the *panniculus carnosus* is present in mouse skin but absent from human dermis (Khavari, 2006, Wong et al., 2010, Löwa et al., 2018). Differences in skin biology are especially evident when trying to dissect more complex

skin conditions, such as in skin diseases where aberrant interactions between the immune system, epidermis and the environment likely occur. Many diseases that occur in humans, do not naturally occur in other animals. For instance, unlike humans, normal mice do not develop atopic dermatitis spontaneously, requiring artificial disease induction to model the disease (Shiohara et al., 2004, Weinhart et al., 2019). There are also differences in the cell signalling and functional profiles of oncogenes and tumor suppressor genes between mice and humans (Ratushny et al., 2012). Moreover, discrepancies exist in both innate and adaptive immunity, including balance of leukocyte subsets, defensins, Toll-like receptors, inducible NO synthase, cytokines and cytokine receptors, Th1/Th2 differentiation, antigen-presenting function of endothelial cells, chemokine and chemokine receptor expression (Mestas and Hughes, 2004). Nevertheless, in dermatological research mouse models are predominantly used despite recent gene analysis which has shown that human and mouse skin share some features, but only approximately 30% of genes primarily expressed in mouse skin overlap with those expressed in human skin (Gerber et al., 2014).

| | Mouse | Human | Skin model |
|---|---|---|---|
| **Histology** | 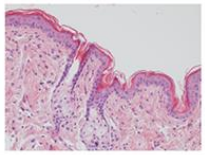 | 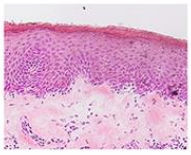 | 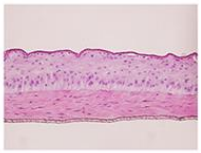 |
| **Epidermal layers** | 2 - 5 | 16 - 18 | 10 - 15 |
| **Skin renewal** | 8 - 10 d | 28 d | No |
| **Hair follicle** | High number & wider diversity | Significantly less than rodents | No |
| **Cutaneous muscle layer** | Panniculus carnosus | No | No |
| **sweat glands** | Eccrine sweat glands (exclusively in the pads) | Apocrine & eccrine | No |
| **Melanocytes** | Follicular location | Interfollicular location | Requires implementation |
| **T-cell population in the skin** | Dendritic epidermal T-cells (DETC) | α/ß T-cells | Requires implementation |
| **Antimicrobial peptides** | Tissue specific different from humans | Yes | Similar to humans |

**Figure 4.** Differences and similarities in anatomy and physiology between mouse skin, human skin and human-based skin equivalents. Reprinted by permission from Wiley (Löwa et al., 2018).

The necessity for better, ideally human-based models in basic and preclinical research cannot be ignored on the grounds of disease accuracy, relevant therapeutic development and animal welfare (Löwa et al., 2018). While the use of animal models is still considered the gold standard for basic, preclinical and pharmacological research, there are now alternative models that have been approved for certain applications (Osuchowski et al., 2014). Recently, law and regulations have become more stringent regarding the safety of products and demand

reduction of laboratory tests on animals. Also, current roadmaps for the pharmaceutical and cosmetics industry encourage the 3R principle, to reduce the number of animals in testing, to refine their use and to find the replacement of animals in experiments (EU Directive 2010/63/EU). Nowadays, the development of alternative models has gained a high priority following the European ban on animal testing for cosmetic ingredients (EU Cosmetics Products Regulation 2009/1223/EU), implementation of the legislative guideline within the registration, evaluation, authorization and restriction of chemicals (REACH Regulation 2006/1907/EC), as well as the recommendation to follow above-mentioned 3R principle for research (Dellambra et al., 2019, Almeida et al., 2017). This was the crucial moment when researches urgently needed to develop physiologically relevant human skin equivalents that could mimic all the characteristics of the human skin and this has given rise to further development and improvement of *in vitro* (3D) skin equivalents.

In the following years, skin equivalents have gained increasing attention in fundamental research of normal and abnormal skin biology studies such as in the disease – atopic dermatitis, psoriasis and ichthyosis vulgaris, but also in preclinical studies (Xie et al., 2010, Eckl et al., 2011, Küchler et al., 2011, van den Broek et al., 2012, Popov et al., 2014). In addition, the use of reconstructed skin equivalents have gained increasing multiple application and have offered several advantages: i) since most are composed of primary human cells, inter-species extrapolation is avoided; ii) in these models, in contrast to *ex vivo* human skin, repeated application of formulations can be performed for couple of days; iii) work with the commercially available skin equivalents does not require advanced knowledge of cell culture techniques because models are delivered “ready to use”, such as the models representing the reconstructed human epidermis (RHE) (EpiSkin, EpiDerm, SkinEthic) or full-thickness human skin equivalents (HSE) (GraftSkin, EpiDermFT); iv) several HSE are accepted in regulatory tests e.g. skin irritation and corrosion testing of chemicals, assessment of phototoxicity; v) the employment of HSE leads to a reduction of laboratory animal use in regulatory toxicology as well as in preclinical studies (Van Gele et al., 2011, Gordon et al., 2015).

## 1.4. Human-based Skin Equivalents

The term “tissue engineering” was officially coined in 1988. Tissue engineering is defined as an interdisciplinary field that applies the principles of engineering and the life sciences toward the development of biological substitutes that restore, maintain or improve tissue function (Langer and Vacanti, 1993). The classical approach of tissue engineering involves the extraction of cells from humans, primary cells or stem cells, their expansion and seeding in a

biomaterial, and the ability to fine tune properties of the final tissue (Vacanti, 2006, Urciuolo et al., 2019). Tissue engineering has been studied and applied for various organs (Griffith and Naughton, 2002), but the need for the organotypic skin models is immense and has profound implications, not only for fundamental dermatological research, but also for preclinical and clinical applications in the fields of pharmaceuticals, cosmetic testing and regenerative medicine, as well as for regulatory authorities and animal welfare organizations (Küchler et al., 2013, Van Smeden et al., 2014, Vávrová et al., 2014, Sriram et al., 2015, Hönzke et al., 2016, Löwa et al., 2020).

The development of organotypic *in vitro* skin models started decades ago and continues to this day due to the limited availability of human skin, ethical and technical issues with regard to animal experimentation. Importantly, it is crucial to study how skin cells and tissue behave as parts of whole living organs that are composed of multiple, tightly opposed and highly dynamic tissue types that are variable in terms of their three dimensional (3D) structure, mechanical properties and biochemical microenvironment. Unfortunately, most studies on cells and tissue regulation have relied on analysis of cells grown in 2D cell cultures that fail to reconstitute the *in vivo* cellular microenvironment (Huh et al., 2011, Teimouri et al., 2018). There are many advantages of 2D cultures; above all, we value them for their simplicity, ease of technical manipulation, and scalability. On the other hand, the monolayer method of cell culture has many disadvantages, e.g., a lack of dimensionality of natural tissue structures or tumor structures and a lack of elements of the microenvironment such as an extracellular matrix (ECM) (Klak et al., 2020). Although easy to establish and maintain, 2D monolayer cell cultures fail to reproduce the complex and dynamic environments of *in vivo* tissues, and commonly do not maintain principal functions of skin, like barrier function, cell sheeting, cell layering, developmental profiles, immune function, blood perfusion and innervation. As a result, growing numbers of studies have reported differences in phenotype, cellular signalling, cell migration, and drug responses when the same cells were grown under 2D as opposed to 3D culture conditions (Mazzoleni et al., 2009, Klicks et al., 2017).

On the other hand, 3D tissue-engineered skin predominantly involves the construction of scaffolds that reproduce the structure of an ECM, into which to support dermal fibroblasts seeded and/or onto which epidermal keratinocytes are seeded. By definition, a reconstructed human epidermis (RHE) consists of just keratinocytes, while full-thickness human skin equivalents (HSE) posses of both the dermal and epidermal layer (Zhang and Michniak-Kohn, 2012). RHE have poor mechanical stability and they are quite fragile, handling them is difficult due to the thin cellular layers and keratinocytes proliferate slower related to HSE dermis (Atiyeh and Costagliola, 2007, Reijnders et al., 2015). However, RHE-based test procedures for *in vitro* re-evaluation of phototoxicity of chemical substances (OECD-432, 2004),

evaluation of skin corrosion (OECD-431, 2014) and assessment of skin irritation (OECD-439, 2015) are already approved by the Organization for Economic Cooperation and Development (OECD) (OECD Council Guidelines, 2016).

| | 2D cultures | 3D tissues equivalents |
|---|---|---|
| **Structure** | Simple monolayer or co-cultures, no stratification | Epidermal differentiation and maturation, stratification |
| **Application** | Initial studies on cell reactivity and cell-cell interactions | Investigation of more complex tissue-specific effects in normal and diseased states |
| **Air-liquid interface** | No | Yes, crucial for stratification |
| **Dynamic cultivation** | No | In principle possible, but improvements still required |
| **Preparation and cultivation time** | Short - few days | Up to several weeks |
| **Costs** | Low costs | High costs |

**Figure 5.** Advantages and disadvantages of *in vitro* 2D and 3D skin equivalents. Reprinted by permission from Wiley (Löwa et al., 2018).

HSE are more representative of skin and constitute a more complex skin equivalents owing to the presence of a dermal compartment (Mathes et al., 2014). Until today, HSE have already provided much information about cell-cell and cell-matrix interactions, responses of dermal and epithelial cells to biological signals and pharmacological agents, as well as the effects of drugs and growth factors on skin reconstruction processes (Fimiani et al., 2005). Therefore, before different approaches of reconstructed skin development can be discussed in more detail, we should look back at the first attempts for skin reconstruction *in vitro*, as described in the following chapter.

### 1.4.1. Historical Overview of Skin Equivalents Development

One of the first approaches of 3D full-thickness HSE were developed in the 1970s. The first successful tissue-engineered skin constructs were developed in 1975 when Rheinwald and Green described a method allowing the *in vitro* culture of human keratinocytes to produce viable epidermal sheets using lethally irradiated murine 3T3 fibroblasts as feeder layers (Rheinwald and Green, 1975). Initiated by the work of Rheinwald and Green, the monolayer culture of human keratinocytes has been the main technique that enabled the production of large quantities of keratinocytes and their expansion in *in vitro* cell culture conditions to study skin biology and (patho)-physiology (Niehues et al., 2018). Early on, cultured human epidermal cells were seeded on decellularized pig dermis (Freeman et al., 1976) or on human de-

epidermized dermis (DED) (Pruniéras et al., 1983). In 1981, a critical step forward was made by Bell and colleagues who were the first to develop and describe a composite skin product reconstituting both the epidermis and the dermis (Bell et al., 1981). They first made the dermis by seeding a collagen gel with dermal fibroblasts isolated from a skin biopsy, then keratinocytes were seeded on the top of the collagen scaffold. Additionally, a better differentiated epidermis was obtained when keratinocytes were seeded on the DED followed with an immersion period and placed at the air-liquid interface (Pruniéras et al., 1983).

Since then, the production of engineered human skin at the air-liquid interface has been achieved by different methods, the principal differences of which involve the construction of the dermal equivalent: culture of fibroblasts in combination with natural or synthetic scaffolds, or stimulating the innate capacity of fibroblasts to secrete and organize extracellular matrix (ECM) without any scaffold, aka by the self-assembly approach (Auxenfans et al., 2009, Ali et al., 2015).

Importantly, a cellular environment that allows cells to function as they do in the native tissue is key to effective tissue engineering. Often, the environment mimics some critical aspects of the *in vivo* setting through proper control of the materials as well as the chemical milieu to which the cells are exposed. The cell scaffolds are the backbones of any tissue-engineered skin substitute (Savoji et al., 2018). Therefore, they usually serve at least one of the following purposes: i) biocompatibility – to allow cells attachment, normal function and perhaps migration; ii) biodegradability – to allow cells to produce their own ECM; iii) mechanical properties – a balance between mechanical properties such as rigidity or flexibility and porous architecture for adequate diffusion of nutrients, retention and presentation of biochemical factors, expressed products and waste is sufficient to allow cell infiltration (Berthiaume et al., 2011, O'brien, 2011).

### 1.4.2. Scaffolds for the Reconstruction of the Dermal Equivalents

Skin equivalents can be generated by seeding keratinocytes on: i) acellular dermal substrates (Pruniéras et al., 1983, Ponec et al., 1988, Zhang et al., 2011, Schechner et al., 2003) or fibroblasts-populated dermal substrates such as DED (Ponec et al., 1997, El Ghalbzouri et al., 2002, Lee and Cho, 2005, Lamb and Ambler, 2013); ii) fibroblasts-populated natural biodegradable polymer scaffolds, such as collagen matrices (Bell et al., 1981, Asselineau and Prunieras, 1984, Tinois et al., 1991, Veves et al., 2001, Campitiello et al., 2005, Tremblay et al., 2005, Fimiani et al., 2005), hyaluronic acid (Caravaggi et al., 2003, Landi et al., 2014), fibrin (Ronfard et al., 2000, Marino et al., 2014, Llames et al., 2004, Panacchia et al., 2010, Sriram et al., 2018) and lyophilized collagen-glycosaminoglycan (-GAG) membranes cross-linked by chemical agents (Supp et al., 2002, Hudon et al., 2003) or iii) synthetic scaffolds

such as hydrogels, polyethylene glycol, polycaprolactone, and polylactic acid (Antoni et al., 2015, Chaudhari et al., 2016).

In all approaches mentioned above, dermal equivalents were prepared by mixing dermal fibroblasts with e.g. collagen or by seeding dermal fibroblasts on the DED. The dermal equivalent was submerged in media. Subsequently, epidermal keratinocytes were seeded on the top of dermal equivalent, allowed to cover the upper surface of the construct, before lifting the whole construct above the liquid to expose the keratinocytes to the air. The constructs were then matured at the air-liquid interface, allowing the keratinocytes to stratify and complete the keratinized epidermis. By this approach, a tissue with biological and morphological resemblance to human skin can be achieved (Lee et al., 2000).

As a major extracellular matrix (ECM) protein of the dermal layer, type I collagen is the most widely studied and clinically utilized natural scaffold available for tissue-engineered skin equivalents. The advantages include good biocompatibility, proper porous structure, as well as low immunogenicity (Bi and Jin, 2013). However, limited availability, contraction of the collagen gel, batch-to-batch variability, technical challenges in handling, and the inability to experimentally vary composition and compliance suggested the need for a more versatile ECM (El Ghalbzouri et al., 2005, Serban et al., 2008). Furthermore, the quality of current HSE may be compromised by the fact that they are largely based on non-human collagen. Collagen originated from rat or bovine tendon, and bovine fibrin, allow successful HSE formation, but they still render the dermal compartment an incomplete approach to human ECM *in vivo*, which contains lipids, fibrin, GAGs and PGs in addition to collagen as its main substituent. As such, the dermal equivalents poorly emulate physiological, human ECM and, thus, tissue architecture. Furthermore, the collagen matrices tend to shrink considerably during model cultivation which limits the applicability of the models (El Ghalbzouri et al., 2009).

To avoid contraction of the dermal compartment, non-contractile matrices can be used such as DED. Although the use of human DED may offer a human alternative to these animal-derived dermal equivalents, the application of this method is limited by uncontrollable variation in DED thickness and low availability of the native tissue (El Ghalbzouri et al., 2009). In addition, all mentioned dermal equivalents serve as exogenous scaffolds that need to be seeded with fibroblasts in order to provide a microenvironment permissive of HSE formation, thereby increasing their artificial character. Another impediment is the short life spam of DED based skin equivalents. After 4-8 weeks of culture, these skin equivalents have an epidermis harbouring only one to two viable cell layers, rendering them unsuitable for long-term studies pertaining to e.g. skin aging and UV carcinogenesis (El Ghalbzouri et al., 2009).

One of the natural scaffolds is also Matrigel. Matrigel is the trade name for the matrix extracted from Engelbreth-Holm-Swarm mouse sarcomas consisting primarily of specialized ECM

proteins that build up basement membranes for cells in most epithelial and endothelial layers, and it has been used for skin-engineering purposes (Sobral et al., 2007, Itoh et al., 2013, Dikici et al., 2020). The primary components of Matrigel are four major basement membrane ECM proteins: laminin, collagen IV, entactin and the heparin sulfate PG – perlecan and several growth factors such as transforming growth factor-beta, epidermal growth factor, fibroblast growth factor, insulin-like growth factor, and tissue plasminogen activator (Uriel et al., 2009, Kamel et al., 2013). However, the exact concentrations of the ingredients are not clearly defined, and it shows high batch-to-batch variations (Reis et al., 2014). In studies where Matrigel was employed successful endothelial cell network formation was described (Andrée et al., 2019, Dikici et al., 2020). However, Matrigel remains a popular option for certain cell culture assays but it does have limitations: it is derived from tumor cells and it is disadvantageous for 3D cultures intended for routine predictive drug testing (Knight and Przyborski, 2015, Aisenbrey and Murphy, 2020).

Lastly, many synthetic biocompatible polymers, biodegradable or not, can be used as supports for fibroblast culture during the production of dermal equivalent (Blackwood et al., 2008, Auxenfans et al., 2009, Bacakova et al., 2019). They include hydrogels, polyethylene glycol, polycaprolactone, and polylactic acid (Kao et al., 2009, Antoine et al., 2014, Chaudhari et al., 2016). However, limited clinical success was achieved because synthetic polymers often have lower rates of cell attachment and proliferation due to the limited biological signals. The combination of two or more different polymers including natural or synthetic is necessary to produce suitable scaffolds for skin equivalents when the advantages or disadvantages of each material are well balanced (Zhong et al., 2010).

### 1.4.3. Dermal Equivalents Based on the Self-assembly Approach

The drawbacks of the scaffolds and disadvantages of the artificial substitute use supported the self-assembly of dermal equivalent approach (El-Serafi et al., 2017). The self-assembly approach is a tissue engineering approach based on the capacity of mesenchymal cells, such as fibroblasts, to create their own ECM in order to obtain a final dermis with a composition relatively similar to those present in *in vivo* human skin, inclusive of the collagen, elastin, hyaluronic acid and fibronectin networks (Auger et al., 2004, Urciuolo et al., 2019).

Hence, in the self-assembly approach, dermal fibroblasts are cultured for around four weeks in an optimized culture medium containing ascorbic acid (50 µg/mL), which sustains the formation of ECM. This results in the formation of flexible dermis sheets that can be manipulated, are superimposed to form the dermal compartment. Keratinocytes are then added on top of these sheets and raised to the air-liquid interface, a condition that induces epidermal cell differentiation (L'heureux et al., 1998, Michel et al., 1999, Auger et al., 2000,

Bellemare et al., 2005, Rochon et al., 2010, Thakoersing et al., 2012). Skin equivalents produced with this approach share many characteristics with native human skin. Besides proper-differentiation of all epidermal strata in the skin equivalents, expression and localization of proliferation and differentiation markers such as filaggrin (FLG), involucrin (IVL) and loricrin (LOR), as well as markers of the dermo-epidermal junction could be observed as in the native human epidermis (L'heureux et al., 1998, Laplante et al., 2001, Jean et al., 2011). Keratinocytes from the basal layer express keratin 14 while keratin 10 is expressed in the suprabasal layers (Trottier et al., 2008). Furthermore, two constituents of the ECM, type I and III collagen, are expressed in a similar way in the dermis of skin equivalents produced with the self-assembly approach as in the normal human skin (Jean et al., 2011). Moreover, in order to produce a pre-vascularized endogenous human dermis model, human umbilical vein endothelial cells (HUVEC) were seeded on the self-assembled dermis by fibroblasts, which allowed the formation of an interconnected capillary network (Mazio et al., 2019).

Finally, producing skin equivalents using the self-assembly approach results in substitutes that are entirely autologous, devoid of exogenous ECM and synthetic materials, thereby avoiding potential immunogenicity or inflammation reactions. Besides that, these skin equivalents are stable for considerably longer culturing period and highly reproducible (Auxenfans et al., 2009).

## 1.5. Current Limitations of the Skin Equivalents

Despite the progress in the field of tissue engineering, reconstructed human skin still exhibits several major drawbacks. As such, existing skin equivalents do not resemble the native tissue complexity since most, if not all of the equivalents in addition to keratinocytes and fibroblasts, lack immune cells, vasculature and multi-cellular composition (Abaci et al., 2017). Almost all skin equivalents lack regenerative capacity, inter-tissue crosstalk and the physical properties of the tissue microenvironment, as well as the external forces that act up on them, alter cell behaviours, tissue organization and cell-generated forces (Weinhart et al., 2019). Also, there is a lack of adequate disease skin equivalents (Löwa et al., 2018). Therefore, there is a growing interest in building more physiological skin equivalents by incorporating different skin components, such as vasculature, pigmentation, immunity, innervation, appendages, glands and adipose tissue (Abaci et al., 2017, Löwa et al., 2018).

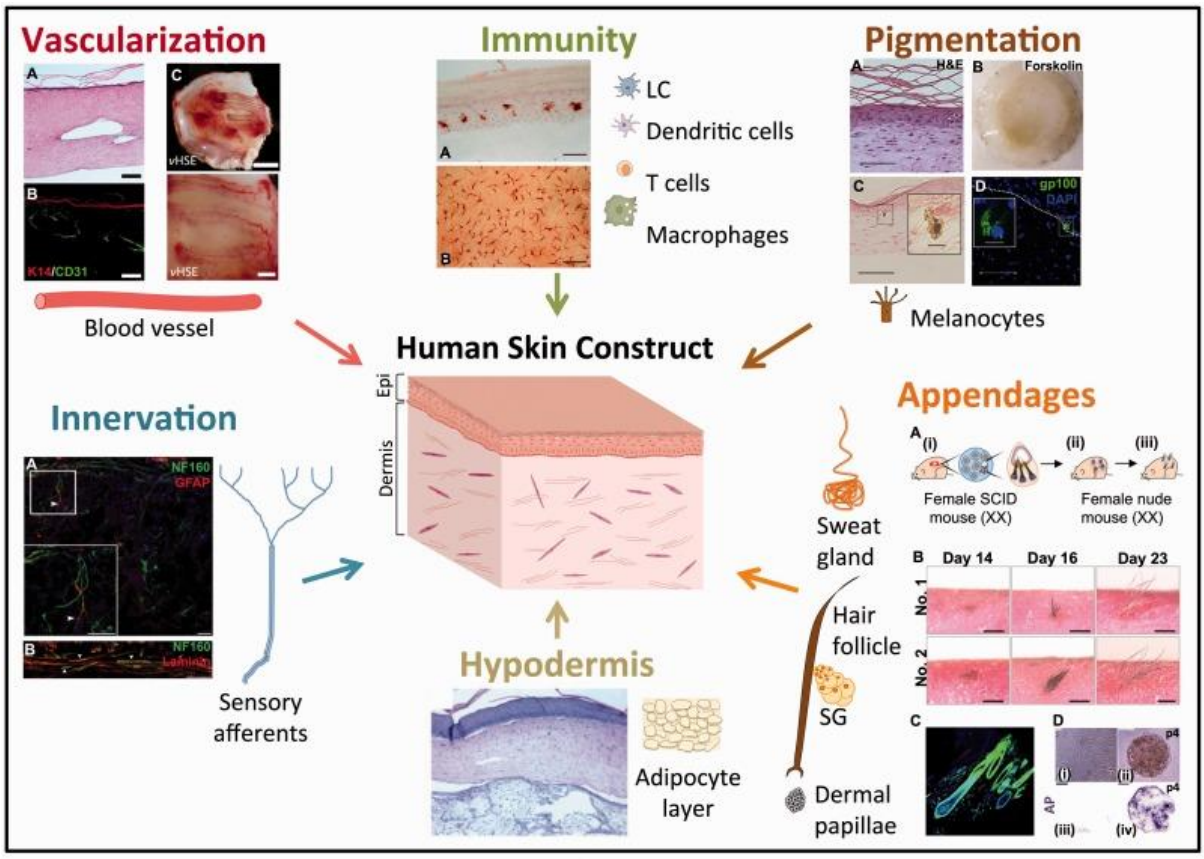


**Figure 6.** Schematic depiction of current skin equivalents reconstruct of epidermis and dermis with vascularization, immunity, pigmentation, innervation, hypodermis and appendages. Reproduced from (Abaci et al., 2017).

With the improvements, reconstructed skin equivalents should become an indispensable tool for investigating dermatology, especially for addressing: i) skin homeostasis and the molecular mechanisms that govern different cell types and their interactions, ii) skin repair, specifically the signalling pathways that drive this process, iii) skin regeneration, by understanding the properties and the behaviour of the skin stem cells residing in various niches and iv) skin diseases, by modelling these diseases using cells from patients or genetically engineered diseased cells to reproduce molecular defects (Ali et al., 2015). Therefore, reconstructed skin equivalents have been improved over the past years by incorporating other cell types as described in the following chapter.

### 1.5.1. Approaches to Overcome the Limitations

Until now, various pigmented human skin equivalents have been reconstructed (Nakazawa et al., 1998, Liu et al., 2011, Duval et al., 2012) by co-seeding of human melanocytes and keratinocytes on dermal compartment, then allowing adhesion and proliferation of cells exposed to the air-liquid interface, which gave rise to a multi-layered, stratified, pigmented

epidermis with a dense horny layer. These human skin equivalents thus mimic the physiological situation of normal human skin, and provide a more physiologically relevant system to study the 3D interactions of melanocyte-keratinocyte and to elucidate the regulatory mechanisms of melanogenic compounds (Yoon et al., 2003). To create immune-competent skin equivalents, immune cells isolated from blood or as cell lines, have been incorporated in the skin equivalents which include Langerhans cells (Ouwehand et al., 2011, Kosten et al., 2015), macrophages (Bechetoille et al., 2011, Linde et al., 2012) and T cells (Van Den Bogaard et al., 2014, Wallmeyer et al., 2017). Subcutaneous adipose tissue has also been integrated (Trottier et al., 2008, Bellas et al., 2013, Xie et al., 2010, Monfort et al., 2013). Furthermore, Vidal and colleagues produced a full-thickness 3D skin construct containing human induced neuronal stem cells within an adipose scaffold hypodermis layer to model the immune-competent skin equivalent (Vidal et al., 2019). However, most HSE are currently cultured under static conditions, resulting in no or low exposure of mechanical forces such as stretching or shear stress. To mimic more physiological skin equivalents, perfusion platform (Strüver et al., 2017) or microfluidic cell cultures (Wufuer et al., 2016) has been used, which allowed dynamic cultivation of *in vitro* skin equivalents. Another drawback of the currently available skin equivalents is that only few *in vitro* diseased skin equivalents are described (Küchler et al., 2011, Vávrová et al., 2014, Hönzke et al., 2016, Wallmeyer et al., 2017, Löwa et al., 2020). Nevertheless, the development of disease skin equivalents is still in its infancy. With regard to skin, disease skin equivalents are currently generated from patient-derived cells, by modulation of disease-associated genes, by co-cultivation with pathogens or malignant cells, or by addition of disease-associated stimuli such as cytokines (Löwa et al., 2018).

The vascularized skin equivalents are still in the early stage of development. Vasculogenesis is the *in situ* assembly of endothelial cells and precursor cells, such as angioblasts, into capillaries, whereas angiogenesis is the formation of new capillaries from pre-existing vessels. Vasculogenesis and angiogenesis are multifactor processes driven by numerous growth factors: vascular endothelial growth factor (VEGF), fibroblast growth factors (FGF), platelet-derived growth factors (PDGF), angiopoeitins, and the transforming growth factors (TGF), released at a precise time and concentration. Originally, vasculogenesis and angiogenesis were considered independent events, with vasculogenesis occurring exclusively during embryogenesis and angiogenesis in adults. It is now recognized that these processes are more complex and both mechanisms may be involved in vessel formation within a single microenvironment (Ferrara et al., 2003, Kaully et al., 2009, Jiang and Brey, 2011).

Proper microvascular structure is essential for normal function of all organs as well as for normal skin function. *In vivo*, the skin is supplied through a dense capillary network in the

dermis and the adipose tissue underneath (Groeber et al., 2013). The microcirculation supplies skin with oxygen, nutrients, immune cells and signalling molecules, while removing by the products and waste (Jain, 2003). Furthermore, the vascular system is a key component in many skin diseases such as melanoma, psoriasis, and atopic dermatitis (Elias and Steinhoff, 2008, Groeber et al., 2013). Nevertheless, with all improvements of the reconstructed skin equivalents, a major weakness of functional skin equivalents is a lack of functional vascularization. Non-vascularized skin equivalents cannot be used as models for studying key features of diseased skin, such as trafficking of leukocytes across vessel endothelium, or for evaluating transdermal drug penetration into the blood stream and/or skin localization of an intravenously administered substance (Dellambra et al., 2019). Therefore, three approaches have been attempted for vascularization of bioengineered tissue: i) incorporation of soluble angiogenic factors, ii) gene transfer approaches and iii) seeding of endothelial cells onto or into matrices and scaffolds (Kaully et al., 2009, Montaño et al., 2010).

Black and colleagues were the first who described the *in vitro* formation of capillary-like structures within the engineered tissue (Black et al., 1998). They co-cultured keratinocytes, fibroblasts, and human umbilical vein endothelial cells (HUVEC) on chitosan/collagen scaffolds and demonstrated that an extensive network of capillary-like structures was spontaneously formed by self-organization, by the cell-cell interaction of HUVEC with fibroblasts and by cell-matrix interactions (Black et al., 1998). Furthermore, Groeber and co-workers used decellularized segment of porcine jejunum, physiologically supplied by a single artery-vein-pair, which was reseeded with human dermal microvascular endothelial cells (HDMEC) and perfused by a bioreactor system generating physiological pulsatile pressure (Groeber et al., 2016). This bioreactor system supports the skin equivalent under submerged conditions or at the air-liquid interface, allowing the formation of typical histological skin architecture and of a functional skin barrier (Groeber et al., 2013, Groeber et al., 2016). In another approach, keratinocytes were genetically modified to overexpress VEGF or PDGF, and the resulting skin equivalents exhibited enhanced vascularization (Supp et al., 2000, Supp et al., 2002, Supp et al., 2004). The same research group has reported the modification of endothelial cells with a caspase-resistant Bcl-2 protein to enhance endothelial cells survival (Supp et al., 2000).

Despite the fact that all approaches mentioned above clearly describe development of capillary-like structures in the dermal compartment of the skin equivalents, there is still need to further increase the resemblance of these skin equivalents to native human skin, to improve the barrier function and *in vitro–in vivo* correlations.

## 2. AIMS OF THE THESIS

## 2.1. Aims

Dermal fibroblasts seem critical for fundamental physiological processes leading to normal keratinocytes differentiation and maturation, tissue homeostasis and cutaneous wound healing (El Ghalbzouri et al., 2004, Tracy et al., 2016), as well as for pathophysiological processes in which diseased fibroblasts may drive skin diseases (Berroth et al., 2013, Löwa et al., 2020). However, very little is known about the actual crosstalk between epidermal keratinocytes and dermal fibroblasts and the impact of dermal fibroblasts on epidermal differentiation and maturation. Therefore, we aimed to gain more fundamental understanding of the impact of the cellular crosstalk between keratinocytes and fibroblasts on the skin differentiation, skin homeostasis and skin barrier formation by using human-based *in vitro* three-dimensional (3D) skin equivalents with and without fibroblasts (Jevtić et al., 2020). Furthermore, recent findings indicate that extracellular vesicles (EVs) operate cell-to-cell communication and there is currently very little information about the content and the function of EVs from dermal fibroblasts. Hence, in this thesis we aimed to confirm the methods for EVs isolation and characterization from the cell culture medium secreted by dermal fibroblasts.

Over the past years, human-based tissue models emerged as novel and promising tools for basic and preclinical research (Brubaker et al., 2019). Advances in the field of tissue engineering of reconstructed human skin equivalents led to the growing interest in the development of well-established test systems closely resembling native human skin *in vitro*, but they still exhibit several major drawbacks such as the lack of immune cells, vasculature and multi-cellular composition (Abaci et al., 2017). Moreover, the dermal equivalent of the vast majority of skin equivalents consist of the animal-derived collagen matrix poorly emulating physiological human extracellular matrix (ECM) and tissue architecture. To overcome these obstacles, this thesis further aims for the ongoing development of completely human-based skin equivalents based on primary human fibroblasts-derived ECM with included endothelial cells, crucial for adequate tissue differentiation and vascularization.

# 3. MATERIALS AND METHODS

## 3.1. Materials

### 3.1.1. Reagents

| | |
|---|---|
| Acrylamide | Sigma-Aldrich, Munich, DE |
| Adenine | Sigma-Aldrich, Munich, Germany |
| Ammonium persulfate (APS) | Sigma-Aldrich, Munich, DE |
| Agar100 (epoxy resin) | Agar Scientific, Stansted, GBR |
| Bovine collagen type I | PureCol; Advanced BioMatrix, San Diego, CA, USA |
| Bovine Serum Albumin (BSA) | Carl Roth, Karlsruhe, DE |
| Benzyl dimethylamine | Agar Scientific, Stansted, GBR |
| Cacodylate buffer (cacodylic acid sodium salt trihydrate) | Roth, Karlsruhe, Germany |
| Caffeine solution | PerkinElmer, Waltham, MA, USA |
| Cholera toxin | Sigma-Aldrich, Munich, Germany |
| DAPI Mounting Medium | Dianova Hamburg, DE |
| Dithiothreitol (DTT) | Sigma-Aldrich, Munich, DE |
| DMEM | Sigma-Aldrich, Munich, DE |
| DMEM/F12 | Sigma-Aldrich, Munich, DE |
| Dodecenyl succinic anhydride | Agar Scientific, Stansted, GBR |
| Dimethylsulfoxide (DMSO) | Carl Roth, Karlsruhe, DE |
| Eosin G | Carl Roth, Karlsruhe, DE |
| Ethanol absolute | Merck, Darmstadt, DE |
| Ethanol 96% | Erkel AHK, Berlin, DE |
| Endothelial cell differentiation medium | Lonza, Walkersville Inc., Walkersville, USA |
| EpiLife medium | Thermo Fisher Scientific, Schwerte, Germany |
| Epidermal growth factor | Sigma-Aldrich, Munich, Germany |
| Exosome-depleted FBS | Sigma-Aldrich, Munich, Germany |
| Filter 0.22 µm | TPP, Melbourn, UK |
| Goat serum | Dianova, Hamburg, DE |
| Hank’s Buffered Salt Solution (HBSS) | Life Technologies, Darmstadt, DE |
| Hematoxylin | Carl Roth, Karlsruhe, DE |
| Human keratinocyte growth supplement | Thermo Fisher Scientific, Schwerte, Germany |
| Hydrocortisone | Sigma-Aldrich, Munich, Germany |

| | |
|---|---|
| Fetal Bovine Serum | Biochrom, Berlin, DE |
| Igepal® CA-630 | Thermo Fisher Scientific, Schwerte, Germany |
| Insulin | Roche, Grenzach-Wühlen, DE |
| Ionic detergent compaitibilty reagent IDCR | Invitrogen, Carlsbad USA |
| Karnovsky`s fixative | Merck Eurolab, Darmstadt, Germany |
| L-Glutamine | Sigma-Aldrich, Munich, DE |
| Lucifer yellow solution | Sigma-Aldrich, Munich, Germany |
| Lipid standards | Merck, Darmstadt, Germany |
| Linomat 5 | Camag, Muttenz, Switzerland |
| N-Methyl-4-nitroaniline | Agar Scientific, Stansted, GBR |
| Nickel-grids | nickel-grids |
| Osmium tetroxide | Chempur, Karlsruhe, Germany |
| Penicillin/Streptomycin | Sigma-Aldrich, Munich, DE |
| Phosphate Buffered Saline (PBS) | Sigma-Aldrich, Munich, DE |
| Protease/Phosphatase Inhibitor Cocktail | Cell Signaling, Massachusetts, US |
| Roti®-Histofix | Carl Roth, Karlsruhe, DE |
| Roti®-Histokit | Carl Roth, Karlsruhe, DE |
| Roti®-Histol | Carl Roth, Karlsruhe, DE |
| Sodium hydroxide (NaOH) | Sigma-Aldrich, Munich, DE |
| Sodium pyruvate/Ham’s F12 | Life Technologies, Darmstadt, Germany |
| TEMED | Carl Roth, Karlsruhe, DE |
| Tris | Carl Roth, Karlsruhe, DE |
| Trypsin/EDTA | Sigma-Aldrich, Munich, DE |
| Tween-20 | Carl Roth, Karlsruhe, DE |
| Testosterone solution | Sigma-Aldrich, Munich, Germany |
| Uranlyess | Science Services GmbH, Munich, Germany |

### 3.1.2. Cell Culture Medium

| | |
|---|---|
| Fibroblasts Growth Medium | DMEM supplemented with:<br>10% FBS<br>1% L-glutamin<br>1% penicillin/streptomycin |
| Keratinocytes Growth Medium | EpiLife medium supplemented with human keratinocyte growth supplement |

| | |
|---|---|
| Keratinocytes Differentiation medium (KDM) | 64.5% DMEM<br>10% FBS,<br>5 µg/ml insulin,<br>10 ng/ml epidermal growth factor,<br>0.4 µg/ml hydrocortisone,<br>0.18mM adenine,<br>0.1nM cholera toxin,<br>4mM L-glutamine<br>21.5% sodium pyruvate/Ham's F12 |
| Conditioned Medium for Extracellular Vesicles (EVs) | DMEM supplemented with:<br>7.5% fetal bovine serum (FBS)<br>2 mM L-glutamine |
| Conditioned Medium for Extracellular Vesicles (EVs) Depleted of Exosomes | DMEM supplemented with:<br>7.5% exosome deptelred fetal bovine serum (FBS)<br>2 mM L-glutamine |

### 3.1.3. Kits

| | |
|---|---|
| Pierce® BCA Protein Assay Kit | Thermo Fisher Scientific, Schwerte, DE |
| SignalFire™ ECL reagent | Cell Signaling, Frankfurt/Main, DE |
| InnuPREP RNA Mini Kit | Analytik Jena, Jena, DE |
| iScript cDNA Kit | Bio-Rad, Munich, DE |
| iTaq™ Universal SYBR® Green Supermix Kit | Bio-Rad, Munich, DE |

### 3.1.4. Antibodies for immunofluorescence and western blot

| Antibody | Isotype | Clone | IF | WB | Company |
|---|---|---|---|---|---|
| ß-actin | mouse IgG1 | monoclonal (15G5A11/E2) | - | 1:10,000 | Sigma-Aldrich, Munich, Germany |
| FLG | mouse IgG | polyclonal | 1:1,000 | 1:1,000 | BioLegend, San Diego, United States of America |
| IVL | rabbit IgG | polyclonal | 1:1,000 | 1:1,000 | Abcam, Cambridge, United Kingdom |
| CLDN1 | mouse IgG2 | monoclonal (1C5-D9) | 1:300 | 1:500 | Novus Biologicals Cambridge, United Kingdom |

| | | | | | |
|---|---|---|---|---|---|
| OCLN | mouse IgG1 | monoclonal (OC-3F10) | 1:300 | 1:500 | ThermoFisher, Cambridge, United Kingdom |
| Ki67 | mouse IgG | monoclonal (Ki-67P) | 1:200 | - | Dianova, Hamburg, Germany |
| vWF | rabbit IgG | polyclonal | 1:400 | - | Abcam, Cambridge, United Kingdom |
| CD31 | mouse IgG1 | monoclonal (JC70A) | 1:50 | - | Dako, Glostrup, Denmark |
| IgG Alexa Fluor®488 | rabbit IgG | - | 1:400 | - | Cell Signaling, Frankfurt/Main, Germany |
| IgG Alexa Fluor®594 | mouse IgG | - | 1:400 | - | Cell Signaling, Frankfurt/Main, Germany |

### 3.1.5. Primers

| Gene | Sense primer (5‘ – 3‘) | Antisense primer (5‘ – 3‘) |
|---|---|---|
| *FLG* | AAggAACTTCTggAAAAggAATTTC | TTgTggTCTATATCCAAgTgATCCAT |
| *IVL* | TCCTCCAgTCAATACCCATCAg | CAgCAgTCATgTgCTTTTCCT |
| *CLDN1* | gCgCgATATTTCTTCTTgCAgg | TTCgTACCTggCATTgACTgg |
| *OCLN* | TgCATgTTCgACCAATgC | AAgCCACTTCCTCCATAAgg |
| *GAPDH* | CTCTCTgCTCCTCCTgTTCgAC | TgAgCgATgTggCTCggCT |

### 3.1.6. Software

| | |
|---|---|
| Bruker OPUS software | Bruker Corp, Billerica, MA |
| ImageJ, Version 1.46r | National Institute of Health, MD, US |
| GraphPad Prism | GraphPad Software, La Jolla, CA, US |
| VisionCats software | Camag, Muttenz, Switzerland |
| WinMDI software, Version 2.8 | Scripps Institute, La Jolla, CA, US |

### 3.1.7. Consumables

| | |
|---|---|
| 12-well cell culture inserts with 3 µm pore size | BD Biosciences, Heidelberg, Germany |
| 12-well inserts with 0.4 µm pore size | Corning, Corning, NY, USA |
| Blotting Pads | VWR, Pennsylvania, US |
| Cell Culture flasks (75 cm², 150 cm²) | TPP, Melbourn, UK |
| Centrifuge tubes (15, 50 mL) | Sarstedt, Nürnbrecht, DE |
| Cover slips | Gerhard Menzel, Braunschweig, DE |
| Embedding molds | Sigma-Aldrich, Munich, DE |
| Forceps | Carl Roth, Karlsruhe, DE |

| | |
|---|---|
| Formvar and carbon coated copper grid | Polyscience, Hirschberg, Germany |
| Franz diffusion cells | Fa. Gauer, Puettling, Germany |
| Filter paper | Schleicher&Schüll, Dassel, Germany |
| HPTLC plates | Merck, Darmstadt, Germany |
| Igepal® CA-630 | Sigma-Aldrich, Munich, Germany |
| Multiwell cell culture plates (6, 12, 96-well) | VWR, Pennsylvania, US |
| Nitrocellulose membrane | Bio-Rad, Munich, DE |
| Nitril gloves | Hansa-Trading HTH, Hamburg, DE |
| Parafilm | Carl Roth, Karlsruhe, DE |
| PCR grade tubes | Sarstedt, Nürnbrecht, DE |
| PCR stripes | Carl Roth, Karlsruhe, DE |
| Pipette tips (10, 100, 1000 µL) | Sarstedt, Nürnbrecht, DE |
| Pipette tips with filter (10, 100, 1000 µL) | Sarstedt, Nürnbrecht, DE |
| Polylysine slides | Gerhard Menzel, Braunschweig, DE |
| Scalpels | Carl Roth, Karlsruhe, DE |
| Serological pipettes (5, 10, 25 mL) | Sarstedt, Nürnbrecht, DE |
| Syringes | Carl Roth, Karlsruhe, DE |
| Syringe filters (0.45 µm) | Sarstedt, Nürnbrecht, DE |
| Tissue freezing medium | Leica Biosystems, Nussloch, Germany |

### 3.1.8. Devices

| | |
|---|---|
| Autoclave V Series | Systec, Wettenberg |
| Avanti J-26 S XP centrifuge | Beckman Coulter, Brea, CA, USA |
| Balance XS205 dualRange | Mettler-Toledo, Giessen, DE |
| Beckman Coulter ultracentrifuge with type 70 Ti rotor | Beckman Coulter, Brea, CA, USA |
| Centrifuge, Eppendorf Centrifuge 5415 C | Eppendorf AG, Hamburg, DE |
| Centrifuge, Megafuge 1.0 R | Heraeus, Hanau, DE |
| CO2 Incubator | Heraeus, Hanau, DE |
| CO2-free Incubator | Heraeus, Hanau, DE |
| Cryotome Leica CM1510 S | Leica Biosystems, Nussloch, DE |
| Flash electron microscope JEM-1400 | JEOL GmbH, Freising, Germany |
| FACSCalibur | BD Biosciences, San Jose, CA, US |
| Fluorescence microscope BZ-8000 | Keyence, Neu-Isenburg, DE |
| FLUOstar Optima | BMG Labtech, Ortenberg, DE |

| | |
|---|---|
| LaminAir HB 2472 | Heraeus, Hanau, DE |
| Light microscope - Olympus CX21 | Olympus, Stuttgart, Germany |
| LightCycler 480 | Roche, Mannheim, DE |
| Microscope, phase contrast Axiovert 135 | Carl Zeiss, Jena, DE |
| Mr. Frosty | Thermo Fisher Scientific, Waltham, UK |
| Neubauer cell counting chamber | Carl Zeiss, Jena, DE |
| Nicolet 6700 FTIR spectrometer | Thermo Fisher Scientific, Schwerte, Germany |
| NanoSight NS500 sample chamber | Malvern, Worcestershire, UK) |
| PCR thermo cycler, Tgradient | Biometra, Jena, DE |
| pH meter 766 | Knick, Berlin, DE |
| Pipettes (10, 100, 1000 µl) | Eppendorf, Hamburg, DE |
| PXi/PXi Touch gel imaging system | Syngene, Cambridge, UK |
| Radiochemical detection | HIDEX 300 SL, HIDEX, Turku, Finland |
| Refrigerator -80°C HERAfreezeTM HFU T Serie | Thermo Scientific, Schwerte, Germany |
| Trans-Blot Turbo Blotting System | BioRad, Munich, DE |
| TissueLyzer | Qiagen, Hilden, Germany |
| Vacuum concentrator (Savant SpeedVac Plus) | Thermo Scientific, Schwerte, Germany |

## 3.2. Methods

### 3.2.1 Cell culture

#### 3.2.1.1. Dermal fibroblasts, epidermal keratinocytes and endothelial cell cultivation

Primary human fibroblasts and keratinocytes were isolated from juvenile foreskin after circumcision surgery (approved by the ethics committee of the Charité-Universitätsmedizin Berlin, Germany, EA1/081/13) using standard procedures. Fibroblasts were cultured in Dulbecco's Modified Eagle's Medium (DMEM) (Sigma-Aldrich, Munich, Germany) supplemented with 10% fetal bovine serum (FBS) Superior (Biochrom, Berlin, Germany), 1% L-glutamin (Sigma-Aldrich, Munich, Germany) and 1% penicillin/streptomycin (10.000U/ml; Sigma-Aldrich, Munich, Germany). Keratinocytes were first cultured in EpiLife medium supplemented with human keratinocyte growth supplement (Thermo Fisher Scientific, Schwerte, Germany), defined as keratinocytes growth medium. Human dermal microvascular endothelial cells (HDMEC) from neonatal foreskin (Lonza, Walkersville Inc., Walkersville, USA) were cultured according to manufacturer's instructions in endothelial cell (EC) differentiation medium (Lonza, Walkersville Inc., Walkersville, USA). All cells were maintained at 37°C in a humidified atmosphere at 95% and 5% $CO_2$. Cell culture medium was changed

every second days. For each experiment, fibroblasts and keratinocytes at passage 2 and HDMEC were used at passage 5.

#### 3.2.1.2. Generation of skin equivalents with and without fibroblasts

For the construction of the dermis equivalent, bovine collagen type I (PureCol; Advanced BioMatrix, San Diego, CA, USA) was mixed with HBSS (Sigma-Aldrich, Germany), brought to a neutral pH using NaOH, and mixed with $6x10^4$ primary human fibroblasts. The collagen-fibroblast mixture was then poured into 12-well cell culture inserts with 3 µm pore size (BD Biosciences, Heidelberg, Germany) and kept at 37°C for 2 h. Subsequently, keratinocyte growth medium was added and $9x10^5$ normal human keratinocytes were seeded on top of the collagen matrix and transferred to an incubator at 37°C with 5% $CO_2$ and 95% humidity. After 24 h, the skin equivalents were lifted to the air-liquid interface and the culture medium was changed to a differentiation medium. The skin equivalents were cultured over 14 days, with medium change every other day, with keratinocytes differentiation medium (KDM) consisting of FBS (Biochrom, Berlin, Germany), 5 µg/ml insulin (Roche, Prenzberg, Germany), 10 ng/ml epidermal growth factor, 0.4 µg/ml hydrocortisone, 0.18mM adenine, 0.1nM cholera toxin, 4mM L-glutamine (all from Sigma-Aldrich, Munich, Germany) in DMEM with sodium pyruvate/Ham's F12 (Life Technologies, Darmstadt, Germany) with medium change every other day (Löwa et al., 2020, Jevtić et al., 2020).

To generate skin equivalents without fibroblasts, the dermis equivalent was initially prepared as described above. After successful solidification of the collagen matrix, sterile distilled water was added to lyse the fibroblasts in the collagen matrix. The distilled water was changed three times every 2 h, and then kept overnight to ensure full fibroblast lysis (Coulomb et al., 1989). Afterwards, the water was removed and keratinocyte growth medium was added for 2 h. Primary keratinocytes were then seeded and the skin equivalents were generated as described above.

#### 3.2.1.3. Generation of skin equivalents with a dermal equivalent based on self-assembled extracellular matrix (ECM)

*Generation of type II skin equivalents - skin equivalent with a dermal equivalent based on self-assembled ECM containing fibroblasts and human dermal microvascular endothelial cells (HDMEC):* First, 2.800 primary human fibroblasts were seeded on 12-well inserts with 0.4 µm pore size (Corning, Corning, NY, USA) and cultured for 10 days. Subsequently, $1.1x10^4$ HDMEC were seeded directly onto the fibroblasts. The co-culture was then incubated for 20 days in a 1:1 ratio of fibroblasts culture medium and EC differentiation medium. Subsequently, $9x10^5$ primary human keratinocytes were seeded on top of the fibroblast/HDMEC co-cultures

and after 24h the skin equivalents were lifted to the air-liquid interface. The skin equivalents were then cultivated over another 14 days using a 1:1 ratio of KDM and the medium used for the fibroblasts/EC co-culture.

*Generation of type III skin equivalents - skin equivalents with a dermal equivalent based on self-assembled ECM containing fibroblasts only:* First, 2.800 primary human fibroblasts were seeded on 12-well inserts with 0.4 µm pore size (Corning, Corning, NY, USA) and cultured for 30 days in a 1:1 ratio of fibroblasts culture medium and EC differentiation medium. Medium was replaced every other day. Subsequently, $9x10^5$ primary human keratinocytes were seeded on top of the fibroblasts cultures and the skin equivalents were generated according to type II skin equivalents.

Self-assembled dermal compartment for the type II and type III skin equivalents has been developed by our collaboration partner Dr.rer.nat. Sabine Kaessmeyer (Department of Veterinary Medicine, Institute for Veterinary Anatomy, Freie Universität Berlin, Germany ).

#### 3.2.1.4. Condition medium preparation for extracellular vesicle (EVs) isolation

Primary human fibroblasts were isolated from juvenile foreskin after circumcision surgery (approved by the ethics committee of the Charité-Universitätsmedizin Berlin, Germany, EA1/081/13) using standard procedures and cultivated in Dulbecco's modified Eagle's medium (DMEM) (Sigma-Aldrich, Munich, Germany) supplemented with 7.5% fetal bovine serum (FBS) (Biochrom, Berlin, Germany) and 2 mM L-glutamine (Sigma-Aldrich, Munich, Germany). On day 4 of dermal fibroblasts cultivation, when the confluence of the cells reached 70-80%, cells were washed three times with PBS and further cultured in EVs-depleted medium, made with exosome-depleted FBS (Sigma-Aldrich, Munich, Germany). After 24h, medium was collected for the EVs isolation. The cells were used in passage 3.

### 3.2.2 Cryopreservation and preparation of cryosection of skin equivalents

For the histological analysis of the skin equivalent, the insert membrane and the skin equivalent was cut out of the insert with a scalpel. The skin equivalent was transferred into disposable embedding mold (Sigma-Aldrich, Munich, Germany) previously filled with a tissue freezing medium to fill the bottom of the mold (Leica Biosystems, Nussloch, Germany) using forceps and then completely covered carefully with tissue freezing medium avoiding air bubbles. The filled embedding mold was then held to the phase boundary of liquid nitrogen for shock freezing, resulting in a homogeneous cryo-bloc. The cryo-blocs were stored at -80°C (HERAfreezeTM HFU T Serie; Thermo Scientific, Schwerte, Germany). Prior to cryosection preparation, the respective cryo-blocs were prewarmed in the cryotome (Leica CM 1510s; Leica Microsystems, Wetzlar, Germany) to the cutting temperature of -18°C to -21°C. The

cryosections 7 µm thin were prepared according to the manufacturer's specifications and were finally transferred to poly-L-lysine coated slides (Gerhard Menzel, Braunschweig, Germany). Finally, the sections were dried at room temperature for at least 30 min and further investigated as described below.

### 3.2.3. Histological analysis of skin equivalents

Sections were stained with hematoxylin and eosin (H&E) according to standard protocols shown in Table 3.1. Room temperature dried cryosections were mounted with Roti®-Histokitt (Carl Roth, Karlsruhe, Germany) and covered with a thin cover glass. Tissue sections were then analysed using a microscopy (BZ-8000; Keyence, Neu-Isenburg, Germany).

**Table 3.1.** H&E staining procedure

| Solution | Incubation time [min] |
|---|---|
| Aqua bidest. | 0.5 |
| Hematoxylin solution (according Mayer) | 5 |
| Tap water | 5 |
| Eosin G solution | 0.5 |
| Ethanol 96% (v/v) I | 2 |
| Ethanol 96% (v/v) II | 2 |
| Ethanol 100% (v/v) I | 2 |
| Ethanol 100% (v/v) II | 2 |
| Roti®-Histol I | 2 |
| Roti®-Histol II | 2 |

### 3.2.4. Immunofluorescence analysis

For immunofluorescence (IF) staining, the skin sections were cut as described in chapter above and fixed with 4% formaldehyde, washed with PBS containing 0.0025% BSA and 0.025% Tween 20 (Carl Roth, Karlsruhe, Germany), and blocked with normal goat serum (1:20 in PBS). The skin sections were then incubated with primary antibodies overnight at 4°C. Subsequently, the skin sections were washed three times and incubated with secondary antibodies IgG Alexa Fluor®488 and IgG Alexa Fluor®594 (Abcam, Cambridge, UK; 1:400) for 1h at room temperature. The skin sections were then embedded in 4′,6-diamidin-2-phenylindol (DAPI) antifading mounting medium (Dianova, Hamburg, Germany) and subjected to fluorescence microscopy analysis (BZ-8000; Keyence, Neu-Isenburg, Germany). Tables displaying the antibodies used for IF analysis are shown in Table 3.1.4.

### 3.2.5. Western blot analysis

For the western blot (WB) analysis, for protein quantification the epidermis was gently peeled-off and lysed in RIPA buffer with 1% Protease-Phosphatase Inhibitor Cocktail (Thermo Scientific, Schwerte, Germany) for sodium dodecyl sulfate polyacrylamide gel electrophoresis (SDS-PAGE). Total proteins were quantified using the BCA Protein Assay Kit (Thermo Scientific, Schwerte, Germany). Subsequently, samples (~25µg protein) were boiled in standard SDS-PAGE sample buffer and separated by 10% SDS-PAGE (Bio-Rad, Munich, Germany) according to their molecular mass based on their different migration rate through a gel under the influence of an electrical field. SDS is a detergent that, together with heat, disrupts the tertiary structure of proteins and coats the proteins with a negative charge. Therefore, samples were diluted in standard SDS-PAGE sample buffer supplemented with 100 mM dithiothreitol (DTT) and boiled at 95 °C. DTT is a reducing agent that breaks down protein-protein disulfide bonds. In parallel, gels were prepared for SDS-PAGE (Table 3.2.).

**Table 3.2.** Running and Stacking gel composition for SDS-PAGE.

| | **$dH_2O$** | **Acrylamid** | **Gel buffer** | **SDS (10%)** |
|---|---|---|---|---|
| **Running gel** | 4.1 ml | 3.3. ml | 2.5 ml 2 M Tris (pH 8.8) | 0.1 ml |
| **Stacking gel** | 6.1 ml | 1.3 ml | 2.5 ml 0.5 M Tris (pH 6.8) | 0.1 ml |

Gels were then blotted onto nitrocellulose membranes (Bio-Rad, Munich, Germany). Gel and membrane together with blotting pads were layered in a transfer cassette (Bio-Rad, Munich, DE). By applying electrical load (200 mA, 30 min), the negatively charged proteins transfer onto the membrane. After blocking with Tris-buffered saline containing 0.1% Tween20 (TBST) supplemented with 5% skimmed milk powder for 1h at 37°C to reduce the amount of unspecific binding of proteins, and the membranes were incubated with primary antibodies at 4°C overnight. Blots were washed in TBST and incubated with anti-rabbit or anti-mouse horseradish-peroxidase-conjugated secondary antibody (Cell Signaling, Frankfurt/Main, Germany) for 1h and washed with TBST. Blots were developed with SignalFire™ ECL reagent (Cell Signaling, Frankfurt/Main, Germany) and visualized by PXi/PXi Touch gel imaging system (Syngene, Cambridge, UK). Immunoblotting quantification was performed using ImageJ software. ImageJ was applied to analyse protein expression via densitometry. Target protein intensity was compared to that of the loading control (β-Actin). Tables displaying the antibodies used for WB analysis are shown in Table 3.1.4.

### 3.2.6. Sample preparation for transmission electron microscopy (TEM)

The skin equivalents were washed with 0.1M cacodylate buffer (cacodylic acid sodium salt trihydrate, Roth, Karlsruhe, Germany) and fixed for 1h at 4°C in Karnovsky`s fixative (Merck Eurolab, Darmstadt, Germany). Then, the skin equivalents were post-fixed in 1% osmium tetroxide (Chempur, Karlsruhe, Germany) in 0.1M sodium cacodylate buffer for 1h and dehydrated by a graded series of ethanol.

### 3.2.7. Transmission electron microscopy (TEM) of the skin equivalents

The transmission electron microscopy (TEM) analysis was performed by our collaboration partner Dr.rer.nat. Sabine Kaessmeyer (Department of Veterinary Medicine, Institute for Veterinary Anatomy, Freie Universität Berlin, Germany ). Also, the description of this method section was provided by Dr.rer.nat. Sabine Kaessmeyer. After washing and fixation, the skin equivalents were embedded in a mixture of Agar100 (epoxy resin), dodecenyl succinic anhydride (softener), N-Methyl-4-nitroaniline (hardener) and benzyl dimethylamine (catalyst) (all: Agar Scientific, Stansted, GBR). Polymerization was carried out at 45°C and 55°C, each for 24h. Semi-thin sections (0.5µm) were cut and stained with modified Richardson solution and examined using a light microscope (Olympus CX21, Olympus, Stuttgart, Germany). Ultra-thin-sections (70nm) were mounted on nickel-grids (Agar Scientific, Stansted, GBR), stained with 2% uranyl acetate and stabilized by lead citrate Ultrostain 2 (Leica, Wetzlar, Germany) and analyzed using an JEM-1400 Flash electron microscope (JEOL GmbH, Freising, Germany).

### 3.2.8. Quantitative real-time polymerase chain reaction (qPCR)

To analyse the gene expression of skin barrier and tight junction proteins, the epidermis was gently peeled-off the dermis equivalents placed into a lysis buffer and then milled for 30s on 25Hz using a TissueLyzer (Qiagen, Hilden, Germany). Afterwards, RNA was isolated using an InnuPREP RNA Mini Kit (Analytik Jena, Jena, Germany) according to the manufacturer's instructions. Prior to qPCR analysis, RNA samples needed to be converted into complementary DNA (cDNA) by using the retroviral enzyme reverse transcriptase. The iScript cDNA Kit (Bio-Rad, Munich, Germany) was used for cDNA synthesis. Subsequently, real-time quantitative polymerase chain reaction was performed using the iTaq™ Universal SYBR® Green Supermix Kit (Bio-Rad, Munich, Germany). Glyceraldehyde-3-phosphate dehydrogenase (GAPDH) served as house-keeping gene. Primer sequences are displayed in Table 3.1.5.

### 3.2.9. Skin absorption testing

To assess the skin barrier function of the skin equivalents, skin permeation assays were performed according to previously published procedures (Wallmeyer et al., 2015). Stock solutions of testosterone (40 µg/ml, 2% [v/v] Igepal® CA-630 and 0.4% ethanol (v/v, %); Sigma-Aldrich, Munich, Germany) and the hydrophilic test compound caffeine (1 mg/ml in PBS) was prepared and spiked with 2,4,6,7-$^{3}$H-testosterone (100 Ci/mmol; Amersham, Freiburg, Germany) or 1-methyl-$^{14}$C-caffeine (100 Ci/mmol; PerkinElmer, Waltham, MA, USA) to achieve a total radioactivity of 2 µCi/ml. The permeation experiments were performed using Franz diffusion cells (Fa. Gauer, Puettling, Germany). After mounting the skin equivalents onto the Franz cells, 110 µl spiked testosterone and caffeine solution were applied topically and 500 µl of the receptor fluid was sampled every 30 min for up to 6 h. The total amount of permeated testosterone and caffeine was quantified using radiochemical detection (HIDEX 300 SL, HIDEX, Turku, Finland). The permeation rate of testosterone and caffeine was calculated as the apparent permeability coefficient ($P_{app}$).

### 3.2.10. Lucifer yellow assay

10 µl Lucifer yellow solution (1 mM; Sigma-Aldrich, Munich, Germany) was applied onto the skin equivalents and incubated for 6 h at 37°C. Subsequently, the skin equivalents were embedded in tissue freezing medium (Leica Biosystems, Nussloch, Germany), shock-frozen in liquid nitrogen and cut into 7 µm sections using a Leica CM1510 S cryotome (Leica Biosystems, Nussloch, Germany). Skin sections were then analysed by fluorescence microscopy (BZ-8000; Keyence, Neu-Isenburg, Germany).

### 3.2.11. Stratum corneum lipid analyses

#### 3.2.11.1. Stratum corneum (SC) isolation for lipid analysis

The skin equivalents were placed on a filter paper (Schleicher&Schüll, Dassel, Germany) soaked with 0.25% trypsin in PBS (Sigma-Aldrich, Munich, Germany). After 4h of incubation at 37°C (CO2 incubator HERAcell 240i; Heraeus, Hanau, Germany), SC was peeled off and washed with sterile water to remove any remaining keratinocytes. Afterwards, SC sheets were vacuum-dried using vacuum concentrator (Savant SpeedVac Plus; Thermo Scientific, Schwerte, Germany), aerated with nitrogen to avoid oxidative processes and stored at -20°C. The lipid organization was studied by infrared spectroscopy and skin lipid profile was determined by high performance thin layer chromatography (Vavrova et al., 2014, Wallmeyer et al., 2015).

### 3.2.11.2. Lipid analysis of stratum corneum (SC) samples

The lipid analysis was performed by our collaboration partner the lab of Prof. Dr. Kateřina Vávrová (Faculty of Pharmacy in Hradec Kralove, Charles University, Czech Republic), who has also described this method. The organization of the skin lipids was determined by infrared spectroscopy. Skin lipid profiles were determined by high performance thin layer chromatography (Vávrová et al., 2014, Wallmeyer et al., 2015). Due to the completeness of this thesis, however, the methods will be described in the following.

### 3.2.11.3. Infrared spectroscopy stratum corneum (SC) samples

Infrared (IR) spectra of hydrated SC samples were collected on a Nicolet 6700 FTIR spectrometer (Thermo Fisher Scientific, Schwerte, Germany) equipped with a single-reflection MIRacle attenuated total reflectance germanium crystal at 23°C. The spectra were generated by coaddition of 256 scans collected at 2 $cm^{-1}$ resolution and analysed with Bruker OPUS software (Bruker Corp, Billerica, MA). The exact peak positions were determined from second derivative spectra. For each sample, the spectra were recorded at two different areas and averaged.

### 3.2.11.4. High-performance thin layer chromatography (HPTLC) of stratum corneum (SC) lipids

The lipids were analysed on silica gel 60 HPTLC plates (20 × 10 $cm^2$, Merck, Darmstadt, Germany). Lipid standards were either purchased from Merck (Darmstadt, Germany) or synthesized as described previously (Opálka et al., 2015, Kováčik et al., 2016). To generate calibration curves, standard lipids were mixed in ratios that approximately correspond to the composition of human SC (Pullmannová et al., 2014). Standard lipid mixtures were analysed along with the samples on the same HPTLC plate (Table 3.3.).

**Table 3.3.** Calibration curve range of lipid standards used for HPTLC analysis.

| Lipid standard | Calibration curve range [µg] |
|---|---|
| Cholesterol | 0.5 – 10 |
| Lignoceric acid | 0.4 – 8 |
| Ceramide (Cicero et al.) EOS | 0.03 – 0.6 |
| Cer NS | 0.2 – 4 |
| Cer EOP | 0.04 – 0.8 |
| Cer NP | 0.1 – 2 |
| Cer AS | 0.08 – 1.6 |
| Cer AP | 0.08 – 1.6 |
| Cholesterol sulfate | 0.1 – 2.5 |
| GlucosylCer | 0.2 – 5 |
| Sphingomyelin | 0.2 – 5 |
| Phospholipid | 0.5 – 12.5 |
| Cer OS | 0.05 – 2.0 |
| Cer OP | 0.05 – 2.0 |
| Cer OH | 0.05 – 2.0 |

| | |
|---|---|
| ω-OH-fatty acid (32-hydroxydotriacontanoic acid) | 0.2 – 10 |

Lipids were applied on a HPTLC plate under stream of nitrogen using Linomat 5 (Camag, Muttenz, Switzerland). Standard lipids mixtures were analysed along with the samples on the same HPTLC plate. The plates were developed in an automatic developing chamber ADC 2 (Camag, Muttenz, Switzerland) with controlled humidity (33 – 36% RH) and temperature (25 – 27°C). To separate the main barrier lipids (cholesterol, free fatty acids and Cer), the plate was developed first to 85 mm and then to 60 mm with $CHCl_3$/MeOH/acetic acid 190:9:1.5 (v/v/v). To separate barrier lipid precursors (glucosylCer, cholesterol sulfate, phospholipids, sphingomyelin), the plate was developed once to 85 mm using $CHCl_3$/MeOH/acetic acid/$H_2O$ 66:25:6:3 (v/v/v/v). To separate CLE lipids (CerOS, CerOP, CerOH, ω-OH-fatty acid and fatty acids), the plate was developed once to the 85 mm using $CHCl_3$/MeOH/acetic acid 190:9:1.5 (v/v/v). The lipids were visualized by dipping in a derivatization reagent (7.5% $CuSO_4$, 8% $H_3PO_4$, and 10% MeOH in water) for 10s and heating at 160°C for 20min. The lipids were then quantified by densitometry using TLC scanner 3 and VisionCats software (Camag, Muttenz, Switzerland) (Vavrova et al., 2014).

#### 3.2.11.5. Extraction of free and covalent stratum corneum (SC) lipids

The free SC lipids were extracted with 1 mL $CHCl_3$/MeOH 2:1 (v/v) per mg of SC for 1.5h, and then with additional 1mL $CHCl_3$/MeOH 2:1 (v/v) per mg of SC for 1.5h. The lipid extracts were combined, filtered, concentrated under a stream of nitrogen, dried under reduced pressure overnight, and stored at -20°C under argon.

For the analysis of covalent lipids from the corneocyte lipid envelope (CLE), the SC samples, from which the free lipids were extracted were shaken with 1mL 10M NaOH/MeOH 1:9 (v/v) per mg of extracted SC for 15 min and then heated at 60°C for 1h. Then the samples were acidified by 2M HCl (pH ~ 4), shaken, filtered and extracted with $CHCl_3$. The extracts were concentrated under a stream of nitrogen, dried under reduced pressure overnight, and stored at -20°C under argon.

### 3.2.12. DigiWest analysis

This description of the DigiWest® protein profiling procedure as well as its realization was conducted by Dr. Gerrit Erdmann from NMI TT Pharmaservices, as described previously (Treindl et al., 2016, Jevtić et al., 2020). In brief, cell pellets were directly lysed in lithium dodecyl sulfate Buffer containing 212 mM Tris HCL, 282 mM Tris base, 4% LDS(w/v), 1.01 mM EDTA and supplemented with 50mM DTT (from NuPage Sample Reducing Reagent, Invitrogen, Carlsbad USA). Protein concentration was determined using the 660 nm assay

with ionic detergent compaitibilty reagent IDCR (Invitrogen, Carlsbad USA). according to manufactures protocol. Subsequently, SDS-PAGE and Western blotting onto PVDF membranes was performed using the NuPAGE system (Invitrogen, Carlsbad USA) loading 15µg total protein per sample and blots were then washed in PBST. Proteins were biotinylated directly on the membrane using NHS-PEG12-Biotin and membranes were washed in PBST afterwards and dried. Each sample lane was cut into 96 size fractions of 0.5 mm each and transferred to a distinct well of 96-well multitier plate. Proteins were eluted from the membrane strip using elution buffer (8 M urea, 1% Triton-X100 in 100 mM Tris-HCl pH 9.5). Eluted proteins from each molecular weight fraction were loaded onto one distinct color of neutravidin coated MagPlex beads (Luminex, Austin USA). Beads from four lanes (4x96 Bead IDs) were pooled afterwards.

Aliquots of DigiWest bead mixes were transfered into 96 well plates containing assay buffer (Blocking Reagent for ELISA (Roche, Basel Schweiz via Sigma Aldrich/Merck, Darmstadt Germany) supplemented with 0.2% milk powder, 0.05% Tween-20 and 0.02% sodium azide) and subsequently incubated with a primary antibody overnight. Bead mixes were washed with PBST, and a Phycoerythrin-labelled secondary antibody was added. Beads were washed twice, and assays were run on a Luminex FlexMAP 3D device. A total of 124 different antibodies and controls were investigated (see Appendix Table A1). Antibody specific signals were quantified using the DigiWest data analysis tool (Treindl et al., 2016).

For clustering, ratios were calculated between three different donors of the skin equivalents with and without fibroblasts followed by log2 transformation. Hierarchical clustering (HCL) was performed on the log2 transformed ratios using MeV 4.9.0 software used (Saeed et al., 2006).

### 3.2.13. Isolation and characterization of extracellular vesicles (EVs)

#### 3.2.13.1. Isolation of extracellular vesicles (EVs) from fibroblast condition medium

To elucidate the characteristics of the EVs, the EVs were isolated from conditioned medium by several ultracentrifugation and filtration steps. Briefly, conditioned medium was centrifuged at 300 x g for 10min at 4$^{o}$C by using Centrifuge, Megafuge 1.0 R (Heraeus, Hanau, Germany) to pellet the cells and filtered through a vacuum-connected 0.22 µm filter (TPP, Melbourn, UK) on top of a sterile bottle, using a vacuum. Supernatant was centrifuged at 10,000 x g for 30min at 4$^{o}$C using Avanti J-26 S XP centrifuge (Beckman Coulter, Brea, CA, USA) and filtered through the 0.22 µm filter again and finally for 100,000 x g for 90min at 4$^{o}$C using an Beckman Coulter ultracentrifuge with type 70 Ti rotor (Beckman Coulter, Brea, CA, USA). The pellet was washed in PBS and re-centrifuged for 100,000 x g for 90 min at 4$^{o}$C before being re-suspended in 200 µl of sterile PBS and stored at -80$^{o}$C.

### 3.2.13.2. Protein concentration of EVs

Total EVs lysate isolated from the conditioned medium was prepared to determine the total protein concentration using the bicinchoninic acid (BCA) protein assay kit (Thermo Scientific, Schwerte, Germany) according to the manufacturer's instructions. Briefly, bovine serum albumin (BSA) standards, included in the kit, were diluted with PBS into the desired concentrations (250 µg / mL, 150 µg / mL, 50 µg / mL, 25 µg / mL, 5 µg / mL and 0 µg / mL). A working solution was then prepared by mixing 50 parts of BCA Reagent A with 1 part of BCA Reagent B. After this, duplicate 25 µL aliquots of each standard or sample were transferred into individual wells of a 96 well microplate (TPP, Melbourn, UK) prior to addition of 200 µL working solution into each well and incubation for 30 min at 60ºC. The plate was then cooled at room temperature and the absorbance was measured at 562 nm on a microplate spectrophotometer FLUOstar Optima (BMG Labtech, Ortenberg, Germany). A standard curve was used to determine the protein concentration of each sample.

### 3.2.13.3. Annexin V/Propidium Iodide (PI) staining

To exclude any potential apoptotic effects of fibroblasts on EVs composition, an Annexin V/PI staining was performed. Annexin V binds to phosphatidylserine residues that appear on the cell surface as an early event in apoptosis. PI, in contrast, is dye that is normally impermeable for the cell membrane of viable cells but intercalates with the DNA of damaged cells. On day 5 of cultivation, fibroblasts were collected for Annexin V/PI staining at the same time as condition medium was collected for EVs isolation. Fibroblasts were detached and centrifuged (300 x g for 5 min). As a positive control, fibroblasts were treated with 10% DMSO. Subsequently, fibroblasts were resuspended in binding buffer (PBS + 2mM EDTA + 0.5% BSA). After an additional centrifugation, 5 µl Annexin V-FITC in 195 µl binding buffer were added and cells were incubated for 10 min at 4°C. Fibroblasts were washed, centrifuged and again resuspended in binding buffer. Prior to analysis, 10 µl PI was added. Cells were assessed via flow cytometry with FACSCalibur (BD, New Jersey, US). After excluding debris by scatter gating, cells were gated for the two fluorophores Annexin V-FITC (FL1) and PI (FL2). Data were analysed using WinMDI software (Version 2.8).

### 3.2.13.4. Nanoparticle tracing analysis (NTA)

Nanoparticle tracking analysis (NTA) is an approach that can measure the size and calculate the concentration of particles in a liquid (Filipe et al., 2010, Gardiner et al., 2013). A volume of 10 µL of EVs suspension was diluted into 450 µL of PBS to make a total volume of 500 µL in a 1 mL tube (Eppendorf, Hamburg, Germany). The EVs suspension then was loaded into the NanoSight NS500 sample chamber (Malvern, Worcestershire, UK) which was subsequently

illuminated by a laser source. The EVs were tracked and analysed by a high-resolution camera and accompanying NTA 3.0 0064 software. The parameters established were optimal for exosome analysis, specifically, a camera level setting of 7; the number of captures was set to 3; capture duration was set at 30 seconds; and a detection threshold set to 2.

#### 3.2.13.5. Transmission electron microscopy (TEM) analysis of EVs

The occurrence of EVs was confirmed by TEM. For TEM analysis we used the scanning electron microscope Hitachi SU 8030 in TEM mode (Hitachi Ltd., Tokyo, Japan). Samples were prepared using the protocol from Rutter and Innes 2016 (Rutter and Innes 2016), without glow discharging grids and replacing uranyl acetate by Uranlyess (Science Services GmbH, Munich, Germany). Briefly, formvar and carbon coated copper grid (Polyscience, Hirschberg, Germany) was placed on Whitman filter paper (Schleicher&Schüll, Dassel, Germany). By using a pipette (Eppendorf, Hamburg, DE), 5 µL of EVs sample was placed on 300 mesh formvar and carbon coated copper grids and incubated 10 min. The grid was gently picked up with fine forceps and gently touched edge of grid to Whitman filter paper to wick off excess solution. The grid was then negatively stained, pipetting 100 µL 2% Uranyless (Science Services GmbH, Munich, Germany) across the grid surface. Fluid excesses were carefully blotted using Kimwipe and the grids dried overnight in a desiccator. Imaging was performed using 30 kV acceleration voltage.

### 3.2.14. Statistical analysis

Statistical testing was performed using GraphPad Prism software (GraphPad Software, La Jolla, CA). The data were presented as the means ± standard error of the mean.

For the skin equivalents with and without fibroblasts, significance was determined with a paired Student's t-test, *p≤0.05, **p≤0.01.

Statistical analysis was performed using a paired Student’s t-test for direct comparison of the control equivalents with type II equivalents since the same cells donors were used for both approaches and a unpaired student’s t-test for comparison of the control equivalent with type III equivalents since different donors were used for these two approaches , *p≤0.05, **p≤0.01.

# 4. RESULTS

## 4.1. Histological analysis of the skin equivalents with and without dermal fibroblasts

As on of the first aims of this thesis was fundamental understanding of the impact of the cellular crosstalk between keratinocytes and fibroblasts on the skin differentiation, skin homeostasis and skin barrier formation, human-based *in vitro* three-dimensional (3D) skin equivalents with and without fibroblasts were cultured. After the cultivation of the skin equivalents with and without fibroblasts for 14 days, firstly a histological analysis was performed. Histological analysis consistently demonstrated that skin equivalents with fibroblasts (control) developed a fully differentiated epidermis (Fig. 4.1. A), whereas the skin equivalents without fibroblasts were characterized by a more disorganised epidermal stratification and a significant epidermal thinning ($p = 0.0130$) (Fig. 4.1. B) (Jevtić et al., 2020).

Ultrahistological analysis performed by Dr.rer.nat. Sabine Kaessmeyer further showed that the control equivalents expressed basal keratinocytes with a polygonal to prismatic cell shape (Fig. 4.1. C) and a stratum spinosum that consisted of several spinous cell layers. In the skin equivalents without fibroblasts, the keratinocytes of all strata exhibited an unphysiological cell shape and were thinner and elongated. Furthermore, the stratum basale and stratum spinosum were not clearly distinguishable, as all cells showed similar shapes (Fig. 4.1. D). Additionally, in the skin equivalents without fibroblasts, only few mitochondria and rough endoplasmic reticulum were observed within the keratinocytes compared to significantly higher expression in the control skin equivalents. Both types of skin equivalents expressed keratohyalin granules in the upper cell layers, indicating the stratum granulosum. While the stratum corneum (SC) of the normal skin equivalents mainly consisted of cornified cells (Fig. 4.1. E), the SC of the skin equivalents without fibroblasts was not fully differentiated and contained keratinized and non-keratinized cells (Fig. 4.1. F) (Jevtić et al., 2020).

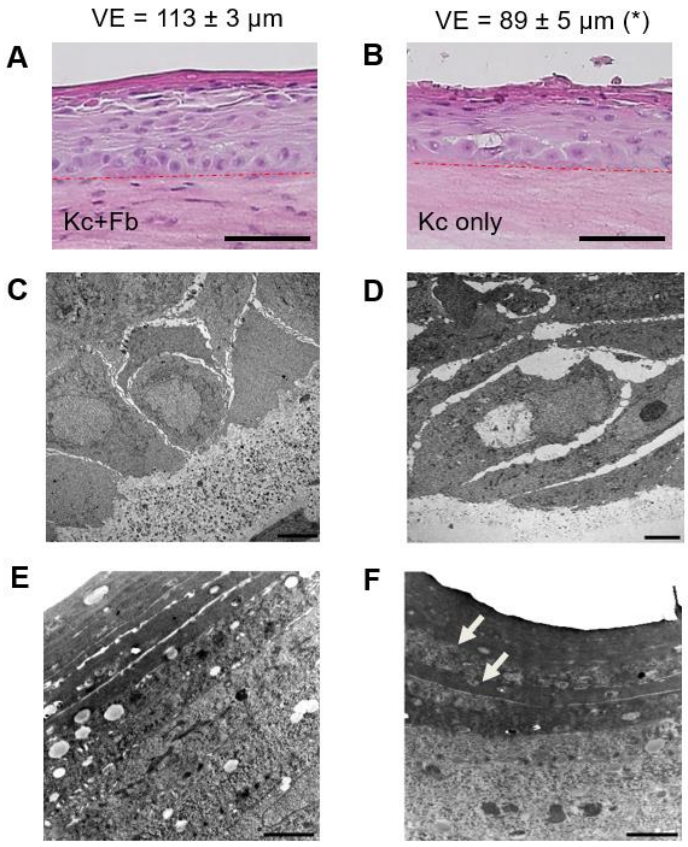


**Fig. 4.1. Histological analysis of the skin equivalents with and without fibroblasts**

Representative histologic staining of skin equivalents **(A)** with and **(B)** without fibroblasts and thickness of viable epidermis (VE). Values are given as mean ± SEM, n = 8. Asterisk indicates statistically significant values, *p ≤ 0.05. Ultrastructure of **(C, E)** skin equivalents with fibroblasts and **(D, F)** skin equivalents without fibroblasts. (C) Basal keratinocytes with polygonal to prismatic cell shapes and (D) thin, elongated basal cells in the stratum basale. **(E)** Corneocytes with cornified envelope and **(F)** undifferentiated keratinocytes (arrows) between corneocytes within the stratum corneum. **(A, B)** Scale bar: 100 µm, (C, D) Scale bar: 5 µm, **(E, F)** Scale bar: 2 µm. SEM = standard error of the mean; Kc+Fb = skin equivalents with fibroblasts; Kc only = skin equivalents without fibroblasts (Jevtić et al., 2020).

## 4.2. Expression of skin barrier and tight junction proteins in the skin equivalents with and without dermal fibroblasts

To determine the temporal influence of fibroblasts on the skin differentiation, investigation of the expression of characteristic skin differentiation and tight junction proteins on gene and protein levels at day 4, 7, 10, 12 and 14 of tissue cultivation was performed. Skin equivalents devoid of fibroblasts showed a reduced filaggrin (FLG) expression between day 4 to 14 ($p = 0.0568$) compared to control skin equivalents (Fig. 4.2. A, B). These findings are in line with the immunofluorescence (IF) staining (Fig. 4.2. C) (Jevtić et al., 2020).

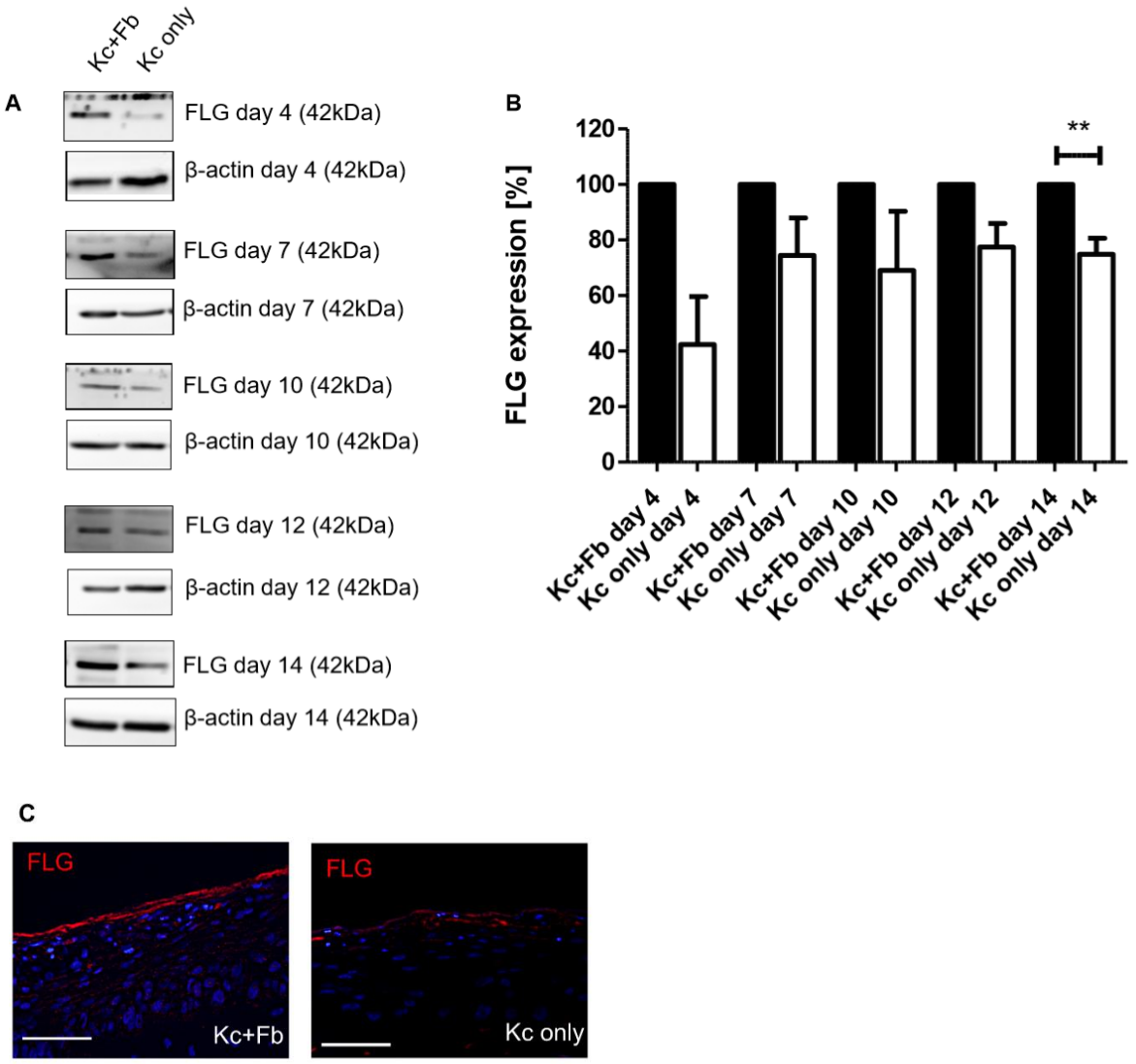


**Figure 4.2. Protein expression and immunofluorescence staining of filaggrin (FLG)**

**(A)** Western blots and **(B)** relative protein expression semi-quantified via densitometry of filaggrin (FLG) in the skin equivalents with and without fibroblasts at day 4, 7, 10, 12 and 14. The expression levels in the control skin equivalents were set to 100%. Values are given as mean ± SEM, n = 3-8. Asterisk indicates statistically significant values, **p ≤ 0.01. Representative immunostaining against **(C)** filaggrin (FLG) in the skin equivalents with and without fibroblasts after 14 days of cultivation, n = 3. Scale bar = 100 µm. Exposure time: blue channel 1/55 s and red channel 1/5 s. Kc+Fb = skin equivalents with fibroblasts; Kc only = skin equivalents without fibroblasts (Jevtić et al., 2020).

Involucrin (IVL), a late-stage differentiation marker, was not detected in both skin equivalents with and without fibroblasts between day 4 to 10 of tissue cultivation; however, a compensatory up-regulation was detected from day 12 onwards (Fig. 4.3 A, B). IF staining further indicates an unphysiological IVL expression pattern in deeper epidermal layers (Fig. 4.1.3 C) (Jevtić et al., 2020).

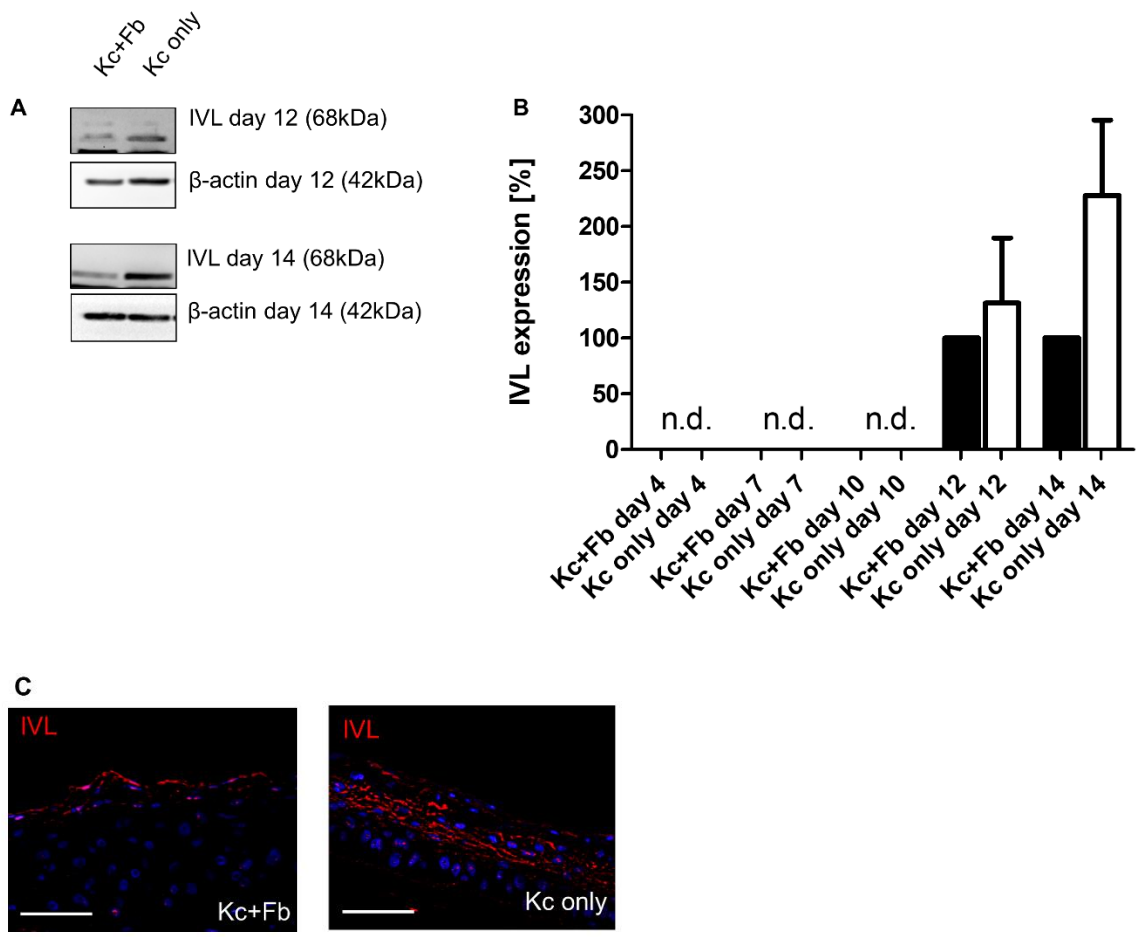


**Figure 4.3. Protein expression and immunofluorescence staining of involucrin (IVL)**

**(A)** Western blots and **(B)** relative protein expression semi-quantified via densitometry of involucrin (IVL) in the skin equivalents with and without fibroblasts at day 4, 7, 10, 12 and 14. The expression levels in the control skin equivalents were set to 100%. Values are given as mean ± SEM, n = 3-8. Representative immunostaining against **(C)** involucrin (IVL), in the skin equivalents with and without fibroblasts after 14 days of cultivation, n = 3. Scale bar = 100 µm. Exposure time: blue channel 1/55 s and red channel 1/5 s. Kc+Fb = skin equivalents with fibroblasts; Kc only = skin equivalents without fibroblasts; n.d. = not detected (Jevtić et al., 2020).

Further, for the tight junction protein claudin-1 (CLDN-1), a clear trend towards decreased expression was observed at day 4 ($p = 0.3184$) and 7 ($p = 0.2317$) when fibroblasts were missing, whereas an increased CLDN-1 expression was found from day 10 onwards (Fig. 4.4) (Jevtić et al., 2020).

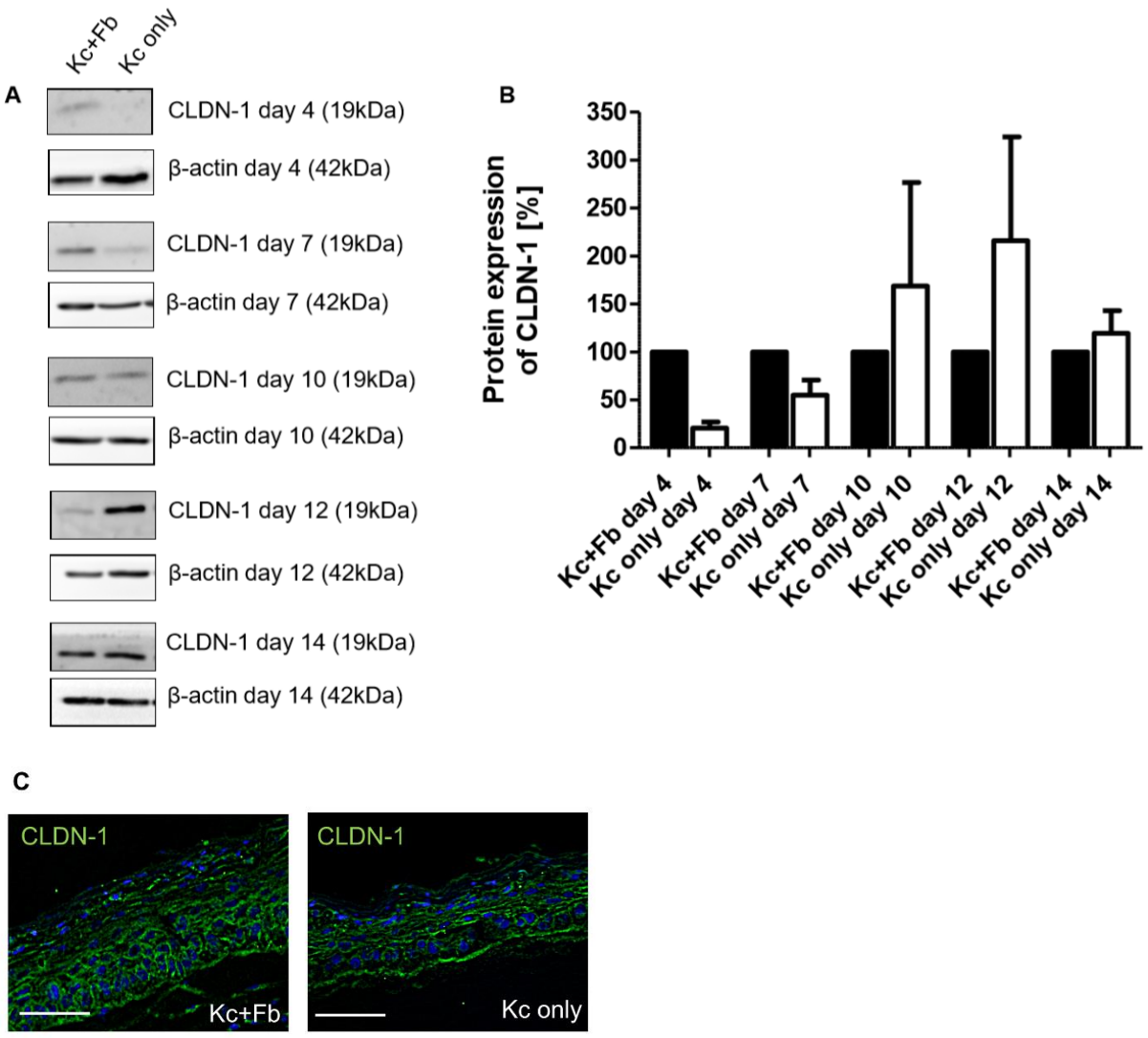


**Figure 4.4. Protein expression and immunofluorescence staining of claudine-1 (CLDN-1)**

**(A)** Western blot and **(B)** relative protein expression semi-quantified via densitometry of claudin-1 (CLDN-1) of the skin equivalents with and without fibroblasts at the day 4, 7, 10, 12 and 14. Values are given as mean ± SEM, n = 3 - 8. The expression levels in the control skin equivalents were set 100%. Representative immunostaining against **(C)** claudin (CLDN-1), in the skin equivalents with and without fibroblasts after 14 days of cultivation, n = 3. Scale bar = 100 µm. Exposure time: blue channel 1/55 s and green channel 1/10 s. Kc+Fb = skin equivalents with fibroblasts; Kc only = skin equivalents without fibroblasts, (Jevtić et al., 2020).

Lastly, for the tight junction protein occludin (OCLN), no major differences were observed in protein level expression and in its distribution within the epidermis (Fig. 4.5.) (Jevtić et al., 2020).

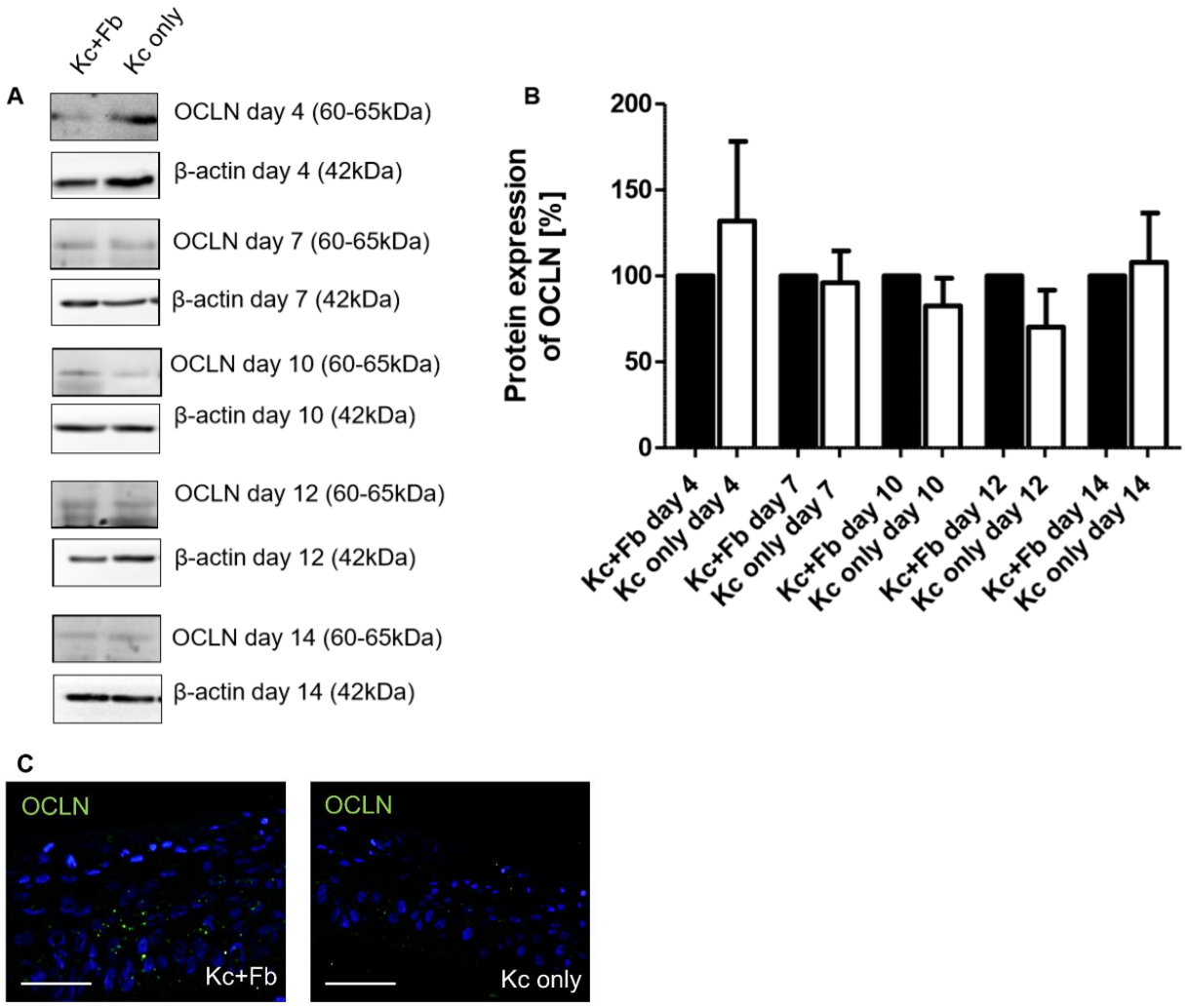


**Figure 4.5. Protein expression and immunofluorescence staining of occludin (OCLN)**

**(A)** Western blot and **(B)** relative protein expression semi-quantified via densitometry of occludin (OCLN) of the skin equivalents with and without fibroblasts at the day 4, 7, 10, 12 and 14. The expression levels in the control skin equivalents were set 100%. Values are given as mean ± SEM, n = 3 - 8. Representative immunostaining against **(C)** occludin (OCLN), in the skin equivalents with and without fibroblasts after 14 days of cultivation, n = 3. Scale bar = 100 µm. Exposure time: blue channel 1/55 s and green channel 1/10 s. Kc+Fb = skin equivalents with fibroblasts; Kc only = skin equivalents without fibroblasts.

Corresponding regulations at the mRNA levels are presented in Fig. 4.6. and they are supporting protein expression levels of cornified envelope proteins FLG and IVL and tight junction proteins CLDN-1 and OCLN (Jevtić et al., 2020).

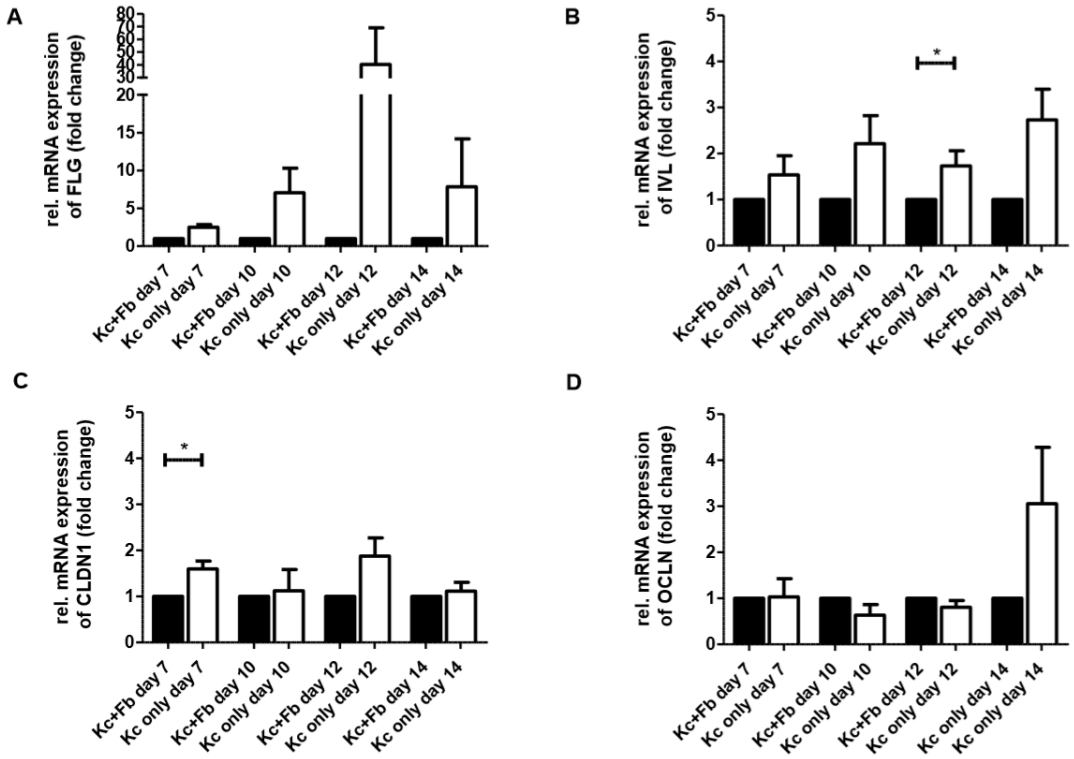


**Figure 4.6. Representative mRNA expression of cornified envelope and tight junction proteins**

Relative mRNA expression of **(A)** filaggrin (*FLG*), **(B)** involucrin (*IVL*), **(C)** claudin-1 (*CLDN1*) and **(D)** occludin (*OCLN*) of the skin equivalents with and without fibroblasts at the day 7, 10, 12 and 14. The expression levels in the control skin equivalents were set to 1. Values are given as mean ± SEM, n = 4 - 7. Asterisk indicates statistically significant values, $*p \leq 0.05$. Kc+Fb = skin equivalents with fibroblasts; Kc only = skin equivalents without fibroblasts (Jevtić et al., 2020).

Additionally, immunofluorescence staining against Ki67 – cells proliferation marker, was performed to determine influence of fibroblasts on proliferation of the cells in the stratum basale. Interestingly, lower expression of Ki67 was observed in skin equivalents without fibroblasts as assessed by IF staining (Fig. 4.7) (Jevtić et al., 2020).

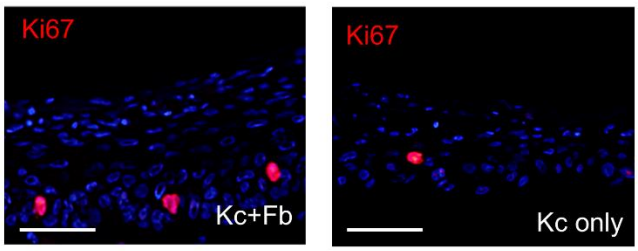


**Figure 4.7. Representative immunostaining against Ki67**

Representative immunostaining against Ki67, in the skin equivalents with and without fibroblasts after 14 days of cultivation, n = 3. Scale bar = 100 µm. Exposure time: blue channel 1/55 s and and red channel 1/5 s. Kc+Fb = skin equivalents with fibroblasts; Kc only = skin equivalents without fibroblasts (Jevtić et al., 2020).

## 4.3. Skin permeability studies in the skin equivalents with and without dermal fibroblasts

The skin barrier function of the skin equivalents with and without fibroblasts was determined by skin permeability studies using radioactively-labelled compounds. Notably, the absence of fibroblasts in the skin equivalents resulted in an increased skin permeability for the hydrophilic model compound caffeine (Fig. 4.8. A) and the lipophilic model drug testosterone (Fig. 4.8. B) compared to the control equivalents. To assess whether this difference derives from the different epidermal thickness of the skin equivalents without fibroblasts, we also investigated the skin absorption pattern of the dye Lucifer yellow. In the skin equivalents without fibroblasts, Lucifer yellow extensively penetrated through the stratum corneum (SC) into the viable epidermal layers, whereas for the normal skin equivalents, significantly less penetration was observed (Fig. 4.8. C, D) (Jevtić et al., 2020).

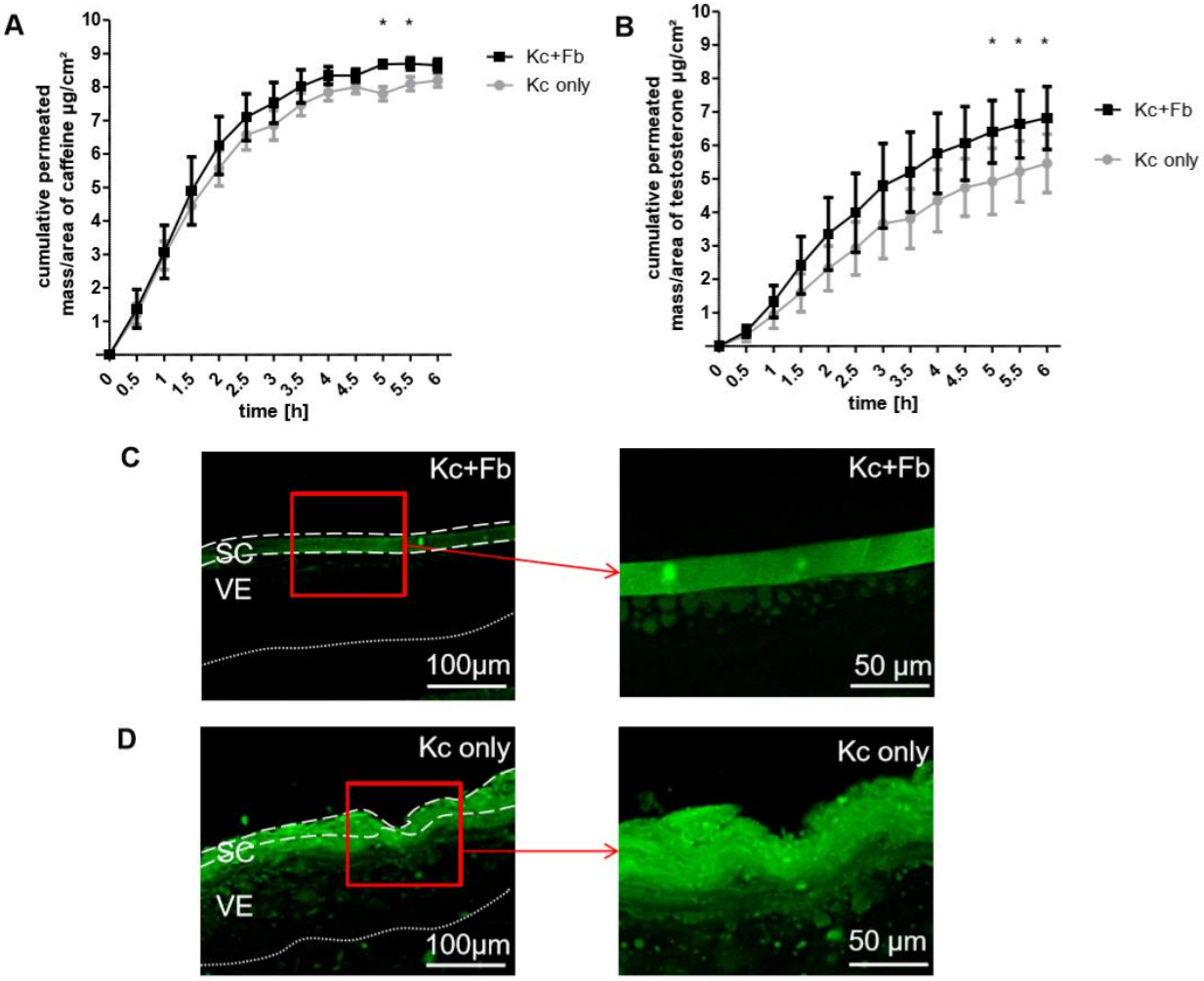


**Figure 4.8. Skin barrier function in the skin equivalents with and without fibroblasts**

Skin permeation profile of **(A)** caffeine and **(B)** testosterone in skin equivalents (■) with and (●) without fibroblasts. Values are given as a mean ± SEM, n = 4. Asterisks indicate statistically significant values, *p ≤ 0.05. Representative images of Lucifer yellow penetration in skin equivalents **(C)** with and **(D)**

without fibroblasts after topical exposure for 6 h, n = 3. Exposure time: green channel 1/12 s. SC = stratum corneum, VE = viable epidermis, Kc+Fb = skin equivalents with fibroblasts, Kc only = skin equivalents without fibroblasts (Jevtić et al., 2020).

## 4.4. Stratum corneum (SC) lipid analysis of the skin equivalents with and without fibroblasts

The isolated SC lipid analysis was probed by our collaboration partner the lab of Prof. Dr. Kateřina Vávrová by FTIR to assess skin lipid and protein organisation. The fibroblast presence apparently improved the lipid chain order as indicated by slightly lower methylene stretching symmetric stretching wavenumber (Fig. 4.9. A), although statistical significance hasn't been reached. The increased ratio of the methylene symmetric stretching and Amide I band intensities suggest an increased relative lipid content in the skin equivalents with fibroblasts over those without fibroblasts (Fig. 4.9. B) (Jevtić et al., 2020).

HPTLC analysis of extracted SC lipids revealed that both types of skin equivalents contained all major barrier lipids (ceramides, free fatty acids and cholesterol) (Fig. 4.9. C, F and 4.10.), but also a significant amount of lipid precursors (sphingomyelin, glucosylceramides, and phospholipids) (Fig. 4.9. G, I) (Jevtić et al., 2020).

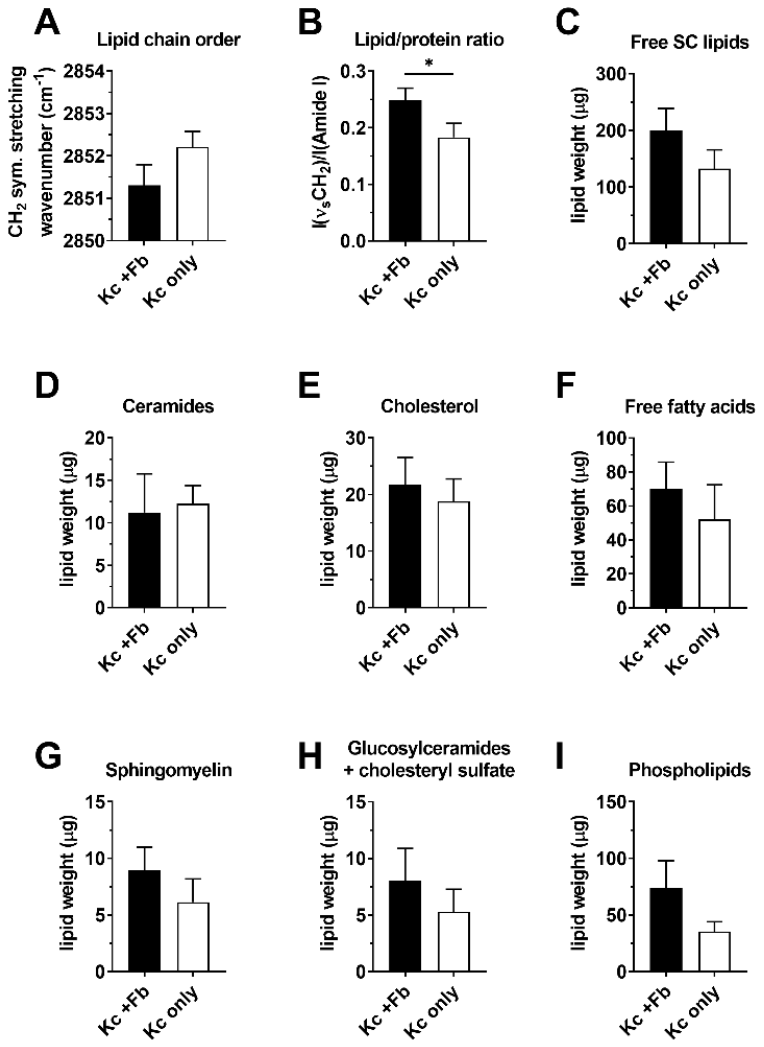


**Figure 4.9. SC lipids organisation and composition in the skin equivalents with and without fibroblasts**

Organisation and composition of the SC lipids in skin equivalents with and without fibroblasts: lipid chain order **(A)**, relative lipid content **(B),** total extractable lipids **(C)**, total ceramides **(D)**, cholesterol **(E)**, free fatty acids **(F)** and barrier lipid precursors **(G-I)** Values are given as means ± SEM, n = 5. Asterisk indicates statistically significant differences at *$p \leq 0.05$. Kc+Fb = skin equivalents with fibroblasts, Kc only = skin equivalents without fibroblasts (Jevtić et al., 2020).

The skin equivalents with fibroblasts apparently synthesize more lipids compared to the equivalents without fibroblasts, but these differences were not significant. No changes were observed in the individual ceramide subclasses (Fig. 4.10.) (Jevtić et al., 2020).

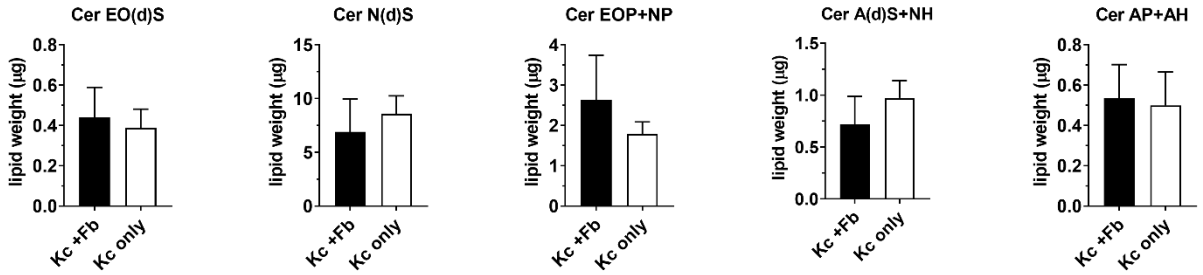


**Figure 4.10. SC ceramide subclasses analysis in the skin equivalents with and without fibroblasts**

HPTLC quantification of SC ceramide subclasses. Results are shown as mean ± SEM; n = 5. Kc+Fb = skin equivalents with fibroblasts; Kc only = skin equivalents without fibroblasts (Jevtić et al., 2020).

## 4.5. Investigation of signalling pathways in the skin equivalents with and without fibroblasts

A bead-based DigiWest analysis, a high-throughput Western blot approach, was performed by Dr. Gerrit Erdmann from NMI TT Pharmaservices to determine a more comprehensive analysis of the impact of fibroblasts on the epidermal-dermal crosstalk. Hierarchical clustering (HCL) analysis showed the upregulation (yellow) or downregulation (blue) of 96 proteins in the skin equivalents without fibroblasts compared to control skin equivalents (Fig. 4.11.).

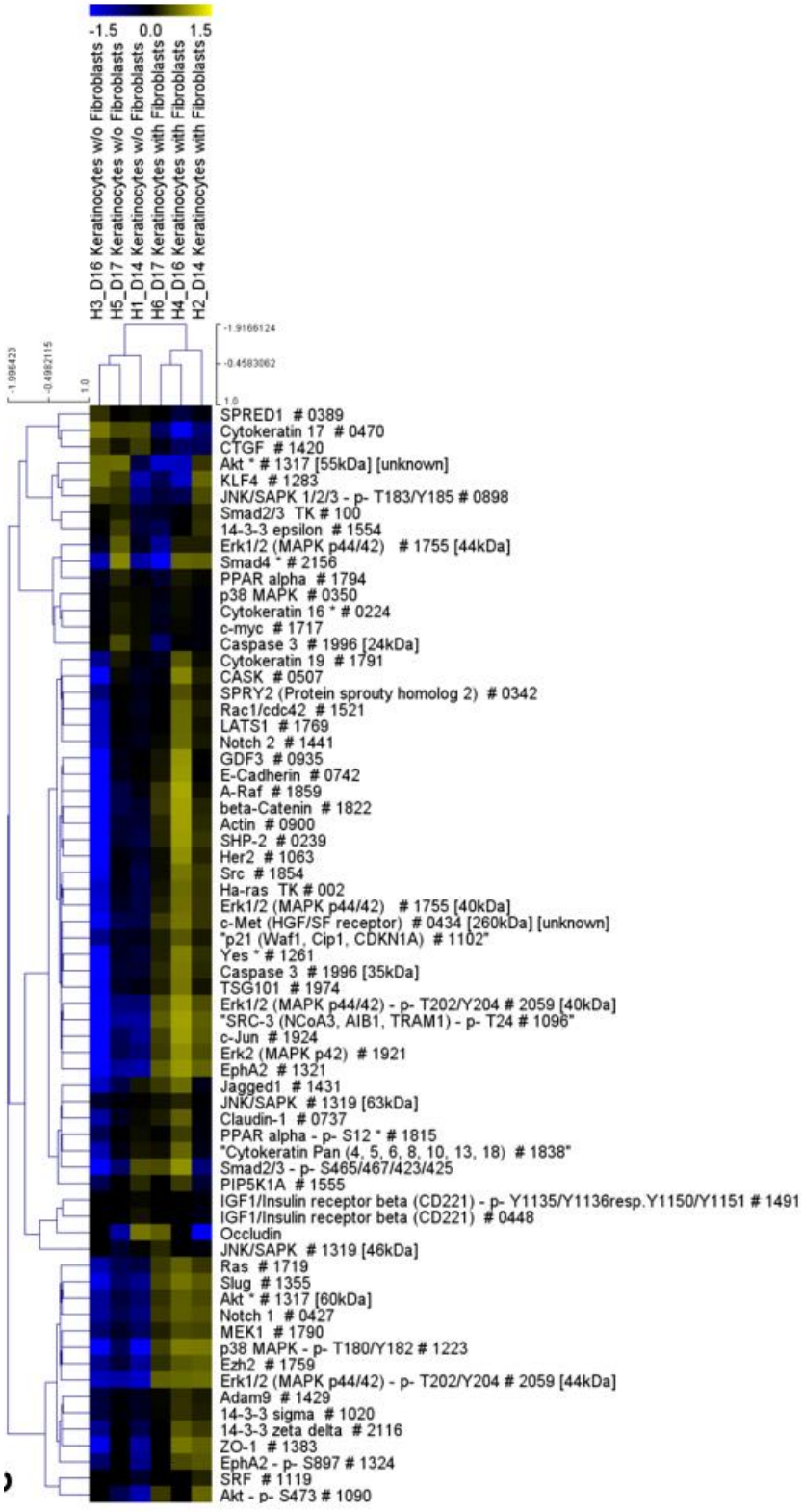


**Figure 4.11. High-throughput analysis of the skin equivalents with and without fibroblasts**

For hierarchical clustering (HCL), ratios were calculated between three different donors of the skin equivalents with and without fibroblasts followed by log2 transformation. HCL was performed on the log2 transformed ratios using MeV 4.9.0 software, n = 3. w/o = without (Jevtić et al., 2020).

Most interestingly, the expression levels of Ras (p = 0.0169), MEK1 (p = 0.0441) and phosphorylated ERK 1/2 (40 kDa (p = 0.0067) and 44 kDa (p = 0.0167)) (Fig. 4.12. A) participants of Ras/Raf/MEK/ERK signalling pathway, were significantly reduced in the skin equivalents devoid of fibroblasts. Furthermore, a significantly decreased expression of Notch1 (p = 0.0155), Slug (p = 0.0375) and Ezh2 (p = 0.0278). Also, a clear trend for decreased protein expression was detected for c-Jun (p = 0.0664) and p38 MAPK-p T180/Y182 (p = 0.0762) but statistical significance hasn't been reached (Fig. 4.12. B). Similarly, a trend for an increased expression of CK17 (p = 0.0732) was found in the absence of fibroblasts (Fig. 4.12. C) (Jevtić et al., 2020).

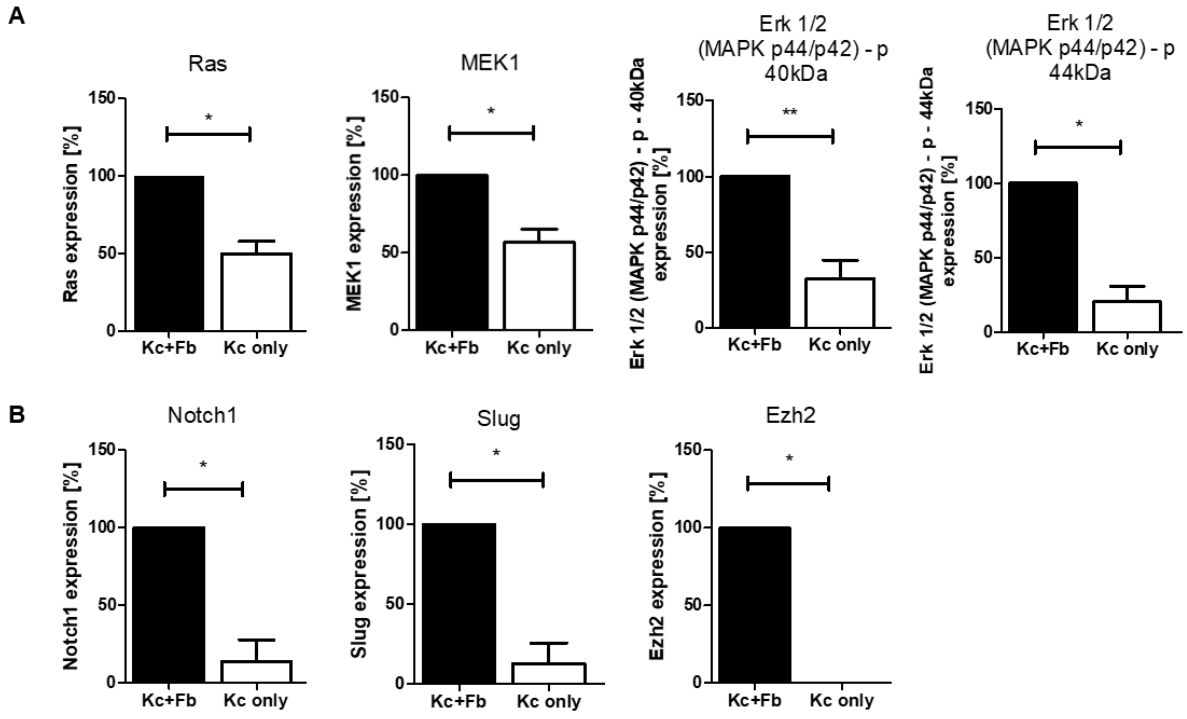


**Figure 4.12. Detailed expression levels of selected proteins for Fig 4.11.**

DigiWest bead-based multiplex WB analysis of skin equivalents with and without fibroblasts after 14 days of cultivation indicates distinct alteration of Ras/Raf/MEK/ERK signaling in skin equivalents without fibroblasts. **(A)** Protein expression levels of Ras, MEK1, Erk 1/2 (MAPK p44/p42) - p - (40 kDa) and Erk 1/2 (MAPK p44/p42) - p - (44 kDa). **(B)** Protein expression levels of Notch1, Slug and Ezh2. The expression levels in the control skin equivalents were set to 100%. Values are given as a mean ± SEM, n = 3. Asterisk indicates statistically significant values, *$p \leq 0.05$ and **$p \leq 0.01$ (Jevtić et al., 2020).

## 4.6. FACS analysis of the dermal fibroblasts

After the idea arose that extracellular vesicles (EVs) might be the possible way of epidermal-dermal crosstalk, fibroblasts-derived EVs were collected with several centrifugation and filtration steps as described in the Material and methods. Firstly it was important to quantify

the percentage of dead cells present in the culture, on day 5 of dermal fibroblasts cultivation, after the condition medium was collected. With FACS analysis of the dermal fibroblasts, we proved that more that 95% of the cells were alive in the culture (Fig. 4.1.12.).

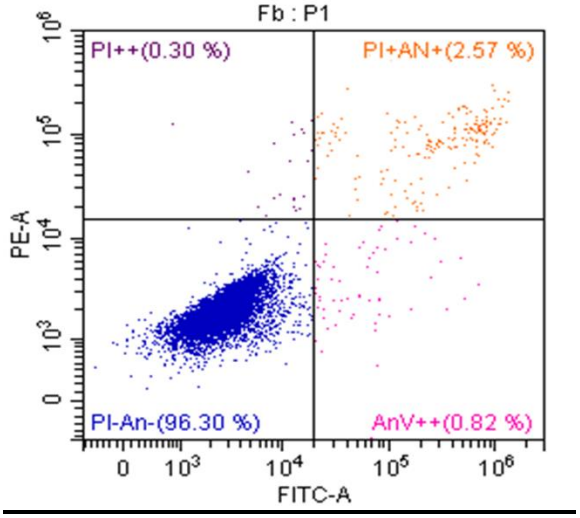


**Figure 4.13. Annexin V/PI staining of the dermal fibroblasts**

Representative Annexin V FITC-A vs. Propidium Iodide-A contour plots of cultured fibroblasts from which condition medium EVs were isolated, n = 2.

## 4.7. Determination of size and morphology of fibroblasts-derived extracellular vesicles (EVs)

To determine the size distribution of fibroblasts-derived EVs, nanoparticle tracking analysis (NTA) was performed. NTA proved the presence of EVs and showed that vast majority of vesicles detected were smaller than 150 nm. Histograms represent the mean of three replicate measurements of the same sample with an average size of 133.5 ± 2.0 nm of fibroblasts derived EVs (Figure 4.14. A).

In addition to the size distribution analysis, we used transmission electron microscopy (TEM) to visualize and to analyse the individual morphology of the content of our EVs samples. The fibroblasts-derived EVs showed round shape and size smaller then 150 nm (Figure 4.14. B).

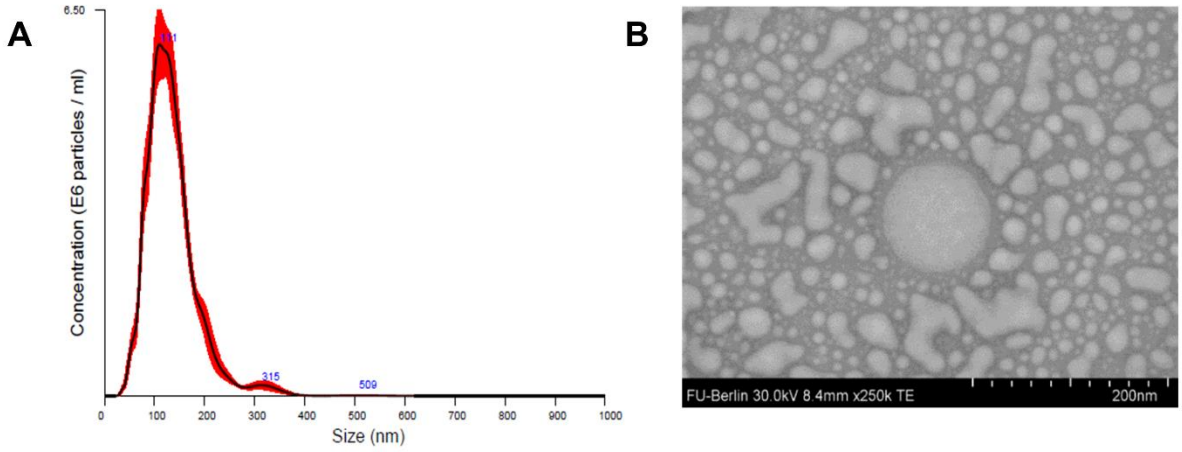


**Figure 4.14. Determination of the size and morphology of extracellular vesicles (EVs)**

**(A)** Representative averaged size/distribution of extracellular vesicles (EVs) obtained by nanoparticle tracking analysis (NTA) derived from fibroblast cell culture medium. Histograms represent the mean of three replicate measurements of the same sample with an average size of 133.5 ± 2.0 nm, n = 2. Red error bars indicate ± SEM **(B)** EVs were negatively stained with 2% uranyl acetate on Formvar/Carbone grids. Transmission electron microscopy (TEM) proved the presence of fibroblasts derived EVs and here we showed their shape and size smaller than 150 nm, n = 1.

## 4.8. Histological analysis of the skin equivalents based on self-assembled extracellular matrix (ECM)

One of the aims of this thesis was development of completely human-based skin equivalents based on primary human fibroblasts-derived ECM with included endothelial cells. For that purpose three types of skin equivalents were generated: i) type I – skin equivalent with a dermal equivalent based on bovine collagen matrix (conventional approach, control model), ii) type II – skin equivalent with a dermal equivalent based on self-assembled ECM containing fibroblasts and HDMEC, and iii) type III – skin equivalents with a dermal equivalent based on self-assembled ECM containing fibroblasts only.

First, a comprehensive histomorphological analysis of the collagen based (control) skin equivalents – type I, skin equivalents based on the self-assembled dermis containing endothelial cells (EC) and fibroblasts – type II and skin equivalents based on the self-assembled dermis containing fibroblasts only – type III was performed. Histological analysis of all three types of skin equivalents stained with hematoxylin and eosin demonstrated that cultured cells were organized into dermal and epidermal tissue compartments, with a well differentiated stratified multi-layered epithelium and a presence of *stratum basale*, *stratum spinosum*, *stratum granulosum*, and finally the *stratum corneum* (Fig. 4.15.). Additionally, the

average thickness of the epidermis of the skin equivalents (measured on 10 different points of each sample) was significantly thinner in type II skin equivalents 54 ± 1 µm (***p ≤ 0.0001), type III skin equivalents 61 ± 3 µm (***p ≤ 0.0001), compared to type I skin equivalents 109 ± 7 µm.

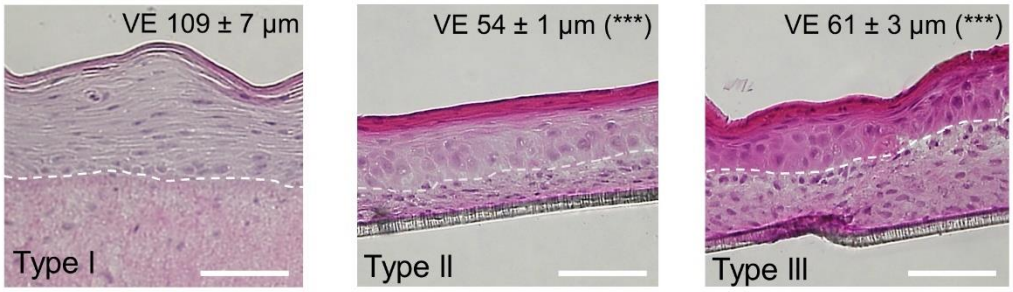


**Figure 4.15. Histological analysis of skin equivalents based on a self-assembled ECM**

Representative hematoxylin and eosin staining with thickness of the viable epidermis (VE) of skin equivalents based on a bovine collagen – type I, skin equivalents based on a self-assembled ECM containing endothelial cells and fibroblasts – type II, and skin equivalents based on a self-assembled ECM with fibroblasts only – type III. Values are given as mean ± SEM, n = 3. Asterisk indicates statistically significant values, ***p ≤ 0.0001. Scale bar = 100 µm.

Ultrastructural analysis, performed by Dr.rer.nat. Sabine Kaessmeyer, of epidermis revealed that the cells shape and layer architecture of type II skin equivalents were closer to those of normal human skin than those of type I or type III skin equivalents. In type II skin equivalents, for example, the cells forming the basal layer were mainly columnar, while the cells of the basal layer in type I and type III skin equivalents were either cuboid or irregular (Fig. 4.16. A). The *stratum spinosum* cells of all skin equivalents formed spinous processes. In the *stratum granulosum*, the cells of all skin types were densely packed and connected by numerous desmosomes. The *stratum corneum* of all types of skin equivalents was characterized by flattened cells with well developed cornified envelope. While in type II skin equivalents nearly all corneocytes where enucleated, in type I and III occasionally nuclei where detected. Keratohyalin granules were found in all investigated skin equivalent types, but more in skin equivalents type II and type III. Intercellularly, a lipid film organized in lamellar lipid bilayers was visible in all skin equivalents.

Interestingly, the presence of hemidesmosomes on the basal side of basal epithelial cells was observed exclusively in type II and III skin equivalents, which is a necessary prerequisite for cohesion between epidermis and dermis in *in vivo* skin. A basement membrane was visible in type II and III skin equivalents, but not in type I equivalents (Fig. 4.16. B).

Only in type II skin equivalents tight junctions (TJs) were regularly detected (Fig. 4.16. C). Moreover, only in type II skin equivalents lamellar bodies with a similar morphology to *in-vivo*-lamellar bodies were present (Fig. 4.16. D).

Furthermore, ultrastructural analysis of the dermal part of the skin equivalents of type II consisted of a densely organized ECM that filled the intercellular spaces. At the ultrastructural level, it became apparent that the ECM consisted of a differentiated network of collagen bundles fibers and fibrils, which surrounded the co-cultured fibroblasts and EC (type II) or the fibroblasts respectively (type III). The type III skin equivalents revealed a similar tissue pattern like type II, however the fibers were arranged slightly looser, less structured and contained vesicles, which is a typical phenomenon of collagen matrix-based skin equivalents. In contrast, the dermal parts of type I skin equivalents showed an irregular mixture of fibroblasts, fibroblasts fragments, numerous vesicles and filaments and fibrils within the homogeneous collagen matrix (Fig. 4.16. B, C, D).

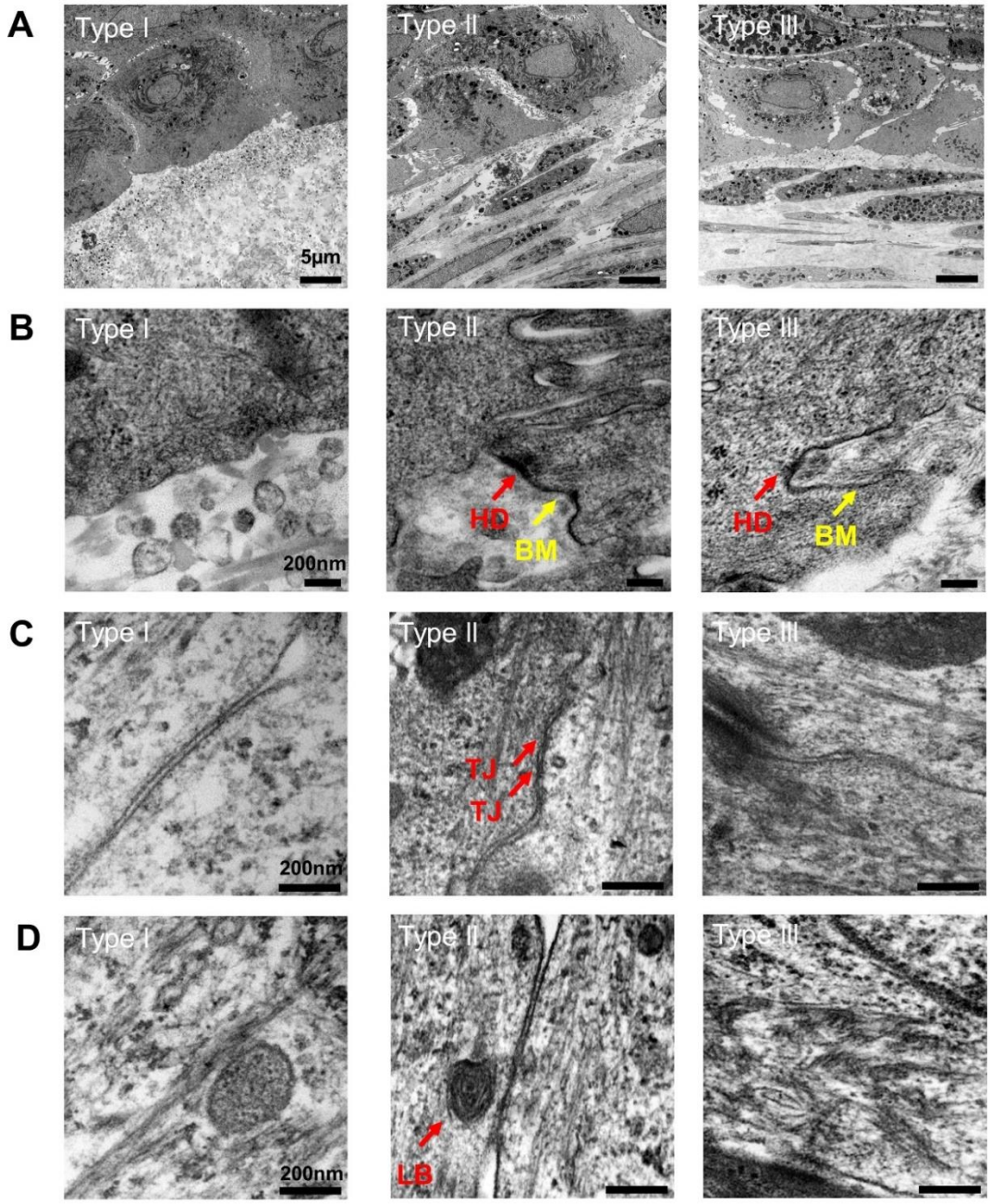


**Figure 4.16. Ultrastructural analysis of skin equivalents based on a self-assembled ECM**

**(A)** Ultrastructural analysis of the skin equivalent type I, type II and type III, n = 3. Scale bar = 5 µm. **(B)** Ultrastructural analysis revealed presence of hemidesmosomes (HD) (red arrow heads) and basement membrane (BM) (yellow arrow heads) in the skin equivalents based on a self-assembled ECM containing endothelial cells and fibroblasts – type II and skin equivalents based on a self-assembled ECM with fibroblasts only – type III, n = 3. Scale bar = 200 nm. **(C)** Tight junctions (TJs) (red arrow heads) connect the neighbouring cells of the *stratum granulosum* in the skin equivalents based on a self-assembled ECM containing endothelial cells and fibroblasts – type II, n = 3. Scale bar = 200 nm. **(D)** In skin equivalents with dermal equivalent consisting of self-assembled ECM by fibroblasts with endothelial cells lamellar bodies (LB) (red arrow heads) are present within the cells of the *stratum granulosum*, n = 3. Scale bar = 200 nm.

## 4.9. Expression of skin barrier and tight junction proteins in the skin equivalents based on self-assembled extracellular matrix (ECM)

To assess the impact of the components and structure of the dermal equivalent on the skin differentiation, the expression of characteristic skin differentiation and tight junction (TJ) proteins on protein and gene levels, as well as expression pattern in all three types of skin equivalents was investigated. Most interestingly, the important skin barrier – filaggrin (FLG) and involucrin (IVL), and TJ proteins – occludin (OCLD) and claudin-1 (CLDN-1) that showed a much stronger and more physiological expression pattern in the skin equivalents with the self-assembled ECM (Fig. 4.17.). Here, an increased expression of IVL was observed in the type II skin equivalents containing endothelial cells (Fig. 4.16.), in line with the IF staining and mRNA levels (Fig. 4.18. and 4.19.). However, statistical significance wasn't reached due to pronounced donor variability. Unexpectedly, a downregulation of IVL was observed in type III equivalents, although this could not be verified at mRNA level (Fig. 4.19.). No differences were observed in the expression of the late stage differentiation marker FLG (Fig. 4.17.).

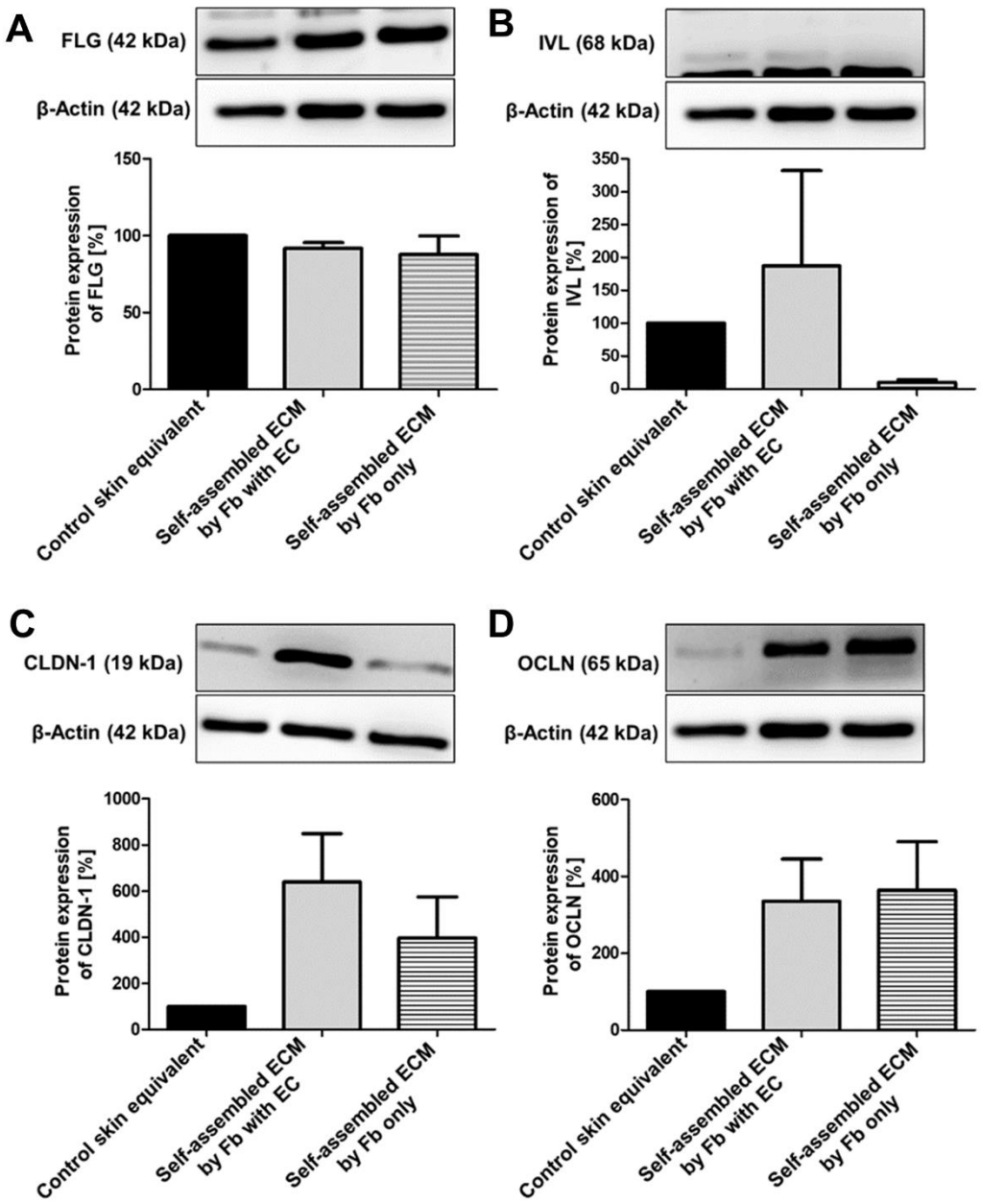


**Figure 4.17. Protein expression levels of cornified envelope and tight junction proteins in the skin equivalents based on a self-assembled ECM**

Representative western blots and relative protein expression semi-quantified via densitometry of important cornified envelope proteins **(A)** filaggrin (FLG) and **(B)** involucrin (IVL) and tight junction proteins **(C)** claudin-1 (CLDN-1) and **(D)** occludin (OCLN) of the skin equivalent with dermal equivalent based on a bovine collagen matrix, control skin equivalent – type I, skin equivalent with dermal equivalent consisting of self-assembled ECM by fibroblasts with endothelial cells – type II, and skin equivalent with a dermal equivalent consisting of self-assembled ECM by fibroblasts only – type III. Values are given as mean ± SEM, n = 3. ECM = extracellular matrix, Fb = fibroblasts, EC = endothelial cells.

A clear trend towards increased expression of TJ proteins CLDN-1 (p=0.0563) and OCLN (p=0.0578) was found in type II and type III equivalents (Fig. 4.17.) in line with gene expression levels (Fig. 4.19.). Whereas the TJ proteins were exclusively found in the *stratum granulosum* in type II and type III skin equivalents, the type I skin equivalents showed strong expression throughout the entire epidermis for CLDN-1 and a very weak expression for OCLD within the *stratum granulosum* (Fig. 4.18.).

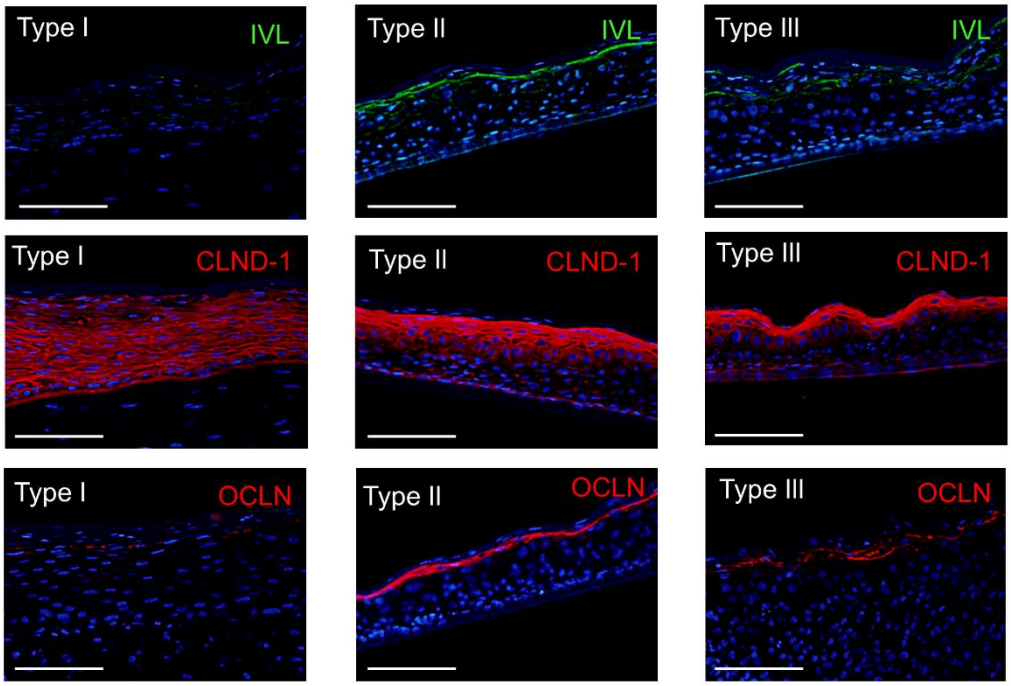


**Figure 4.18. Representative immunofluorescence staining of cornified envelope and tight junction proteins in the skin equivalents based on a self-assembled ECM**

Representative immunostaining against involucrin (IVL), claudin-1 (CLDN-1) and **)** occludin (OCLN) of the skin equivalent with dermal equivalent based on a bovine collagen matrix – type I, skin equivalent with dermal equivalent consisting of self-assembled ECM by fibroblasts with endothelial cells – type II, and skin equivalent with a dermal equivalent consisting of self-assembled ECM by fibroblasts only – type III. Counterstaining of cell nuclei was performed with 4',6'-diamin-2-phenylindol (DAPI). Scale bar = 100 µm. Exposure time: blue channel 1/55 s, green channel 1/10 s and red channel 1/5 s. ECM = extracellular matrix, Fb = fibroblasts, EC = endothelial cells.

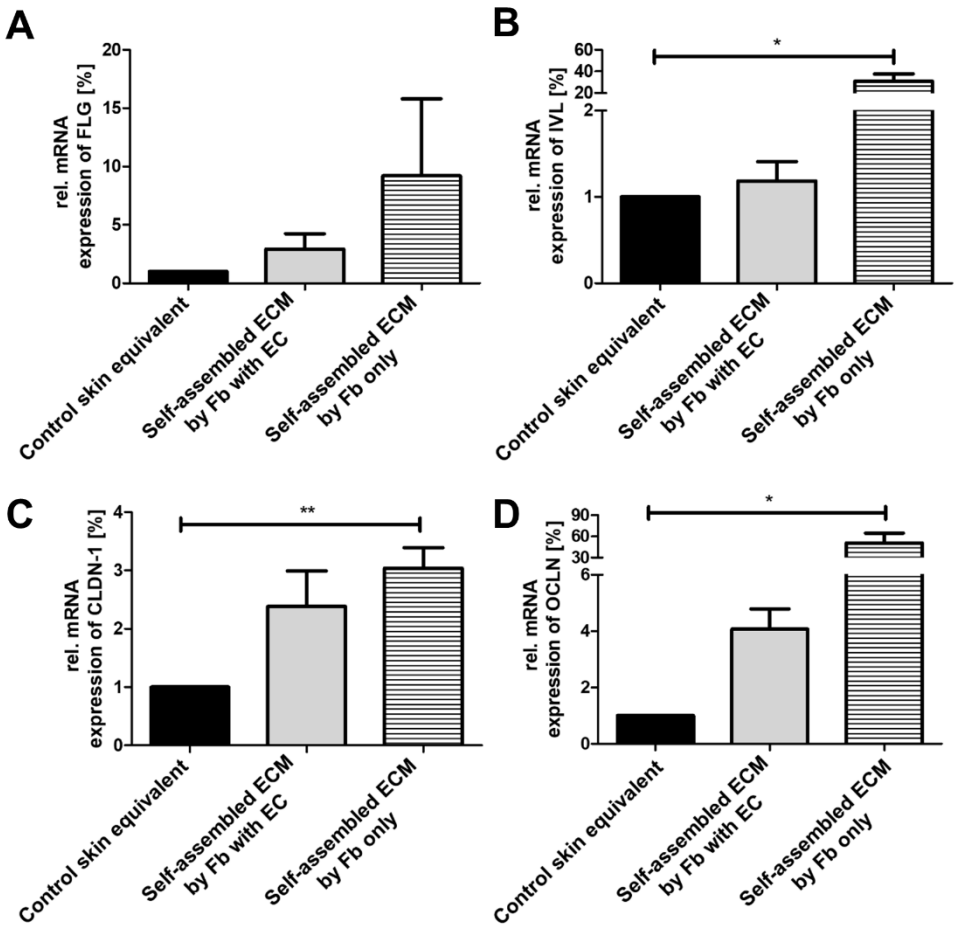


**Figure 4.19. Representative mRNA expression of cornified envelope and tight junction proteins in the skin equivalents based on a self-assembled ECM**

Relative mRNA expression of **(A)** filaggrin - *FLG*, **(B)** involucrin - *IVL*, **(C)** claudin-1 *CLDN-1* and **(D)** occludin - *OCLN* of the skin equivalent with dermal equivalent based on a bovine collagen matrix, control skin equivalent – type I, skin equivalent with dermal equivalent consisting of self-assembled ECM by fibroblasts with endothelial cells – type II, and skin equivalent with a dermal equivalent consisting of self-assembled ECM by fibroblasts only – type III. Values are given as mean ± SEM, n = 3. Asterisk indicates statistical significance *$p \leq 0.05$, **$p \leq 0.01$. ECM = extracellular matrix, Fb = fibroblasts, EC = endothelial cells.

## 4.10. Observation of the pre-formed blood vessels formation in the skin equivalents based on self-assembled extracellular matrix (ECM)

We aimed to observe the formation of pre-formed blood vessels in all three types of skin equivalents. In type ll skin equivalents, endothelial cells migrated forming capillary-like structures in the newly synthesized ECM by fibroblasts. The identity and integrity of the capillary-like structures were confirmed by IF staining against the endothelial cell markers cluster of differentiation 31 (CD31) and von Willebrand factor (vWF) (Fig. 4.20.). CD31 and

vWF staining were detected surrounding the tubular structures in the dermis. In the control and type III skin equivalent, no such capillary-like structures and no immunostaining of CD31 and vWF were detected (Fig. 4.20.).

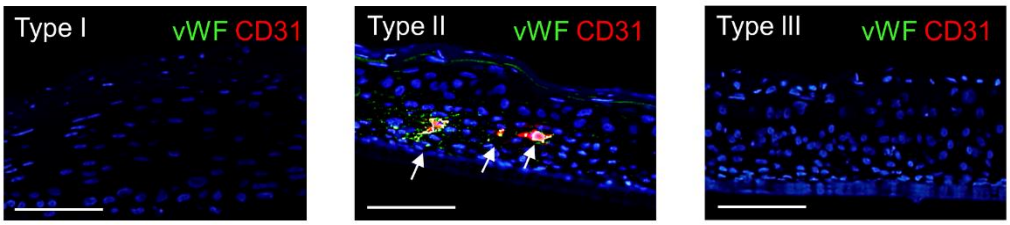


**Figure 4.20. Representative immunofluorescence staining of CD31 and vWF in the skin equivalents based on a self-assembled ECM**

Immunohistochemical analysis of the skin equivalent with dermal equivalent based on a bovine collagen matrix – type I, skin equivalent with dermal equivalent consisting of self-assembled ECM by fibroblasts with endothelial cells – type II and skin equivalent with a dermal equivalent consisting of self-assembled ECM by fibroblasts only – type III, with representative von Willebrand factor (vWF) and cluster of differentiation 31 (CD31). Counterstaining of cell nuclei was performed with 4',6'-diamin-2-phenylindol (DAPI). Scale bar = 100 µm, n = 3. Exposure time: blue channel 1/55 s, green channel 1/10 s and red channel 1/5 s.

## 4.11. Skin permeability studies in the skin equivalents based on self-assembled extracellular matrix (ECM)

The skin barrier function of the skin equivalents was determined by skin permeability studies using radioactively-labelled compounds. To assess the effects of improved differentiation of the skin equivalents with the self-assembled ECM, the permeability of the control skin equivalent and type II skin equivalent were compared. Notably, the skin permeability for radioactively labelled testosterone was clearly reduced in type II compared to the control models (Fig. 4.21.) indicating an improved skin barrier function.

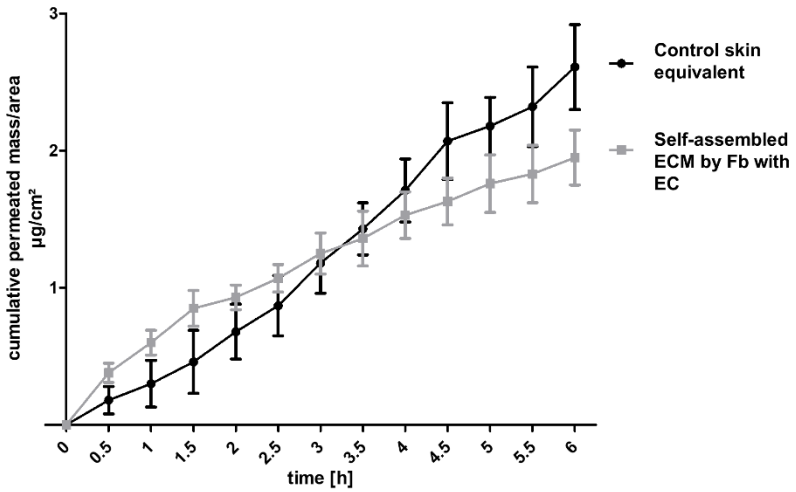


**Figure 4.21. Skin barrier function in the skin equivalents based on a self-assembled ECM**

Skin permeability of radioactively labelled testosterone in (●) skin equivalents with dermal equivalent based on a bovine collagen matrix and (■) skin equivalent with dermal equivalent consisting of self-assembled ECM by fibroblasts with endothelial cells. Values are given as mean ± SEM, n = 3. ECM = extracellular matrix, Fb = fibroblasts, EC = endothelial cells

## 4.12. Stratum corneum (SC) lipid analysis of the skin equivalents based on self-assembled ECM

The lipid analysis was performed by our collaboration partner the lab of Prof. Dr. Kateřina Vávrová. The stratum corneum (SC) lipid chain order was probed by infrared spectroscopy and both free (extractable) SC lipids and covalent lipids in the corneocyte lipid envelope were analysed by high-performance thin layer chromatography (Fig. 4.1.22. and Fig. 4.1.23.).

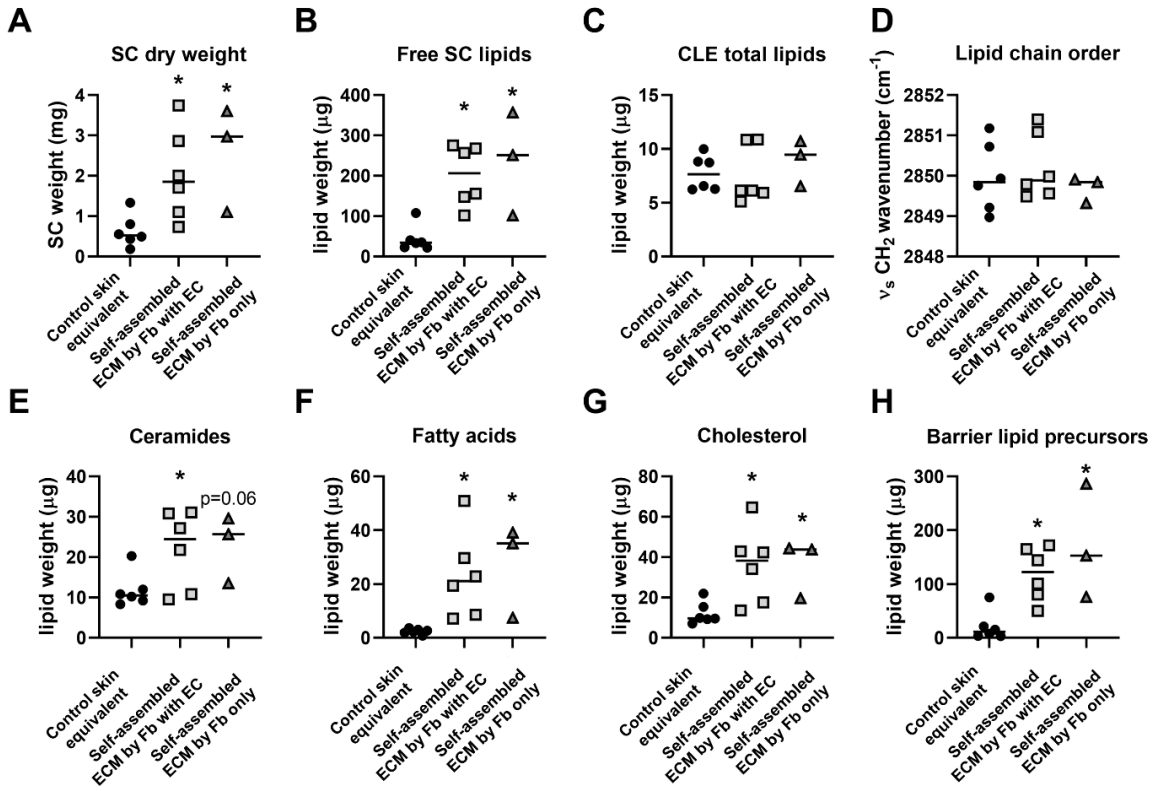


**Figure 4.22. Stratum corneum lipid analysis of the skin equivalents based on a self-assembled ECM**

SC weight and characterization of the SC lipids in skin equivalents having self-assembled ECM by Fb with or without EC compared to control equivalents with Fb in collagen matrix: SC dry weight **(A)**, total extractable SC lipids **(B)**, total covalent SC lipids in CLE **(C)**, lipid chain order **(D)**, total ceramides **(E)**, free fatty acids **(F)**, cholesterol **(G)**, and barrier lipid precursors **(H)**. Asterisk indicates statistically significant differences at *p ≤ 0.05. ECM = extracellular matrix, Fb = fibroblasts, EC = endothelial cells, CLE = corneocyte lipid envelope.

The skin equivalents with self-assembled ECM – both type II and III had thicker SC (4 – 6-fold greater SC dry weight) and 6 – 7-fold more free SC lipids than control equivalents, whereas the covalent lipids were unchanged. All barrier lipid classes (ceramides 2-fold, fatty acids ~10-fold, and cholesterol 4-fold) and also their precursors (~12-fold) were increased in the skin equivalents with self-assembled ECM compared to control. Notably, the most polar ceramides AP and AH, which are hardly detectable in controls, were ~12-fold increased in type II and type III skin equivalents. In all skin equivalents mostly well-ordered SC lipids were found (as indicated by methylene symmetric stretching below 2850 $cm^{-1}$) with no significant differences among the groups.

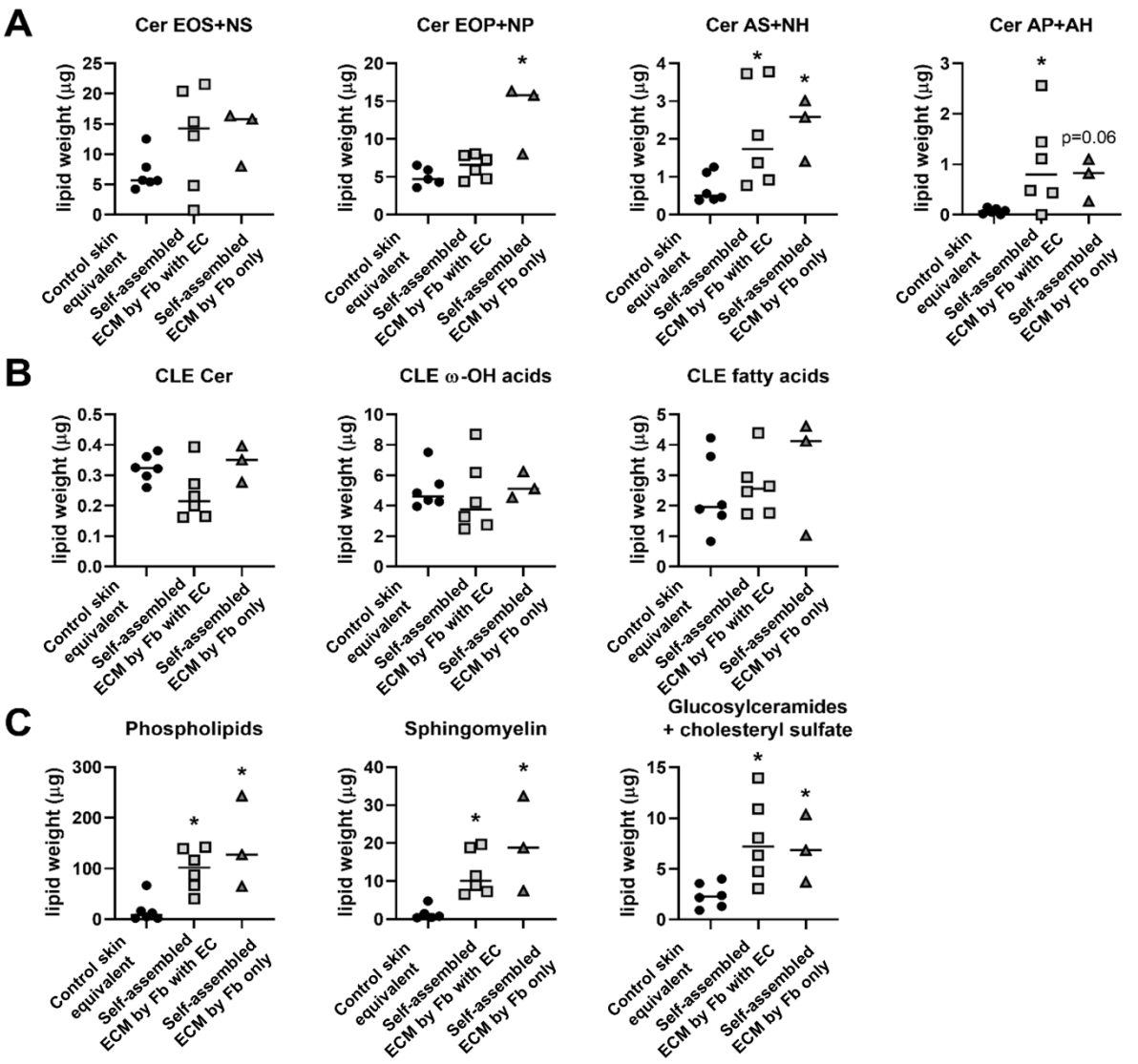


**Figure 4.23. Detailed stratum corneum lipid analysis of the skin equivalents based on a self-assembled ECM**

Detailed composition of the SC lipids in skin equivalents having self-assembled ECM by Fb with or without EC compared to control equivalents with Fb in collagen matrix: graphs in top row (panel A) show ceramide subclasses (Cer EOS+NS, EOP+NP, AS+NH and AP+AH). Panel B shows the covalent lipids in CLE (Cer, ω-hydroxy acids, and fatty acids). Bottom row (panel C) shows the barrier lipid precursors (phospholipids, sphingomyelin and glucosylceramides + cholesteryl sulfate). Asterisk indicates statistically significant differences at *$p \leq 0.05$. ECM = extracellular matrix, Fb = fibroblasts, EC = endothelial cells, CLE = corneocyte lipid envelope.

# 5. DISCUSSION

## 5.1. 3D full-thickness skin equivalents – a model system to study keratinocyte-fibroblast crosstalk

Until now, epidermal keratinocytes and dermal fibroblasts have been analysed extensively and these studies have shown that crosstalk between keratinocyte and fibroblast is critical for the maintenance of the skin homeostasis and the formation of a functional epidermis (Smola et al.,1993, Tracy et al., 2016), as well as cutaneous wound healing (El Ghalbzouri et al. 2004, Sorrell et Caplan, 2004, Tracy et al., 2016), but also it is critical in pathophysiological conditions (Berroth et al., 2013, Kühbacher et al., 2017, Löwa et al., 2020).

Investigation of the cellular growth, signalling processes, cell-cell interactions between keratinocytes and fibroblasts, and the effects of specific soluble factors in more details have been mainly done in monolayer cell culture systems (Maas-Szabowski et al. 1999, Maas-Szabowski et al. 2001). These studies have shown that dermal fibroblasts can interact with epidermal keratinocytes either via soluble mediators or via secreted vesicles (Huang et al., 2015). Although these investigations provided important insights, the impact of the cellular crosstalk on the spatial organization of the skin is difficult to assess with this setup (Jevtić et al., 2020). So far, however, the actual impact of the keratinocyte-fibroblast crosstalk on the skin differentiation is still not fully understood. Furthermore, the interactions between cells are difficult to study in living organisms such as humans or animals due to complexity of the skin and interactions with other organ systems. Therefore, a systematic approach that investigates the impact of fibroblasts on skin differentiation, homeostasis and barrier function is lacking (Jevtić et al., 2020). Thus, alternatives are required. The use of organotypic 3D full-thickness skin equivalents gives us the opportunity to close this research gap by providing a model system that offers the possibility to examine cell-cell interaction without confounding factors, but also more closely mimic characteristics of native human skin than 2D culture systems.

Therefore, to shed a bit more light onto the role of this epidermal-dermal axis, the potential of 3D full-thickness skin equivalents composed of primary human keratinocytes and fibroblasts has been leveraged to study the keratinocyte-fibroblast crosstalk in the skin in more detail (Jevtić et al., 2020). Skin equivalents have been generated with and without fibroblasts, the latter by inducing an osmotic shock which removes previously seeded fibroblasts (Coulomb et al., 1989, Marionnet et al., 2006).

Firstly, the histology of the skin equivalents was investigated. In the skin equivalents without fibroblasts, a disturbed maturation and differentiation was observed as well as significant epidermal thinning **(Fig. 4.1. A, B)**, which is in line with previous reports (El Ghalbzouri, Lamme et al., 2002, El Ghalbzouri, Gibbs et al., 2002, Marionnet et al. 2006). On the contrary,

in the control skin equivalents, where both keratinocytes and fibroblasts were present in epidermal and dermal compartment, it has been found that dermal fibroblasts promoted the development of normal epidermal morphology and keratinocytes differentiation in addition to promoting keratinocytes proliferation (El Ghalbzouri, Lamme et al., 2002, El Ghalbzouri, Gibbs et al., 2002). Further, the keratinocytes in the *stratum basale* were flat and not discernible from the superimposed *stratum spinosum* and a distinct *stratum granulosum* was lacking **(Fig. 4.1. C, D, E, F)**. These findings arose the idea to examine the expression of a protein critical for keratinocytes proliferation – Ki67. Notably, Ki67 was lower expressed in the *stratum basale* of the skin equivalents without fibroblasts **( Fig. 4.7.)**, which is consistent with previous studies by El Ghalbzouri and colleagues (el-Ghalbzouri et al., 2002, El Ghalbzouri et al., 2002). Overall, these findings indicate that without the direction given by the fibroblasts, the keratinocytes lack critical information during their differentiation which results in disturbed epidermal morphology and unphysiological cell shapes **(Fig. 4.1.)** (Jevtić et al., 2020).

Further, the temporal and spatial effects of fibroblasts on tissue differentiation were analysed. This data brings new insights in the time course appearance of cornified envelope proteins filaggrin (FLG) and involucrin (IVL), markers of terminally differentiated keratinocytes. A decreased expression of FLG **(Fig. 4.2.)** and a compensatory upregulation of IVL **(Fig. 4.3.)** was observed in the skin equivalents devoid of fibroblasts indicating that fibroblasts orchestrate the skin differentiation. The upregulation of IVL likely aims to compensate for the lack of FLG, a phenomenon that has been repeatedly shown in FLG-deficient skin equivalents (Hönzke et al., 2016, Wallmeyer et al., 2017). Another consequence of the dysregulated epidermal differentiation is an impaired skin barrier function as indicated by the increased permeability of the test compounds testosterone, caffeine **(Fig. 4.1.8 A and B)** and Lucifer yellow **(Fig. 4.1.8 C and D)**. These findings are in line with the apparently lower stratum corneum (SC) lipid content in the fibroblast-free skin equivalents **(Fig. 4.9. and Fig. 4.10.)** although overall the effects on the skin lipids were surprisingly minor (Jevtić et al., 2020).

Another poorly understood aspect is the direct interplay of keratinocytes and fibroblast signalling pathways that orchestrate epidermal proliferation and differentiation (Jevtić et al., 2020). In skin, homeostasis of the epidermis relies on a tightly regulated balance between proliferation and differentiation, where a continuous proliferation of keratinocytes in the *stratum basale* is a prerequisite to replace the shedded material of the SC (Maas-Szabowski et al., 2000). Key players of the epidermal stratification are the cells in *stratum spinosum* and their different missions. They have to carry out simultaneously a suppression of genes particularly expressed in *stratum basale*, upregulation of specific genes needed for suprabasal cell differentiation, maintenance of their immature and proliferative status, prevention of premature terminal differentiation and initiation of the terminal differentiation program to

differentiate into granular cells (Massi and Panelos, 2012). Once cells exit the *stratum basale*, they downregulate proliferation-associated genes and execute a terminal differentiation program that is marked by a stepwise transcriptional transition from early differentiation spinous layers to late differentiation granular layers. In the last step, all metabolic activity ceases as dead squames of the protective SC are formed and subsequently sloughed from the skin surface (Watt et al., 2006). Hence, it is particularly interesting that in the skin equivalents without fibroblasts, the cells in the *stratum basale* and *stratum spinosum* did not show any morphological differences **(Fig. 4.1. C, D, E, F)** which is indicative for a lack of proper differentiation (Jevtić et al., 2020). Fibroblasts are also involved in the synthesis of critical components of the basal membrane such as type IV and VII collagen and laminin-1. The cells of the *stratum basale* are attached to basal membrane and proliferate, and they ultimately leave the basal cell layer through asymmetric mitosis and, thus, exit the cell cycle. If the basement membrane components have not been properly synthesized, consequently the basal cells lack the information about proper cell polarization and shape, as well as the information about when to leave the cell cycle (Sorrell et al., 2004, Simpson et al., 2012).

To unravel the impact of fibroblasts on this regulation in more detail, DigiWest analysis was performed **(Fig. 4.11. and Fig. 4.12.)**. Currently, the complex network of intercellular crosstalk between keratinocytes and fibroblasts is not fully understood as well as signalling pathways involved in this crosstalk (Jevtić et al., 2020). Interestingly, results of this thesis indicate a disbalance in Ras/Raf/ERK/MEK signalling **(Fig. 4.12. A)**. In general, this pathway can be considered as a double-edged sword which is critical for epidermal survival and proliferative self-renewal of the human skin. *In vitro* studies provided conflicting results regarding the role of Ras/Raf/ERK/MEK signalling in epidermal keratinocyte growth and differentiation; however, subsequent work in tissue models have demonstrated that an activation of this cascade promotes epidermal proliferation and inhibits differentiation (Khavari et al., 2007). Results from the present study clearly indicate that signals from fibroblasts are critical for Ras/Raf/ERK/MEK signalling in epidermal keratinocytes which ultimately guides their proliferation and differentiation. If fibroblasts are missing, Ras/Raf/ERK/MEK signalling is significantly downregulated **(Fig. 4.12. A)** resulting in an impaired differentiation of the skin equivalents as indicated by, e.g. their impaired stratification **(Fig. 4.1.)** or the unphysiological expression of IVL in deeper epidermal layers **(Fig. 4.3. C)** (Jevtić et al., 2020).

In addition to Ras/Raf/ERK/MEK, Notch1, a regulator of cell adhesion, the basal-to-suprabasal switch and expressed widely in the *stratum basale* (Watt et al., 2008; Blanpain et al., 2009) was significantly downregulated in the skin equivalents without fibroblasts **(Fig. 4.12. B)**. Loss-of-function and gain-of-function studies in cell culture and animal models have demonstrated that Notch signalling regulates late-stage granular layer differentiation of the epidermis (Lin et

al., 2011). Postnatal ablation of the Notch1 gene in mice caused epidermal hyperproliferation and thickening as well as increased Ki67 and FLG expression (Rangarajan et al., 2001; Nicolas et al., 2003) which is exactly the opposite of what we found in our study. Interestingly, conditional ablation of Notch signalling during embryogenesis in mice resulted in a loss of the spinous and granular layers due to hypoproliferation of the epidermis, indicating that Notch signalling is also required during epidermal development (Blanpain et al., 2006), which in fact is in line with findings from this thesis **(Fig. 4.1)**. These seemingly contradictory findings may result from an activation of different Notch pathways – canonical or non-canonical (Moriyama et al., 2008) that are stimulated by signals from dermal fibroblasts (Jevtić et al., 2020).

A significant downregulation of Slug **(Fig. 4.1.12. B)** – a transcription factor, was also observed. Slug is involved in epithelial to mesenchymal transition (Mani et al., 2008; Lim et al, 2012), and plays a role in prevention of the differentiation of skin stem cells (Mistry et al., 2014). Depletion of Slug in an organotypic human tissue model resulted in premature differentiation which is in line with our findings and again may explain, for example, the aberrant expression pattern of IVL in the skin equivalents without fibroblasts **(Fig. 4.3.)** and thinning of the epidermis **(Fig. 4.1.)**. Along this line, a significant downregulation of Ezh2 was also detected in the skin equivalents lacking fibroblasts **(Fig. 4.1. B)**. In fully developed epidermis, Ezh2 is strongly expressed mainly in basal cells, and both *in vitro and in vivo* studies showed that an inhibition or loss-of-function of Ezh2 results in impaired keratinocyte differentiation (Ezhkova et al., 2009, Wurm et al., 2015). Furthermore, genes that are involved in terminal differentiation are upregulated when Ezh2 is missing which is in line with the increased expression of *FLG* and *IVL* on gene level in skin equivalents without fibroblast **(Fig. 4.1.6.)** (Jevtić et al., 2020).

In summary, these findings demonstrate that fibroblasts significantly impact and orchestrate epidermal differentiation and maturation as well as the skin barrier formation. When fibroblasts are missing, the differentiation of epidermal keratinocytes and, thus, the epidermal stratification is impaired. Data from the present study also shows a disbalance in Ras/Raf/MEK/ERK signalling, then downregulation of Notch1, Slug and Ezh2 signalling that are mainly expressed in the basal cells, implicating that signals from fibroblasts are necessary to ultimately guides proliferation in basal keratinocytes but also regulates late-state granular layer differentiation of the epidermis. Further investigations are necessary to provide a better understanding of the epidermal-dermal signalling and future studies should include microarray studies, single-cell sequencing and -omics approaches which would provide further insights into the crosstalk of keratinocytes and fibroblasts and unravel these interdependencies in full detail (Jevtić et al., 2020).

## 5.2. Extracellular vesicles (EVs) as a potential cell-to-cell communication mechanism between epidermal keratinocytes and dermal fibroblasts

During the investigation of epidermal-dermal crosstalk, the idea arose that extracellular vesicles (EVs) may have important role in intercellular communication between keratinocytes and fibroblasts. EVs have been found in *ex vivo* sections of the human papillary dermis, at wounds and in the stroma of human skin tumors. In addition, *in vitro* vesicular crosstalk has been observed between several types of skin cells, including keratinocytes, fibroblasts, melanocytes, dermal papillary cells, outer root sheath cells of the hair follicle and microvascular endothelial cells (Terlecki-Zaniewicz et al., 2019). For instance, keratinocytes have been previously reported to secrete exosomes containing stratifin that stimulate the activity of the metalloprotease-1 (MMP-1) in fibroblasts (Chavez-Muñoz et al., 2009). Findings from another group have highlighted a novel mode of communication between keratinocytes and melanocytes and have attributed a novel function for exosomes in the regulation of skin pigmentation (Cicero et al., 2015). Furthermore, it has been reported that melanocytes are important players in the protection against UV light, not only by distribution of melanin but through rapid generation of EVs which might alter proliferation rate in the recipient cells, keratinocytes (Wäster et al., 2016). Huang et al. have shown that keratinocytes can transfer information to fibroblasts in the form of microvesicles (MVs) that can then regulate fibroblast gene and protein expression, leading to increased fibroblast migration and fibroblast-mediated angiogenesis during wound healing. In addition, defective MVs secretion/function may contribute to aberrant wound healing and chronic wounds that fail to re-epithelialize (Huang et al., 2015). Moreover, studies on MVs produced by serum-activated wound myofibroblasts have shown that these MVs can be incorporated into endothelial cells and significantly stimulated microvascular endothelial cells growth, migration rate and capillary-like structure formation, demonstrating that MVs secreted by myofibroblasts can promote angiogenesis (Merjaneh et al., 2017). The most recent data have unravelled the ubiquitous presence of EVs in human skin and their ability to deliver miRNA cargo from fibroblasts through the collagen matrix into the epidermal layer of 3D human skin equivalents (Terlecki-Zaniewicz et al., 2019).

In all of these studies it has been shown that the cargo of EVs is reflective of their cellular origin and modulated by the surrounding environmental stimuli and consists of various biomolecules – proteins, lipids, DNA, mRNA and miRNA (Iraci et al., 2016, Haraszti et al., 2016). Consequently, the isolation, quantification and characterization of exosomes and MVs have become a major initiative in both basic research and clinical applications (Li et al., 2017). This cargo can be transferred to an acceptor cell and may have functional effect on molecular

processes, such as changes in cellular structure and function. Therefore, EVs are emerging as a potential delivery vehicle of signalling molecules (Nawaz and Fatima, 2017), for intercellular crosstalk between epidermal keratinocytes and dermal fibroblasts. However, it is still not known how fibroblasts-derived EVs regulate keratinocyte function. Hence, preliminary isolation of fibroblasts-derived EVs from the primary human dermal fibroblasts condition medium was performed for further characterization in terms of morphology and composition.

A group of scientists at the International Society of Extracellular Vesicles (ISEV) with collective long-term expertise in the field of EVs biology has established the Minimal Information for Studies of EVs in 2018 (MISEV 2018). MISEV 2018 represents comprehensive detailed guidelines which provides researchers with a minimal set of biochemical, biophysical and functional standards that should be used to attribute any specific biological cargo or functions to EVs (Théry et al., 2018, Lötvall et al., 2014). Therefore, we followed these guidelines.

Firstly, it is important to note that primary dermal fibroblasts were cultured in foetal calf serum (FCS) free medium 24h prior to EVs isolation, since it is known that FCS consists EVs and RNAs (Théry et al., 2006). On the day of EVs isolation, dermal fibroblasts were analysed in terms of the presence of abundant dead or dying cells, which lead to contamination of live cell-derived EVs by dead-cell-derived vesicles. Indeed, dying cells release vesicles of various sizes, and eventually break into cell fragments, which can in turn fragment into smaller vesicles upon ultracentrifugation (Witwer et al., 2013). 5% is the maximum acceptable cell death percentage in culture to provide reasonably pure EVs released by live cells (Witwer et al., 2013). This is in fact something what was proved with FACS analysis **(Fig. 4.13.)**, thus, isolated pure EVs were released by living cells. The techniques widely used so far for EVs isolation include ultracentrifugation, density gradient flotation, ultrafiltration, chromatography, polymer-based precipitation and immunoprecipitation (Sadik et al., 2018). To date, most of the researchers who studied EVs from cell culture medium have been using differential centrifugation with or without size filtration to concentrate and partially purify EV (Raposo et al., 2013, Théry et al., 2006). Therefore, for realization of this thesis it has been relied on this technic. After the isolation, the size and morphology of fibroblast-derived EVs were analysed to classify them into one of three categories: exosomes, microvesicles (MVs) and apoptotic bodies (Doyle and Wang, 2019). Nanoparticle tracking analysis (NTA) and transmission electron microscopy (TEM) confirmed that the isolated EVs were within the size expected for exosomes – less then 150 nm, and they showed round shape **(Fig 4.14. A and B)**.

Nevertheless, these are preliminary data and it would be important to further characterize fibroblasts derived EVs – exosomes, in terms of proteome to understand the biomolecular cargo of these exosomes which are by now not fully understood.

## 5.3. Development of completely human-based skin equivalents

The use of animal models for dermatological research studies has increased enormously in the past decades, giving a strong boost to the comprehension of skin (patho)-physiological mechanisms and to testing therapeutic approaches at preclinical level (Schmook et al., 2001, Avci et al., 2013). Mice are widely used in all areas of dermatological interest, from immunological diseases to cancer, skin repair, genetic diseases, and hair disorders (Dellambra et al., 2019). However, besides the ethical concerns related to the use of animals, but also due to the recent regulatory changes, the accuracy of animal to human extrapolation has been an important issue and often results obtained in mouse models cannot be reproduced in the human context (Seok et al., 2013). Such differences underline the need for other, more representative and reliable models.

Human-based organ models gained a lot of attention during the past decades. Reconstructed epidermis constructs and 3D full-thickness skin constructs have become well accepted as potential alternatives to animal use for basic and preclinical studies in dermatological research (Suhail et al., 2019). Hence, human skin equivalents became an attractive tool to study cell-cell, cell-matrix and dermal-epidermal interactions, as well as for preclinical pharmaco-toxicological testing (El Ghalbzouri et al., 2008).

Along with active progress in the field, skin tissue engineering strategies have focused on exploring different tools to attain the complexity of skin tissue. Most skin constructs consist of co-cultured skin-derived cells, particularly keratinocytes which constitute the epidermal equivalent and fibroblasts, that are embedded in a 3D scaffold representing the dermal equivalent (Khiao In et al., 2015, El Ghalbzouri et al., 2009). Hence, different approaches have been reported: fibroblasts seeded onto natural or synthetic biomaterials or fibroblasts stimulated to secrete and organize their own ECM with or without scaffolds (Auger et al., 2004, Auxenfans et al., 2009). Although they are already successfully applied in basic and preclinical research (Skardal et al., 2016, Jodat et al., 2018) further improvements are urgently required.

The most commonly used protocols for skin tissue engineering rely on exogenous material such as animal-derived collagen originated from rat or bovine, for the generation of dermal equivalents. This approach comes along with several limitations such as the lack of a human-based extracellular matrix (ECM) and microstructure as well as significant contractions, shrinkage and low mechanical stability of the connective tissue (Stark et al., 2006, Parenteau-Bareil et al., 2010).

Acknowledging the pivotal role fibroblasts-derived ECM plays in skin tissue, providing a microenvironment for cellular development, homeostasis, and regeneration (Neve et al., 2014,

Cox and Erler, 2011), there is a growing interest in building more physiological skin constructs deploying purely human-based components. Additionally, in order to more closely mimic the architecture of human skin, different groups worked on the implementation of different cell types that are residents of the skin such as human umbilical vein endothelial cells (HUVEC) (Black et al., 1998, Schechner et al., 2000, Hudon et al., 2003, Schechner et al., 2003, Tremblay et al., 2005) or human dermal microvascular endothelial cells (HDMEC) (Supp et al., 2002, Montano et al., 2009, Groeber et al., 2013, Marino et al., 2014) into the dermis of the full-thickness skin equivalent aiming for an endothelialized skin equivalent with capillary-like structures. In contrast with other *in vitro* models of angiogenesis that contain exogenous extracellular matrix (ECM) or biomaterials such as collagen-glycosaminoglycan (Supp et al., 2002, Hudon et al., 2003), fibrin hydrogels (Marino et al., 2014), or acellular dermis (Sahota et al., 2003, Schechner et al., 2003), the cultured endothelial cells in some models are embedded in a complex fibroblasts secreted human ECM and self organized (Rochon et al., 2010). ECM production and maintenance is an important feature of endothelial cells functionality crucial for the development of blood vessels, and endothelial cells signalling responses to this natural matrix *vice versa* (Rhodes and Simons, 2007, Anderson and Hinds, 2012, Witjas et al., 2019).

In the approach used for realization of this thesis, it has been exclusively relied on the use of primary human cells without any exogenous biomaterials. To overcome the limitations of collagen matrices, a long-term co-culture was established between primary human fibroblasts, responsible for the ECM production and human dermal microvascular endothelial cells (HDMEC) that are crucial for adequate tissue differentiation and drive vascularization (Rafii et al., 2016, Sasine et al., 2017). To assess the impact of the components and structure of the dermal equivalent on the skin tissue homeostasis, three types of skin equivalents were generated and compared: i) skin equivalents based on a bovine collagen matrix – type I (conventional approach, as control), ii) skin equivalents based on a self-assembled ECM containing fibroblasts and HDMEC – type II, and iii) skin equivalents based on a self-assembled ECM with fibroblasts only – type III.

Initially, in the self-assembled approach fibroblasts were seeded to allow the production, organization and maintenance of the main ECM components in the presence of ascorbic acid as already shown in previous studies (Black et al., 1998, Supp et al., 2004, Schechner et al., 2003, Hudon et al., 2003, Tonello et al., 2005, Tonello et al., 2003). This approach originates from two main discoveries (Saba et al., 2018). Firstly, in 1972, Switzer and Summer found that ascorbate, an enzymatic cofactor of lysyl- and prolyl-hydroxylase, was shown to stimulate the production of type I collagen by human dermal fibroblasts (Switzer and Summer, 1972).

Secondly, a key experiment followed in 1989 that demonstrated that fibroblasts can deposit enough ECM within few days to create a 3D stromal sheet (Hata and Senoo, 1989).

Therefore, one of the first observation during handling with the skin equivalents based on the self-assembled approach for further processing steps, was their mechanical stability and a distinct robustness. It has been noticed earlier that the mechanical stability represents a challenging problem for biological tissues produced by tissue engineering (Pouliot et al., 2002). Despite the frequent presence of this problem, self-assembled approach developed for realization of this thesis resulted in a very stable biomatrix in a well-preserved form where no contraction occurred, which was, by contrast, frequently occurring during the culturing process of type I skin equivalents. However, this has been already reported, the extent of collagen contraction is dependent on the collagen concentration, the number of fibroblasts present in the matrix and the culture time of the matrices prior to seeding of keratinocytes in collagen based skin equivalents (El Ghalbzouri et al., 2002). Further, the skin equivalents based on the self-assembled approach – type II and type III, exhibited a much denser cyto- and tissue structure as previously demonstrated (Pouliot et al., 2002) compared to the collagen based skin equivalents – type I **(Fig. 4.15.)**. These finding are also supported with findings that incorporation of endothelial cells in the reconstructed dermis resulted in an increase in tissue elasticity and mechanical strength (Chabaud et al., 2017).

Next, the histology and morphology of the skin equivalents were observed. Histological analyses showed in all three skin equivalents types expression of all expected epidermal layers and organisation of the strata was the same as in native human skin, although thinner epidermis was observed in self-assembled approach **(Fig. 4.15.)**.

Further, ultrastructural analysis of the skin equivalents was performed. Here, firstly, I would first like to emphasize above mentioned importance of keratinocyte-fibroblast crosstalk in the skin tissue differentiation and formation of dermal-epidermal junction. Studies on *in vitro* human skin equivalents based on type I collagen and de-epidermized dermis (DED) have shown the importance of intercellular communication between fibroblasts and keratinocytes in the formation of dermal-epidermal junction which is essential for attachment of the epidermis to the dermis and that in turn, can influence the keratinocyte phenotype (El Ghalbzouri et al., 2004, Spiekstra et al., 2007). In-depth ultrastructural analysis of self-assembled skin equivalents revealed interesting findings. Although some typical features of the human skin such as basement membrane and hemidesmosomes were not observable by transmission electron microscopy (TEM) in the type I skin equivalents after 14 days of cultivation **(Fig. 4.16. B)**, these findings are in line with a previous study (Khiao In et al., 2015). Nevertheless, this might be explained with different spatial and temporal expression of basement membrane components during skin morphogenesis as already shown by (Fleischmajer et al., 1998,

Marionnet et al., 2006, Stark et al., 2006). In the Fleischmajer's study, it has been shown that hemidesmosomes were not present after 7 days, were immature after 14 days of skin equivalents cultivation, but they were present, as well as *lamina lucida* and *lamina densa*, after 28 days of skin equivalents cultivation. Interestingly, ultrastructural analysis revealed formation and presence of basement membrane, *lamina lucida* and *lamina densa* and hemidesmosome in the type II and III skin equivalents **(Fig. 4.1.16. B)** in a similar fashion to *in vivo* human skin, also in line with findings in self-assembled approach (Fleischmajer et al., 1998, Michel et al., 1999, Pouliot et al., 2002, Lee et al., 2005, El Ghalbzouri et al., 2009, Rochon et al., 2010). The primary role of fibroblasts seems to be instructive effects on keratinocytes, by promoting the production of basement membrane components such as laminin 1, type IV and VII collagen, their optimal localization and appropriate organization of the basement membrane (Marinkovich et al., 1993, Smola et al., 1993, Smola et al., 1998, Marionnet et al., 2006). However, further analysis targeting specific basement membrane proteins such as collagen IV and VII, nidogen, laminin 5 and 10/11 would be of interest to further investigate kinetics of expression of these proteins during skin equivalent differentiation in self-assembled approach.

Further, the production of ECM by fibroblasts in the self-assembled approach was observed and formation of dermal equivalent by histological staining **(Fig. 4.15.)**. Here, it was noticed differences regarding the thickness of dermal equivalent and produced ECM in the self-assembled approach. This might be related to different proliferation rates of the fibroblasts and subsequently the formation of ECM, but also due to the production of matrix metalloproteinases (MMPs). MMPs are enzymes responsible for the collagen and other protein degradation in ECM (Nagase et al., 2006). It has been reported that endothelial cells (EC) produce MMP-1, MMP-2, MT1-MMP (Taraboletti et al., 2002, Van Doren, 2015), all implicated in the degradation of collagen fibrils. This might be an explanation why in the self-assembled skin equivalents by fibroblast with endothelial cells, dermal equivalent is thinner compared to the self-assembled skin equivalents by fibroblast only. On the other hand, ECM production can be increased by the supplementation of chemical inhibitors of MMPs in cell cultures, such as tissue inhibitor of metalloproteinases-1 (TIMP-1) as already shown *in vitro* (Simon et al., 2012). Hence, fine-tuning seems to be required to tightly control the balance between the synthesis of ECM elements and their degradation (Carver and Goldsmith, 2013). Nevertheless, further characterization of the components of dermal equivalent in self-assembled approach will be necessary to define key parameters of ECM biology, that are relevant for the positive impact of the ECM structure onto the keratinocytes, thus controlling epidermal differentiation, proliferation, and morphogenesis in these skin equivalents.

So far, two types of tissue-engineered skin equivalents are available – reconstructed human epidermis and full-thickness skin equivalents (HSE) – both non-vascularized and of limited value with regard to their ability to reflect the physiological conditions of a full organ. The cutaneous vasculature is crucial for several physiological and pathophysiological processes including the wound healing, development of skin diseases, metastasizing of malignant melanoma, tumor-angiogenesis, and the transdermal penetration of substances (Groeber et al., 2016). Nevertheless, the vascular system is an absolute requirement for the survival of most long term engineered tissues since it ensures the distribution of essential nutrients and oxygen, guaranteeing its survival (da Silva et al., 2020). In the absence of a model that represents the physiological conditions of a full organ, there remains a scientific and medical need for animal models (Groeber et al., 2016).

In order to overcome these limitations and to mimic the architecture and cellular environment of human skin more closely, endothelial cells have been implemented into the dermal part of full-thickness skin equivalents, aiming to create a microcapillary network inside the dermal layer (Tonello et al., 2005, Montaño et al., 2010). Therefore, primary human fibroblasts which produced ECM were co-cultured with HDMEC in our type II skin equivalents. Providing a 3D support for endothelial cells proliferation and survival, the ECM has a dual role – it acts as an adequate substrate for the organisation of endothelial cells into microvessels, simultaneously retaining and concentrating growth factors in the cellular microenvironment (Berthod et al., 2006). Furthermore, ECM production and maintenance also influences endothelial cells functions and gene expression by storing pro- and anti-angiogenic growth factors, cytokines and integrins and their release on demand that are crucial for the development of blood vessels, but also endothelial cells signalling responses to this natural matrix *vice versa* (Soucy and Romer, 2009, Costa-Almeida et al., 2015, Kaessmeyer et al., 2017, Anderson and Hinds, 2012, Witjas et al., 2019).

Accordingly, after 44 days of cultivation, the formation of pre-formed blood vessels in type II skin equivalents was observed **(Fig. 4.20.)**. ECM molecules secreted by fibroblasts provide the physiological environment needed for endothelial cells proliferation and organization into capillary-like structures (Black et al., 1998, Black et al., 1999, Supp et al., 2002, Sehchner et al., 2003, Hudon et al., 2003, Tonello et al., 2003, Tonello et al., 2005). Findings from this thesis are also consistent with previous reports in which dermal constructs were produced with fibroblasts and EC embedded in chitosan-bovine collagen (Black et al., 1998, Hudon et al., 2013, Tremblay et al., 2004), collagen-glycosaminoglycan (Supp et al., 2002, Hudon et al., 2003), fibrin hydrogels (Marino et al., 2014), hyaluronic acid (Tonello et al., 2003, Tonello et al., 2005) and acellular dermis (Schechner et al., 2003, Sahota et al. 2003). This was supported with the fact that fibroblasts and keratinocytes secrete angiogenic growth factors

such as vascular endothelial growth factor (VEGF) and platelet derived growth factor (PDGF), which induce endothelial cells migration and angiogenesis (Trampezinski et al., 2004).

The impact of different components and structure of the dermal equivalent on epidermal differentiation and barrier function were analysed. Although in all three types skin equivalents expression of all expected epidermal layers and organisation of the strata were the same as in native human skin, differentiation of the type II skin equivalents was improved **(Fig. 4.17. and Fig. 4.19.)**. It has been previously reported an unphysiological localization of terminally differentiation marker – involucrin (IVL) – in the self-assembled human skin equivalents cultured for 13 weeks or longer, where IVL was shifted from the *stratum granulosum* also to the *stratum spinosum* (El Ghalbzouri et al., 2009), in contrast to our finding. An increased expression of IVL was discovered and its expression pattern in the *stratum granulosum* exclusively **(Fig. 4.17. and Fig. 4.18.)** which is normal for native human skin (El Ghalbzouri et al., 2002).

Interestingly, physiological tight junctions (TJs) expression pattern **(Fig. 4.17. and Fig. 4.18.)** and improved skin barrier function **(Fig. 4.21.)** were observed in self-assembled approach, since it is known that TJs are involved in differentiation, proliferation, cell polarity and signal transduction processes of cells (Bäsler et al., 2016). CLDN-1 was expressed in all viable epidermis, with a low expression in *stratum basale* **(Fig. 4.18.)** and OCLN was expressed in *stratum granulosum* **(Fig. 4.18.)** which is typical localization in the native human skin (Bäsler et al., 2016, Brandner and Schulzke, 2015, Roger et al., 2019). This is remarkable since the TJs expression pattern is unphysiological in most of the skin equivalents described so far which also holds true for our control skin equivalents. This findings was also confirmed with transmission electron microscopy. To the best of the knowledge, TJs in such a skin equivalent have thus been detected ultra-structurally for the first time (**Fig. 4.16. C)**. Furthermore, the main function of TJs is sealing of the paracellular pathway to restrict the movement of molecules within the intercellular space (Bäsler et al., 2016), that is exactly what was seen in the permeation study for radioactively labelled testosterone which was clearly reduced in type II skin equivalents **(Fig. 4.21.)**.

The improved barrier function of the skin equivalents with self-assembled ECM compared to controls and is, at least partly, connected with the increased lipid synthesis, which is consistent with (Thakoersing et al., 2012). The lack of improvement of the *stratum corneum* lipid arrangement in type II and III equivalents may be explained by the fact that not only the barrier lipids (ceramides, fatty acids and cholesterol), but also their precursors were elevated **(Fig. 4.22. and Fig. 4.23.)**. The lipid precursors sphingomyelin (Pullmannova et al., 2014), glucosylceramides (Sochorová et al., 2017) and phospholipids (Gooris et al., 2018), disturb the *stratum corneum* lipid organization. Notably, the increased free *stratum corneum* lipids

were not paralleled by an increase in the covalent lipids of the corneocyte lipid envelope, which is an essential structure for the skin barrier function (Akiyama, 2017). Thus, the fibroblasts generated ECM induced lipid synthesis in keratinocytes but did not affect in a similar manner the lipid processing at the *stratum granulosum-stratum corneum* interface.

Since one of the goals of this thesis was establishment of the new self-assembled approach, it is remarkable to compare self-assembly of dermal equivalent preparation used for realization of this thesis with other methods based on scaffold-free methods. Different research groups have reported different cultivation time of dermal fibroblasts to allow the development of ECM and dermis, before further co-culture with other cell types e.g. keratinocytes and/or endothelial cells, was performed. Cultivation time varies from 3 weeks (Lee et al., 2005, El Ghalbzouri et al., 2008, Thakoersking et al., 2012), 4 weeks (Rochon et al., 2010), up to 5 weeks respectively (Michel et al., 1999, Jean et al., 2011).

Therefore, it is interesting to contrast scaffold-free method of the self-assembly approach used for realization of this thesis with self-assembly method reported by Rochon and colleagues (Rochon et al., 2010). In that study, dermal fibroblasts were cultured for 4 weeks and then co-cultured with endothelial cells for one week to form endothelialized stromal sheets. These were then detached, superimposed and cultured for another week. Keratinocytes were then seeded on top and the construct were cultured for three more weeks in an air-liquid interface (Rochon et al., 2010). However, the time frame of cultivation in our approach for the cultivation of skin equivalents based on the self-assembly approach was prolonged in comparison to conventional skin equivalent cultivation that requires around 14 days. Nevertheless, self-assembled approach developed for realization of this thesis is shorter than method described by Rochon. In type II skin equivalents, the fibroblasts proliferated and synthesized their own ECM for 10 days alone, before endothelial cells have been seeded for 20 days of co-culture, including two more weeks at the air-liquid interface with seeded keratinocytes, leading into well-differentiated epidermis mimicking many attributes of human *in vivo* microenvironment. Importantly, all of these steps were processed in the same inserts without additional manipulation of cells and tissues such as detachment or superimposed step described by (Rochon et al., 2010), decreasing the manufacturing issues.

In summary, these data demonstrate a simple approach for the generation of completely human-based skin equivalents using a long-term co-culture of fibroblasts and endothelial cells. In addition to the beneficial direct impact of ECM produced by fibroblasts on the epidermal proliferation and differentiation in the skin equivalents and the formation of network of capillary-like structures by endothelial cells, but also likewise a direct effects of keratinocytes on endothelial cells to establish and form the network of capillary-like structures enable us to

generate relevant skin equivalents that closely emulate human anatomy and physiology. In the future, we can build on this approach aiming for fully vascularised skin equivalents.

# 6. OUTLOOK

## 6.1. Outlook

Significant efforts in tissue engineering are currently focused on the development of *in vitro* tissue engineered skin with more (patho)-physiological functions, in order to overcome the challenges with regards to resemblance to the complex human skin. So far, the limited applicability of conventional *in vitro* skin equivalents and strategies in preclinical research such as disease modelling and drug discovery, and basic research of skin biology can be explained by the fact that standard approaches do not recapitulate key components of the hierarchical architecture and dynamic nature of human tissues and organ function (Martinez et al., 2019). However, recent research of novel bioengineering tools, techniques and technologies has shifted towards more complex 3D *in vitro* skin equivalents in order to recreate a more realistic biochemical and biomechanical microenvironment (Duval et al., 2017).

For example, incorporating vasculature into bioengineered skin is essential for improving the lifespan, graftability, and for studying the systemic delivery of drugs from/to the skin (Abaci et al., 2017). Skin receives its essential nutrients and oxygen via the blood vessels spreading within the dermis. Therefore, the reconstruction blood vessels within a skin equivalent can improve the longevity of the model through supplying nutrients for the cultured cells. Although this thesis describes the successful formation of capillary-like network from endothelial cells in the skin equivalent, vascular system in *in vivo* human skin is much more complex and orchestrates a multitude of different cells such as pericytes in microvasculature and smooth muscle cells in the larger venules as well as resident perivascular leukocytes, including T cells, macrophages, mast cells, and dendritic cells (Braverman, 2000). Nevertheless, the precise mechanism of fibroblasts, endothelial cells and keratinocytes crosstalk which is critical for capillary-like structure formation is unknown at present. Therefore, incorporation of pericytes and/or smooth muscle cells would further increase the validity of vasculature in bioengineered skin. Moreover, cultivation of vascularized skin equivalents in dynamic perfusion platform would allow the continuous supply with oxygen and nutrients and would also increase the skin barrier homeostasis due to mechanical shear stress (Strüver et al., 2017).

During skin aging (Makrantonaki and Zouboulis, 2007), wound healing (Gurtner et al., 2008) and in different skin diseases such as skin cancer, psoriasis, atopic dermatitis and rosacea (Huggenberger and Detmar, 2011) changes are marked in ECM expression and production. Therefore, to study influence of diseased fibroblasts on ECM production and capillary-like network formation with employment of patient derived fibroblasts to produce their own ECM, co-cultured with endothelial cells and keratinocytes could be of interest for future studies.

From our preliminary data it is confirmed that fibroblasts release EVs – exosomes. Besides the importance of understanding the biomolecular cargo of these exosomes, specifically the proteins and mRNA, it would be interesting to determine the functional effect of fibroblasts-derived exosomes on keratinocytes by supplementing of *in vitro* skin equivalents (without fibroblasts) with them.

Overall, building the next generation skin constructs by including various skin components and patient-specific cells, while optimizing methodologies, integration with other organs and of biomarkers/biosensors for high-throughput readouts will revolutionize help in numerous areas of research on (patho)-physiological, pharmacological mechanisms and the early stages of drug development by creating reliable evaluations of patient-specific effects of pharmaceutical agents (Auger et al., 2000; Abaci et al., 2017).

# 7. REFERENCES

ABACI, H., GUO, Z., DOUCET, Y., JACKÓW, J. & CHRISTIANO, A. 2017. Next generation human skin constructs as advanced tools for drug development. *Experimental Biology and Medicine,* 242**,** 1657-1668.
ABD, E., YOUSEF, S. A., PASTORE, M. N., TELAPROLU, K., MOHAMMED, Y. H., NAMJOSHI, S., GRICE, J. E. & ROBERTS, M. S. 2016. Skin models for the testing of transdermal drugs. *Clinical pharmacology: advances and applications,* 8**,** 163.
AGARWAL, S. & KRISHNAMURTHY, K. 2019. Histology, skin. *StatPearls [Internet]. StatPearls Publishing*.
AISENBREY, E. A. & MURPHY, W. L. 2020. Synthetic alternatives to Matrigel. *Nature Reviews Materials***,** 1-13.
AKIYAMA, M. 2017. Corneocyte lipid envelope (CLE), the key structure for skin barrier function and ichthyosis pathogenesis. *Journal of Dermatological Science,* 88**,** 3-9.
ALI, N., HOSSEINI, M., VAINIO, S., TAIEB, A., CARIO-ANDRÉ, M. & REZVANI, H. 2015. Skin equivalents: skin from reconstructions as models to study skin development and diseases. *British Journal of Dermatology,* 173**,** 391-403.
ALMEIDA, A., SARMENTO, B. & RODRIGUES, F. 2017. Insights on in vitro models for safety and toxicity assessment of cosmetic ingredients. *International journal of pharmaceutics,* 519**,** 178-185.
ANDERSON, D. E. & HINDS, M. T. 2012. Extracellular matrix production and regulation in micropatterned endothelial cells. *Biochemical and biophysical research communications,* 427**,** 159-164.
ANDRÉE, B., ICHANTI, H., KALIES, S., HEISTERKAMP, A., STRAUß, S., VOGT, P.-M., HAVERICH, A. & HILFIKER, A. 2019. Formation of three-dimensional tubular endothelial cell networks under defined serum-free cell culture conditions in human collagen hydrogels. *Scientific reports,* 9**,** 1-11.
ANTOINE, E. E., VLACHOS, P. P. & RYLANDER, M. N. 2014. Review of collagen I hydrogels for bioengineered tissue microenvironments: characterization of mechanics, structure, and transport. *Tissue Engineering Part B: Reviews,* 20**,** 683-696.
ANTONI, D., BURCKEL, H., JOSSET, E. & NOEL, G. 2015. Three-dimensional cell culture: a breakthrough in vivo. *International journal of molecular sciences,* 16**,** 5517-5527.
ARDA, O., GÖKSÜGÜR, N. & TÜZÜN, Y. 2014. Basic histological structure and functions of facial skin. *Clinics in dermatology,* 32**,** 3-13.
ASSELINEAU, D. & PRUNIERAS, M. 1984. Reconstruction of 'simplified'skin: control of fabrication. *British Journal of Dermatology,* 111**,** 219-222.
ATIYEH, B. S. & COSTAGLIOLA, M. 2007. Cultured epithelial autograft (CEA) in burn treatment: three decades later. *Burns,* 33**,** 405-413.
AUGER, F. A., BERTHOD, F., MOULIN, V., POULIOT, R. & GERMAIN, L. 2004. Tissue-engineered skin substitutes: from in vitro constructs to in vivo applications. *Biotechnology and applied biochemistry,* 39**,** 263-275.
AUGER, F. A., POULIOT, R., TREMBLAY, N., GUIGNARD, R., NOËL, P., JUHASZ, J., GERMAIN, L. & GOULET, F. 2000. Multistep production of bioengineered skin substitutes: sequential modulation of culture conditions. *In Vitro Cellular & Developmental Biology-Animal,* 36**,** 96-103.
AUXENFANS, C., FRADETTE, J., LEQUEUX, C., GERMAIN, L., KINIKOGLU, F., BECHETOILLE, N., BRAYE, F., AUGER, F. & DAMOUR, O. 2009. Evolution of three dimensional skin equivalent models reconstructed in vitro by tissue engineering.
AVCI, P., SADASIVAM, M., GUPTA, A., DE MELO, W. C., HUANG, Y.-Y., YIN, R., CHANDRAN, R., KUMAR, R., OTUFOWORA, A. & NYAME, T. 2013. Animal models of skin disease for drug discovery. *Expert opinion on drug discovery,* 8**,** 331-355.
BACAKOVA, L., ZIKMUNDOVA, M., PAJOROVA, J., BROZ, A., FILOVA, E., BLANQUER, A., MATEJKA, R., STEPANOVSKA, J., MIKES, P. & JENCOVA, V. 2019. Nanofibrous scaffolds for skin tissue engineering and wound healing based on synthetic polymers. *Applications of Nanobiotechnology.* IntechOpen.

BARONI, A., BUOMMINO, E., DE GREGORIO, V., RUOCCO, E., RUOCCO, V. & WOLF, R. 2012. Structure and function of the epidermis related to barrier properties. *Clinics in dermatology,* 30**,** 257-262.
BARONI, A., BUOMMINO, E., DE GREGORIO, V., RUOCCO, E., RUOCCO, V. & WOLF, R. 2012. Structure and function of the epidermis related to barrier properties. *Clin Dermatol,* 30**,** 257-62.
BÄSLER, K., BERGMANN, S., HEISIG, M., NAEGEL, A., ZORN-KRUPPA, M. & BRANDNER, J. M. 2016. The role of tight junctions in skin barrier function and dermal absorption. *Journal of Controlled Release,* 242**,** 105-118.
BATAILLON, M., LELIÈVRE, D., CHAPUIS, A., THILLOU, F., AUTOURDE, J. B., DURAND, S., BOYERA, N., RIGAUDEAU, A.-S., BESNÉ, I. & PELLEVOISIN, C. 2019. Characterization of a new reconstructed full thickness skin model, T-Skin™, and its application for investigations of anti-aging compounds. *International journal of molecular sciences,* 20**,** 2240.
BECHETOILLE, N., VACHON, H., GAYDON, A., BOHER, A., FONTAINE, T., SCHAEFFER, E., DECOSSAS, M., ANDRÉ-FREI, V. & MUELLER, C. G. 2011. A new organotypic model containing dermal-type macrophages. *Experimental dermatology,* 20**,** 1035-1037.
BELL, E., EHRLICH, H. P., BUTTLE, D. J. & NAKATSUJI, T. 1981. Living tissue formed in vitro and accepted as skin-equivalent tissue of full thickness. *Science,* 211**,** 1052-1054.
BELLAS, E., MARRA, K. G. & KAPLAN, D. L. 2013. Sustainable three-dimensional tissue model of human adipose tissue. *Tissue Engineering Part C: Methods,* 19**,** 745-754.
BELLEMARE, J., ROBERGE, C. J., BERGERON, D., LOPEZ-VALLÉ, C. A., ROY, M. & MOULIN, V. J. 2005. Epidermis promotes dermal fibrosis: role in the pathogenesis of hypertrophic scars. *The Journal of Pathology: A Journal of the Pathological Society of Great Britain and Ireland,* 206**,** 1-8.
BENÍTEZ, J. M. & MONTÁNS, F. J. 2017. The mechanical behavior of skin: Structures and models for the finite element analysis. *Computers & Structures,* 190**,** 75-107.
BERGMANN, S., VON BUENAU, B., VIDAL-Y-SY, S., HAFTEK, M., WLADYKOWSKI, E., HOUDEK, P., LEZIUS, S., DUPLAN, H., BÄSLER, K. & DÄHNHARDT-PFEIFFER, S. 2020. Claudin-1 decrease impacts epidermal barrier function in atopic dermatitis lesions dose-dependently. *Scientific reports,* 10**,** 1-12.
BERROTH, A., KÜHNL, J., KURSCHAT, N., SCHWARZ, A., STÄB, F., SCHWARZ, T., WENCK, H., FÖLSTER-HOLST, R. & NEUFANG, G. 2013. Role of fibroblasts in the pathogenesis of atopic dermatitis. *Journal of allergy and clinical immunology,* 131**,** 1547-1554. e6.
BERTHIAUME, F., MAGUIRE, T. J. & YARMUSH, M. L. 2011. Tissue engineering and regenerative medicine: history, progress, and challenges. *Annual review of chemical and biomolecular engineering,* 2**,** 403-430.
BERTHOD, F., GERMAIN, L., TREMBLAY, N. & AUGER, F. A. 2006. Extracellular matrix deposition by fibroblasts is necessary to promote capillary-like tube formation in vitro. *Journal of cellular physiology,* 207**,** 491-498.
BI, H. & JIN, Y. 2013. Current progress of skin tissue engineering: Seed cells, bioscaffolds, and construction strategies. *Burns & trauma,* 1**,** 2321-3868.118928.
BLACK, A. F., BERTHOD, F., L'HEUREUX, N., GERMAIN, L. & AUGER, F. A. 1998. In vitro reconstruction of a human capillary-like network in a tissue-engineered skin equivalent. *The FASEB journal,* 12**,** 1331-1340.
BLACKWOOD, K. A., MCKEAN, R., CANTON, I., FREEMAN, C. O., FRANKLIN, K. L., COLE, D., BROOK, I., FARTHING, P., RIMMER, S. & HAYCOCK, J. W. 2008. Development of biodegradable electrospun scaffolds for dermal replacement. *Biomaterials,* 29**,** 3091-3104.
BLANPAIN, C. & FUCHS, E. 2009. Epidermal homeostasis: a balancing act of stem cells in the skin. *Nature reviews Molecular cell biology,* 10**,** 207-217.

BRANDNER, J. M. & SCHULZKE, J. D. 2015. Hereditary barrier-related diseases involving the tight junction: lessons from skin and intestine. *Cell and tissue research,* 360**,** 723-748.
BRAVERMAN, I. M. The cutaneous microcirculation. Journal of Investigative Dermatology Symposium Proceedings, 2000. Elsevier, 3-9.
BREITKREUTZ, D., KOXHOLT, I., THIEMANN, K. & NISCHT, R. 2013. Skin basement membrane: the foundation of epidermal integrity—BM functions and diverse roles of bridging molecules nidogen and perlecan. *BioMed research international,* 2013.
BROWN, T. M. & KRISHNAMURTHY, K. 2018. Histology, dermis. *StatPearls [Internet].* StatPearls Publishing.
BRUBAKER, D. K., PROCTOR, E. A., HAIGIS, K. M. & LAUFFENBURGER, D. A. 2019. Computational translation of genomic responses from experimental model systems to humans. *PLoS computational biology,* 15**,** e1006286.
CAMPITIELLO, E., DELLA CORTE, A., FATTOPACE, A., D'ACUNZI, D. & CANONICO, S. 2005. The use of artificial dermis in the treatment of chronic and acute wounds: regeneration of dermis and wound healing. *Acta Biomed,* 76**,** 69-71.
CANDI, E., SCHMIDT, R. & MELINO, G. 2005. The cornified envelope: a model of cell death in the skin. *Nature reviews Molecular cell biology,* 6**,** 328-340.
CARAVAGGI, C., DE GIGLIO, R., PRITELLI, C., SOMMARIA, M., DALLA NOCE, S., FAGLIA, E., MANTERO, M., CLERICI, G., FRATINO, P. & DALLA PAOLA, L. 2003. HYAFF 11-based autologous dermal and epidermal grafts in the treatment of noninfected diabetic plantar and dorsal foot ulcers: a prospective, multicenter, controlled, randomized clinical trial. *Diabetes care,* 26**,** 2853-2859.
CARVER, W. & GOLDSMITH, E. C. 2013. Regulation of tissue fibrosis by the biomechanical environment. *BioMed research international,* 2013.
CHABAUD, S., ROUSSEAU, A., MARCOUX, T. L. & BOLDUC, S. 2017. Inexpensive production of near-native engineered stromas. *Journal of tissue engineering and regenerative medicine,* 11**,** 1377-1389.
CHAUDHARI, A. A., VIG, K., BAGANIZI, D. R., SAHU, R., DIXIT, S., DENNIS, V., SINGH, S. R. & PILLAI, S. R. 2016. Future prospects for scaffolding methods and biomaterials in skin tissue engineering: a review. *International journal of molecular sciences,* 17**,** 1974.
CHAVEZ-MUÑOZ, C., KILANI, R. T. & GHAHARY, A. 2009. Profile of exosomes related proteins released by differentiated and undifferentiated human keratinocytes. *Journal of cellular physiology,* 221**,** 221-231.
CHERMNYKH, E., KALABUSHEVA, E. & VOROTELYAK, E. 2018. Extracellular matrix as a regulator of epidermal stem cell fate. *International journal of molecular sciences,* 19**,** 1003.
CICERO, A. L., STAHL, P. D. & RAPOSO, G. 2015. Extracellular vesicles shuffling intercellular messages: for good or for bad. *Current opinion in cell biology,* 35**,** 69-77.
COSTA-ALMEIDA, R., GOMEZ-LAZARO, M., RAMALHO, C., GRANJA, P. L., SOARES, R. & GUERREIRO, S. G. 2015. Fibroblast-endothelial partners for vascularization strategies in tissue engineering. *Tissue Engineering Part A,* 21**,** 1055-1065.
COULOMB, B., LEBRETON, C. & DUBERTRET, L. 1989. Influence of human dermal fibroblasts on epidermalization. *J Invest Dermatol,* 92**,** 122-5.
COULOMB, B., LEBRETON, C. & DUBERTRET, L. 1989. Influence of human dermal fibroblasts on epidermalization. *Journal of Investigative Dermatology,* 92**,** 122-125.
COX, T. R. & ERLER, J. T. 2011. Remodeling and homeostasis of the extracellular matrix: implications for fibrotic diseases and cancer. *Disease models & mechanisms,* 4**,** 165-178.
CRESCITELLI, R., LÄSSER, C., SZABÓ, T. G., KITTEL, A., ELDH, M., DIANZANI, I., BUZÁS, E. I. & LÖTVALL, J. 2013. Distinct RNA profiles in subpopulations of extracellular vesicles: apoptotic bodies, microvesicles and exosomes. *Journal of extracellular vesicles,* 2**,** 20677.

D'ISCHIA, M., WAKAMATSU, K., CICOIRA, F., DI MAURO, E., GARCIA-BORRON, J. C., COMMO, S., GALVÁN, I., GHANEM, G., KENZO, K. & MEREDITH, P. 2015. Melanins and melanogenesis: from pigment cells to human health and technological applications. *Pigment cell & melanoma research,* 28**,** 520-544.

DA SILVA, L. P., KUNDU, S. C., REIS, R. L. & CORRELO, V. M. 2020. Electric phenomenon: A disregarded tool in tissue engineering and regenerative medicine. *Trends in biotechnology,* 38**,** 24-49.

DELLAMBRA, E., ODORISIO, T., D'ARCANGELO, D., FAILLA, C. M. & FACCHIANO, A. 2019. Non-animal models in dermatological research. *ALTEX-Alternatives to animal experimentation,* 36**,** 177-202.

DIKICI, S., ALDEMIR DIKICI, B., BHALOO, S. I., BALCELLS, M., EDELMAN, E. R., MACNEIL, S., REILLY, G. C., SHERBORNE, C. & CLAEYSSENS, F. 2020. Assessment of the angiogenic potential of 2-deoxy-D-ribose using a novel in vitro 3D dynamic model in comparison with established in vitro assays. *Frontiers in Bioengineering and Biotechnology,* 7**,** 451.

DOYLE, L. M. & WANG, M. Z. 2019. Overview of extracellular vesicles, their origin, composition, purpose, and methods for exosome isolation and analysis. *Cells,* 8**,** 727.

DUVAL, C., CHAGNOLEAU, C., POURADIER, F., SEXTIUS, P., CONDOM, E. & BERNERD, F. 2012. Human skin model containing melanocytes: essential role of keratinocyte growth factor for constitutive pigmentation—Functional response to α-Melanocyte stimulating hormone and forskolin. *Tissue Engineering Part C: Methods,* 18**,** 947-957.

DUVAL, K., GROVER, H., HAN, L.-H., MOU, Y., PEGORARO, A. F., FREDBERG, J. & CHEN, Z. 2017. Modeling physiological events in 2D vs. 3D cell culture. *Physiology,* 32**,** 266-277.

ECKL, K.-M., ALEF, T., TORRES, S. & HENNIES, H. C. 2011. Full-thickness human skin models for congenital ichthyosis and related keratinization disorders. *Journal of investigative dermatology,* 131**,** 1938-1942.

EL-GHALBZOURI, A., GIBBS, S., LAMME, E., VAN BLITTERSWIJK, C. A. & PONEC, M. 2002. Effect of fibroblasts on epidermal regeneration. *Br J Dermatol,* 147**,** 230-43.

EL-SERAFI, A. T., EL-SERAFI, I. T., ELMASRY, M. & SJÖBERG, F. 2017. Skin regeneration in three dimensions, current status, challenges and opportunities. *Differentiation,* 96**,** 26-29.

EL-GHALBZOURI, A., GIBBS, S., LAMME, E., VAN BLITTERSWIJK, C. & PONEC, M. 2002. Effect of fibroblasts on epidermal regeneration. *British Journal of Dermatology,* 147**,** 230-243.

EL GHALBZOURI, A., COMMANDEUR, S., RIETVELD, M. H., MULDER, A. A. & WILLEMZE, R. 2009. Replacement of animal-derived collagen matrix by human fibroblast-derived dermal matrix for human skin equivalent products. *Biomaterials,* 30**,** 71-78.

EL GHALBZOURI, A., HENSBERGEN, P., GIBBS, S., KEMPENAAR, J., VAN DER SCHORS, R. & PONEC, M. 2004. Fibroblasts facilitate re-epithelialization in wounded human skin equivalents. *Laboratory investigation,* 84**,** 102-112.

EL GHALBZOURI, A., JONKMAN, M. F., DIJKMAN, R. & PONEC, M. 2005. Basement membrane reconstruction in human skin equivalents is regulated by fibroblasts and/or exogenously activated keratinocytes. *Journal of investigative dermatology,* 124**,** 79-86.

EL GHALBZOURI, A., LAMME, E. & PONEC, M. 2002. Crucial role of fibroblasts in regulating epidermal morphogenesis. *Cell and tissue research,* 310**,** 189-199.

EL GHALBZOURI, A., LAMME, E. & PONEC, M. 2002. Crucial role of fibroblasts in regulating epidermal morphogenesis. *Cell Tissue Res,* 310**,** 189-99.

ELIAS, P. M. & STEINHOFF, M. 2008. "Outside-to-inside"(and now back to "outside") pathogenic mechanisms in atopic dermatitis. *Journal of Investigative Dermatology,* 128**,** 1067-1070.

EZHKOVA, E., PASOLLI, H. A., PARKER, J. S., STOKES, N., SU, I.-H., HANNON, G., TARAKHOVSKY, A. & FUCHS, E. 2009. Ezh2 orchestrates gene expression for the stepwise differentiation of tissue-specific stem cells. *Cell,* 136**,** 1122-1135.
FEINGOLD, K. R. 2012. Lamellar bodies: the key to cutaneous barrier function. *Journal of Investigative Dermatology,* 132**,** 1951-1953.
FEINGOLD, K. R., SCHMUTH, M. & ELIAS, P. M. 2007. The regulation of permeability barrier homeostasis. *J Invest Dermatol,* 127**,** 1574-6.
FERRARA, N., GERBER, H.-P. & LECOUTER, J. 2003. The biology of VEGF and its receptors. *Nature medicine,* 9**,** 669-676.
FILIPE, V., HAWE, A. & JISKOOT, W. 2010. Critical evaluation of Nanoparticle Tracking Analysis (NTA) by NanoSight for the measurement of nanoparticles and protein aggregates. *Pharmaceutical research,* 27**,** 796-810.
FIMIANI, M., PIANIGIANI, E., DI SIMPLICIO, F. C., SBANO, P., CUCCIA, A., POMPELLA, G., DE ALOE, G. & PETRAGLIA, F. 2005. Other uses of homologous skin grafts and skin bank bioproducts. *Clinics in dermatology,* 23**,** 396-402.
FLAMANT, S. & TAMARAT, R. 2016. Extracellular vesicles and vascular injury: new insights for radiation exposure. *Radiation research,* 186**,** 203-218.
FLEISCHMAJER, R., UTANI, A., MACDONALD, E., PERLISH, J. S., PAN, T.-C., CHU, M.-L., NOMIZU, M., NINOMIYA, Y. & YAMADA, Y. 1998. Initiation of skin basement membrane formation at the epidermo-dermal interface involves assembly of laminins through binding to cell membrane receptors. *Journal of cell science,* 111**,** 1929-1940.
FRANZ, T., LEHMAN, P. & RANEY, S. 2009. Use of excised human skin to assess the bioequivalence of topical products. *Skin pharmacology and physiology,* 22**,** 276-286.
FREEMAN, A. E., IGEL, H. J., HERRMAN, B. J. & KLEINFELD, K. L. 1976. Growth and characterization of human skin epithelial cell cultures. *In vitro,* 12**,** 352-362.
GANGADARAN, P., RAJENDRAN, R. L., LEE, H. W., KALIMUTHU, S., HONG, C. M., JEONG, S. Y., LEE, S.-W., LEE, J. & AHN, B.-C. 2017. Extracellular vesicles from mesenchymal stem cells activates VEGF receptors and accelerates recovery of hindlimb ischemia. *Journal of Controlled Release,* 264**,** 112-126.
GARCIA, M., ESCAMEZ, M. J., CARRETERO, M., MIRONES, I., MARTINEZ-SANTAMARIA, L., NAVARRO, M., JORCANO, J. L., MEANA, A., DEL RIO, M. & LARCHER, F. 2007. Modeling normal and pathological processes through skin tissue engineering. *Molecular Carcinogenesis: Published in cooperation with the University of Texas MD Anderson Cancer Center,* 46**,** 741-745.
GARDINER, C., FERREIRA, Y. J., DRAGOVIC, R. A., REDMAN, C. W. & SARGENT, I. L. 2013. Extracellular vesicle sizing and enumeration by nanoparticle tracking analysis. *Journal of extracellular vesicles,* 2**,** 19671.
GERBER, P. A., BUHREN, B. A., SCHRUMPF, H., HOMEY, B., ZLOTNIK, A. & HEVEZI, P. 2014. The top skin-associated genes: a comparative analysis of human and mouse skin transcriptomes. *Biological chemistry,* 395**,** 577-591.
GHETTI, M., TOPOUZI, H., THEOCHARIDIS, G., PAPA, V., WILLIAMS, G., BONDIOLI, E., CENACCHI, G., CONNELLY, J. & HIGGINS, C. 2018. Subpopulations of dermal skin fibroblasts secrete distinct extracellular matrix: implications for using skin substitutes in the clinic. *British Journal of Dermatology,* 179**,** 381-393.
GOORIS, G., KAMRAN, M., KROS, A., MOORE, D. & BOUWSTRA, J. 2018. Interactions of dipalmitoylphosphatidylcholine with ceramide-based mixtures. *Biochimica et Biophysica Acta (BBA)-Biomembranes,* 1860**,** 1272-1281.
GORDON, S., DANESHIAN, M., BOUWSTRA, J., CALONI, F., CONSTANT, S., DAVIES, D. E., DANDEKAR, G., GUZMAN, C. A., FABIAN, E. & HALTNER, E. 2015. Non-animal models of epithelial barriers (skin, intestine and lung) in research, industrial applications and regulatory toxicology. *Altex,* 32**,** 327-378.
GRIFFITH, L. G. & NAUGHTON, G. 2002. Tissue engineering--current challenges and expanding opportunities. *science,* 295**,** 1009-1014.
GRIFFITHS, C., BARKER, J., BLEIKER, T. O., CHALMERS, R. & CREAMER, D. 2016. *Rook's textbook of dermatology*, John Wiley & Sons.

GROEBER, F., ENGELHARDT, L., LANGE, J., KURDYN, S., SCHMID, F. F., RÜCKER, C., MIELKE, S., WALLES, H. & HANSMANN, J. 2016. A first vascularized skin equivalent as an alternative to animal experimentation. *ALTEX-Alternatives to animal experimentation,* 33**,** 415-422.
GROEBER, F., KAHLIG, A., LOFF, S., WALLES, H. & HANSMANN, J. 2013. A bioreactor system for interfacial culture and physiological perfusion of vascularized tissue equivalents. *Biotechnology journal,* 8**,** 308-316.
GURTNER, G. C., WERNER, S., BARRANDON, Y. & LONGAKER, M. T. 2008. Wound repair and regeneration. *Nature,* 453**,** 314-321.
HAAKE, A., SCOTT, G. & HOLBROOK, K. 2001. Structure and function of the skin: overview of the epidermis and dermis. *The biology of the skin,* 2001**,** 19-45.
HARASZTI, R. A., DIDIOT, M.-C., SAPP, E., LESZYK, J., SHAFFER, S. A., ROCKWELL, H. E., GAO, F., NARAIN, N. R., DIFIGLIA, M. & KIEBISH, M. A. 2016. High-resolution proteomic and lipidomic analysis of exosomes and microvesicles from different cell sources. *Journal of extracellular vesicles,* 5**,** 32570.
HARDING, C. V., HEUSER, J. E. & STAHL, P. D. 2013. Exosomes: looking back three decades and into the future. *Journal of Cell Biology,* 200**,** 367-371.
HATA, R. I. & SENOO, H. 1989. L-ascorbic acid 2-phosphate stimulates collagen accumulation, cell proliferation, and formation of a three-dimensional tissuelike substance by skin fibroblasts. *Journal of cellular physiology,* 138**,** 8-16.
HENKLER, F., TRALAU, T., TENTSCHERT, J., KNEUER, C., HAASE, A., PLATZEK, T., LUCH, A. & GÖTZ, M. E. 2012. Risk assessment of nanomaterials in cosmetics: a European union perspective. *Archives of toxicology,* 86**,** 1641-1646.
HOARAU-VÉCHOT, J., RAFII, A., TOUBOUL, C. & PASQUIER, J. 2018. Halfway between 2D and animal models: are 3D cultures the ideal tool to study cancer-microenvironment interactions? *International journal of molecular sciences,* 19**,** 181.
HÖNZKE, S., WALLMEYER, L., OSTROWSKI, A., RADBRUCH, M., MUNDHENK, L., SCHÄFER-KORTING, M. & HEDTRICH, S. 2016. Influence of Th2 cytokines on the cornified envelope, tight junction proteins, and β-defensins in filaggrin-deficient skin equivalents. *Journal of Investigative Dermatology,* 136**,** 631-639.
HUANG, P., BI, J., OWEN, G. R., CHEN, W., ROKKA, A., KOIVISTO, L., HEINO, J., HÄKKINEN, L. & LARJAVA, H. 2015. Keratinocyte microvesicles regulate the expression of multiple genes in dermal fibroblasts. *Journal of Investigative Dermatology,* 135**,** 3051-3059.
HUDON, V., BERTHOD, F., BLACK, A., DAMOUR, O., GERMAIN, L. & AUGER, F. A. 2003. A tissue-engineered endothelialized dermis to study the modulation of angiogenic and angiostatic molecules on capillary-like tube formation in vitro. *British Journal of Dermatology,* 148**,** 1094-1104.
HUGGENBERGER, R. & DETMAR, M. The cutaneous vascular system in chronic skin inflammation. Journal of Investigative Dermatology Symposium Proceedings, 2011. Elsevier, 24-32.
HUH, D., HAMILTON, G. A. & INGBER, D. E. 2011. From 3D cell culture to organs-on-chips. *Trends in cell biology,* 21**,** 745-754.
IRACI, N., LEONARDI, T., GESSLER, F., VEGA, B. & PLUCHINO, S. 2016. Focus on extracellular vesicles: physiological role and signalling properties of extracellular membrane vesicles. *International journal of molecular sciences,* 17**,** 171.
ITOH, M., UMEGAKI-ARAO, N., GUO, Z., LIU, L., HIGGINS, C. A. & CHRISTIANO, A. M. 2013. Generation of 3D skin equivalents fully reconstituted from human induced pluripotent stem cells (iPSCs). *PloS one,* 8**,** e77673.
JAIN, R. K. 2003. Molecular regulation of vessel maturation. *Nature medicine,* 9**,** 685-693.
JAITLEY, S. & SARASWATHI, T. 2012. Pathophysiology of Langerhans cells. *Journal of oral and maxillofacial pathology: JOMFP,* 16**,** 239.
JAMES, W. D., BERGER, T. G. & ELSTON, D. M. 2006. Acne. Andrews' Diseases of the Skin. *Clinical Dermatology, 10th ed. Philadelphia, PA: Saunders/Elsevier Inc***,** 231-250.

JANSEN VAN RENSBURG, S., FRANKEN, A. & DU PLESSIS, J. L. 2019. Measurement of transepidermal water loss, stratum corneum hydration and skin surface pH in occupational settings: A review. *Skin Research and Technology,* 25**,** 595-605.
JEAN, J., GARCIA-PÉREZ, M. E. & POULIOT, R. 2011. Bioengineered skin: the self-assembly approach. *J Tissue Sci Eng S,* 5**,** 2.
JEVTIĆ, M., LÖWA, A., NOVÁČKOVÁ, A., KOVÁČIK, A., KAESSMEYER, S., ERDMANN, G., VÁVROVÁ, K. & HEDTRICH, S. 2020. Impact of intercellular crosstalk between epidermal keratinocytes and dermal fibroblasts on skin homeostasis. *Biochimica et Biophysica Acta (BBA)-Molecular Cell Research***,** 118722.
JIANG, B. & BREY, E. M. 2011. Formation of stable vascular networks in engineered tissues. *Regenerative Medicine and Tissue Engineering—Cells and Biomaterials***,** 477-502.
JODAT, Y. A., KANG, M. G., KIAEE, K., KIM, G. J., MARTINEZ, A. F., ROSENKRANZ, A., BAE, H. & SHIN, S. R. 2018. Human-derived organ-on-a-chip for personalized drug development. *Current pharmaceutical design,* 24**,** 5471-5486.
JOSEPH, J. S., MALINDISA, S. T. & NTWASA, M. 2018. Two-dimensional (2D) and three-dimensional (3D) cell culturing in drug discovery. *Cell. Culture,* 2**,** 1-22.
KAESSMEYER, S., SEHL, J., KHIAO IN, M., MERLE, R., RICHARDSON, K. & PLENDL, J. 2017. Subcellular interactions during vascular morphogenesis in 3D cocultures between endothelial cells and fibroblasts. *International journal of molecular sciences,* 18**,** 2590.
KALRA, H., DRUMMEN, G. P. & MATHIVANAN, S. 2016. Focus on extracellular vesicles: introducing the next small big thing. *International journal of molecular sciences,* 17**,** 170.
KAMEL, R. A., ONG, J. F., ERIKSSON, E., JUNKER, J. P. & CATERSON, E. J. 2013. Tissue engineering of skin. *Journal of the American College of Surgeons,* 217**,** 533-555.
KAO, B., KADOMATSU, K. & HOSAKA, Y. 2009. Construction of synthetic dermis and skin based on a self-assembled peptide hydrogel scaffold. *Tissue Engineering Part A,* 15**,** 2385-2396.
KAULLY, T., KAUFMAN-FRANCIS, K., LESMAN, A. & LEVENBERG, S. 2009. Vascularization—the conduit to viable engineered tissues. *Tissue Engineering Part B: Reviews,* 15**,** 159-169.
KHAVARI, P. A. 2006. Modelling cancer in human skin tissue. *Nature Reviews Cancer,* 6**,** 270-280.
KHIAO IN, M., WALLMEYER, L., HEDTRICH, S., RICHARDSON, K., PLENDL, J. & KAESSMEYER, S. 2015. The effect of endothelialization on the epidermal differentiation in human three-dimensional skin constructs–A morphological study. *Clinical Hemorheology and Microcirculation,* 61**,** 157-174.
KLAK, M., BRYNIARSKI, T., KOWALSKA, P., GOMOLKA, M., TYMICKI, G., KOSOWSKA, K., CYWONIUK, P., DOBRZANSKI, T., TUROWSKI, P. & WSZOLA, M. 2020. Novel Strategies in Artificial Organ Development: What Is the Future of Medicine? *Micromachines,* 11**,** 646.
KLICKS, J., VON MOLITOR, E., ERTONGUR-FAUTH, T., RUDOLF, R. & HAFNER, M. 2017. In vitro skin three-dimensional models and their applications. *Journal of Cellular Biotechnology,* 3**,** 21-39.
KNIGHT, E. & PRZYBORSKI, S. 2015. Advances in 3D cell culture technologies enabling tissue-like structures to be created in vitro. *Journal of anatomy,* 227**,** 746-756.
KOLARSICK, P. A., KOLARSICK, M. A. & GOODWIN, C. 2011. Anatomy and physiology of the skin. *Journal of the Dermatology Nurses' Association,* 3**,** 203-213.
KOSTEN, I. J., SPIEKSTRA, S. W., DE GRUIJL, T. D. & GIBBS, S. 2015. MUTZ-3 derived Langerhans cells in human skin equivalents show differential migration and phenotypic plasticity after allergen or irritant exposure. *Toxicology and Applied Pharmacology,* 287**,** 35-42.

KOVÁČIK, A., OPÁLKA, L., ŠILAROVÁ, M., ROH, J. & VÁVROVÁ, K. 2016. Synthesis of 6-hydroxyceramide using ruthenium-catalyzed hydrosilylation–protodesilylation. Unexpected formation of a long periodicity lamellar phase in skin lipid membranes. *RSC advances,* 6**,** 73343-73350.
KÜCHLER, S., HENKES, D., ECKL, K.-M., ACKERMANN, K., PLENDL, J., KORTING, H.-C., HENNIES, H.-C. & SCHÄFER-KORTING, M. 2011. Hallmarks of atopic skin mimicked in vitro by means of a skin disease model based on FLG knock-down. *Alternatives to Laboratory Animals,* 39**,** 471-480.
KÜCHLER, S., STRÜVER, K. & FRIESS, W. 2013. Reconstructed skin models as emerging tools for drug absorption studies. *Expert opinion on drug metabolism & toxicology,* 9**,** 1255-1263.
KÜHBACHER, A., BURGER-KENTISCHER, A. & RUPP, S. 2017. Interaction of Candida species with the skin. *Microorganisms,* 5**,** 32.
L'HEUREUX, N., PAQUET, S., LABBÉ, R., GERMAIN, L. & AUGER, F. A. 1998. A completely biological tissue-engineered human blood vessel. *The FASEB Journal,* 12**,** 47-56.
LAI-CHEONG, J. E. & MCGRATH, J. A. 2017. Structure and function of skin, hair and nails. *Medicine,* 45**,** 347-351.
LAMB, R. & AMBLER, C. A. 2013. Keratinocytes propagated in serum-free, feeder-free culture conditions fail to form stratified epidermis in a reconstituted skin model. *PloS one,* 8**,** e52494.
LANDI, A., GARAGNANI, L., LETI ACCIARO, A., LANDO, M., OZBEN, H. & GAGLIANO, M. 2014. Hyaluronic acid scaffold for skin defects in congenital syndactyly release surgery: a novel technique based on the regenerative model. *Journal of Hand Surgery (European Volume),* 39**,** 994-1000.
LANGER, R. & VACANTI, J. 1993. Tissue engineering. *Science,* 260**,** 920-926.
LAPLANTE, A. M., GERMAIN, L., AUGER, F. & MOULIN, V. 2001. Mechanisms of wound reepithelialization: hints from a tissue-engineered reconstructed skin to long-standing questions. *FASEB journal : official publication of the Federation of American Societies for Experimental Biology,* 15 13**,** 2377-89.
LEE, D.-Y., AHN, H.-T. & CHO, K.-H. 2000. A new skin equivalent model: dermal substrate that combines de-epidermized dermis with fibroblast-populated collagen matrix. *Journal of dermatological science,* 23**,** 132-137.
LEE, D.-Y. & CHO, K.-H. 2005. The effects of epidermal keratinocytes and dermal fibroblasts on the formation of cutaneous basement membrane in three-dimensional culture systems. *Archives of dermatological research,* 296**,** 296-302.
LI, P., KASLAN, M., LEE, S. H., YAO, J. & GAO, Z. 2017. Progress in exosome isolation techniques. *Theranostics,* 7**,** 789.
LINDE, N., GUTSCHALK, C. M., HOFFMANN, C., YILMAZ, D. & MUELLER, M. M. 2012. Integrating macrophages into organotypic co-cultures: a 3D in vitro model to study tumor-associated macrophages. *PloS one,* 7**,** e40058.
LIU, F., LUO, X. S., SHEN, H. Y., DONG, J. S. & YANG, J. 2011. Using human hair follicle-derived keratinocytes and melanocytes for constructing pigmented tissue-engineered skin. *Skin Research and Technology,* 17**,** 373-379.
LLAMES, S. G., DEL RIO, M., LARCHER, F., GARCÍA, E., GARCÍA, M., ESCAMEZ, M. J., JORCANO, J. L., HOLGUÍN, P. & MEANA, A. 2004. Human plasma as a dermal scaffold for the generation of a completely autologous bioengineered skin. *Transplantation,* 77**,** 350-355.
LOBB, R. J., BECKER, M., WEN WEN, S., WONG, C. S., WIEGMANS, A. P., LEIMGRUBER, A. & MÖLLER, A. 2015. Optimized exosome isolation protocol for cell culture supernatant and human plasma. *Journal of extracellular vesicles,* 4**,** 27031.
LÖTVALL, J., HILL, A. F., HOCHBERG, F., BUZÁS, E. I., DI VIZIO, D., GARDINER, C., GHO, Y. S., KUROCHKIN, I. V., MATHIVANAN, S. & QUESENBERRY, P. 2014. Minimal experimental requirements for definition of extracellular vesicles and their

functions: a position statement from the International Society for Extracellular Vesicles. Taylor & Francis.
LÖWA, A., GRAFF, P., KAESSMEYER, S. & HEDTRICH, S. 2020. Fibroblasts from atopic dermatitis patients trigger inflammatory processes and hyperproliferation in human skin equivalents. *Journal of the European Academy of Dermatology and Venereology*.
LÖWA, A., JEVTIĆ, M., GORREJA, F. & HEDTRICH, S. 2018. Alternatives to animal testing in basic and preclinical research of atopic dermatitis. *Experimental dermatology,* 27**,** 476-483.
MAAS-SZABOWSKI, N. & FUSENIG, N. E. 1996. Interleukin-1-induced growth factor expression in postmitotic and resting fibroblasts. *Journal of investigative dermatology,* 107**,** 849-855.
MAAS-SZABOWSKI, N., SHIMOTOYODOME, A. & FUSENIG, N. E. 1999. Keratinocyte growth regulation in fibroblast cocultures via a double paracrine mechanism. *Journal of cell science,* 112**,** 1843-1853.
MAAS-SZABOWSKI, N., SZABOWSKI, A., ANDRECHT, S., KOLBUS, A., SCHORPP-KISTNER, M., ANGEL, P., STARK, H.-J. & FUSENIG, N. E. 2001. Organotypic cocultures with genetically modified mouse fibroblasts as a tool to dissect molecular mechanisms regulating keratinocyte growth and differentiation. *Journal of Investigative Dermatology,* 116**,** 816-820.
MAKRANTONAKI, E. & ZOUBOULIS, C. 2007. Molecular mechanisms of skin aging: state of the art. *Annals of the New York Academy of Sciences,* 1119**,** 40-50.
MARINKOVICH, M. P., KEENE, D. R., RIMBERG, C. S. & BURGESON, R. E. 1993. Cellular origin of the dermal-epidermal basement membrane. *Developmental Dynamics,* 197**,** 255-267.
MARINO, D., LUGINBÜHL, J., SCOLA, S., MEULI, M. & REICHMANN, E. 2014. Bioengineering dermo-epidermal skin grafts with blood and lymphatic capillaries. *Science translational medicine,* 6**,** 221ra14-221ra14.
MARIONNET, C., PIERRARD, C., VIOUX-CHAGNOLEAU, C., SOK, J., ASSELINEAU, D. & BERNERD, F. 2006. Interactions between fibroblasts and keratinocytes in morphogenesis of dermal epidermal junction in a model of reconstructed skin. *Journal of investigative dermatology,* 126**,** 971-979.
MARTINEZ, E., ST-PIERRE, J.-P. & VARIOLA, F. 2019. Advanced bioengineering technologies for preclinical research. *Advances in Physics: X,* 4**,** 1622451.
MASSI, D. & PANELOS, J. 2012. Notch signaling and the developing skin epidermis. *Notch Signaling in Embryology and Cancer.* Springer.
MATHES, S. H., RUFFNER, H. & GRAF-HAUSNER, U. 2014. The use of skin models in drug development. *Advanced drug delivery reviews,* 69**,** 81-102.
MAZIO, C., CASALE, C., IMPARATO, G., URCIUOLO, F., ATTANASIO, C., DE GREGORIO, M., RESCIGNO, F. & NETTI, P. A. 2019. Pre-vascularized dermis model for fast and functional anastomosis with host vasculature. *Biomaterials,* 192**,** 159-170.
MAZZOLENI, G., DI LORENZO, D. & STEIMBERG, N. 2009. Modelling tissues in 3D: the next future of pharmaco-toxicology and food research? *Genes & nutrition,* 4**,** 13.
MENON, G. K., CLEARY, G. W. & LANE, M. E. 2012. The structure and function of the stratum corneum. *International journal of pharmaceutics,* 435**,** 3-9.
MERJANEH, M., LANGLOIS, A., LAROCHELLE, S., CLOUTIER, C. B., RICARD-BLUM, S. & MOULIN, V. J. 2017. Pro-angiogenic capacities of microvesicles produced by skin wound myofibroblasts. *Angiogenesis,* 20**,** 385-398.
MESTAS, J. & HUGHES, C. C. 2004. Of mice and not men: differences between mouse and human immunology. *The Journal of Immunology,* 172**,** 2731-2738.
MICHEL, M., L'HEUREUX, N., POULIOT, R., XU, W., AUGER, F. A. & GERMAIN, L. 1999. Characterization of a new tissue-engineered human skin equivalent with hair. *In Vitro Cellular & Developmental Biology-Animal,* 35**,** 318.

MISTRY, D. S., CHEN, Y., WANG, Y., ZHANG, K. & SEN, G. L. 2014. SNAI2 controls the undifferentiated state of human epidermal progenitor cells. *Stem Cells,* 32**,** 3209-3218.
MOJUMDAR, E., GOORIS, G., GROEN, D., BARLOW, D. J., LAWRENCE, M., DEMÉ, B. & BOUWSTRA, J. 2016. Stratum corneum lipid matrix: Location of acyl ceramide and cholesterol in the unit cell of the long periodicity phase. *Biochimica et Biophysica Acta (BBA)-Biomembranes,* 1858**,** 1926-1934.
MONFORT, A., SORIANO-NAVARRO, M., GARCÍA-VERDUGO, J. M. & IZETA, A. 2013. Production of human tissue-engineered skin trilayer on a plasma-based hypodermis. *Journal of tissue engineering and regenerative medicine,* 7**,** 479-490.
MONTAÑO, I., SCHIESTL, C., SCHNEIDER, J., PONTIGGIA, L., LUGINBÜHL, J., BIEDERMANN, T., BÖTTCHER-HABERZETH, S., BRAZIULIS, E., MEULI, M. & REICHMANN, E. 2010. Formation of human capillaries in vitro: the engineering of prevascularized matrices. *Tissue Engineering Part A,* 16**,** 269-282.
MUIZNIEKS, L. D. & KEELEY, F. W. 2013. Molecular assembly and mechanical properties of the extracellular matrix: A fibrous protein perspective. *Biochimica et Biophysica Acta (BBA)-Molecular Basis of Disease,* 1832**,** 866-875.
MURPHREE, R. W. 2017. Impairments in skin integrity. *Nursing Clinics,* 52**,** 405-417.
NAGASE, H., VISSE, R. & MURPHY, G. 2006. Structure and function of matrix metalloproteinases and TIMPs. *Cardiovascular research,* 69**,** 562-573.
NAKAZAWA, K., KALASSY, M., SAHUC, F., COLLOMBEL, C. & DAMOUR, O. 1998. Pigmented human skin equivalent—as a model of the mechanisms of control of cell-cell and cell-matrix interactions. *Medical and Biological Engineering and Computing,* 36**,** 813-820.
NAWAZ, M. & FATIMA, F. 2017. Extracellular vesicles, tunneling nanotubes, and cellular interplay: synergies and missing links. *Frontiers in molecular biosciences,* 4**,** 50.
NEVE, A., CANTATORE, F. P., MARUOTTI, N., CORRADO, A. & RIBATTI, D. 2014. Extracellular matrix modulates angiogenesis in physiological and pathological conditions. *BioMed research international,* 2014.
NGUYEN, A. V. & SOULIKA, A. M. 2019. The dynamics of the skin's immune system. *International journal of molecular sciences,* 20**,** 1811.
NIEHUES, H., BOUWSTRA, J. A., EL GHALBZOURI, A., BRANDNER, J. M., ZEEUWEN, P. L. & VAN DEN BOGAARD, E. H. 2018. 3D skin models for 3R research: The potential of 3D reconstructed skin models to study skin barrier function. *Experimental dermatology,* 27**,** 501-511.
O'BRIEN, F. J. 2011. Biomaterials & scaffolds for tissue engineering. *Materials today,* 14**,** 88-95.
OPÁLKA, L. S., KOVÁČIK, A., SOCHOROVÁ, M., ROH, J., KUNES, J., LENČO, J. & VÁVROVÁ, K. I. 2015. Scalable synthesis of human ultralong chain ceramides. *Organic Letters,* 17**,** 5456-5459.
OSUCHOWSKI, M. F., REMICK, D. G., LEDERER, J. A., LANG, C. H., AASEN, A. O., AIBIKI, M., AZEVEDO, L. C., BAHRAMI, S., BOROS, M. & COONEY, R. 2014. Abandon the mouse research ship? Not just yet! *Shock (Augusta, Ga.),* 41**,** 463.
OUWEHAND, K., SPIEKSTRA, S., WAAIJMAN, T., SCHEPER, R., DE GRUIJL, T. & GIBBS, S. 2011. Langerhans cells derived from a human cell line in a full-thickness skin equivalent undergo allergen-induced maturation and migration. *Tech Adv,* 90**,** 1028-33.
PANACCHIA, L., DELLAMBRA, E., BONDANZA, S., PATERNA, P., MAURELLI, R., PAIONNI, E. & GUERRA, L. 2010. Nonirradiated human fibroblasts and irradiated 3T3-J2 murine fibroblasts as a feeder layer for keratinocyte growth and differentiation in vitro on a fibrin substrate. *Cells Tissues Organs,* 191**,** 21-35.
PARENTEAU-BAREIL, R., GAUVIN, R. & BERTHOD, F. 2010. Collagen-based biomaterials for tissue engineering applications. *Materials,* 3**,** 1863-1887.
PFUHLER, S., FAUTZ, R., OUEDRAOGO, G., LATIL, A., KENNY, J., MOORE, C., DIEMBECK, W., HEWITT, N., REISINGER, K. & BARROSO, J. 2014. The

Cosmetics Europe strategy for animal-free genotoxicity testing: Project status update. *Toxicology in Vitro,* 28**,** 18-23.
PITT, J. M., KROEMER, G. & ZITVOGEL, L. 2016. Extracellular vesicles: masters of intercellular communication and potential clinical interventions. *The Journal of clinical investigation,* 126**,** 1139-1143.
PONEC, M., WEERHEIM, A., KEMPENAAR, J., MOMMAAS, A.-M. & NUGTEREN, D. H. 1988. Lipid composition of cultured human keratinocytes in relation to their differentiation. *Journal of lipid research,* 29**,** 949-961.
PONEC, M., WEERHEIM, A., KEMPENAAR, J., MULDER, A., GOORIS, G. S., BOUWSTRA, J. & MOMMAAS, A. M. 1997. The formation of competent barrier lipids in reconstructed human epidermis requires the presence of vitamin C. *Journal of investigative dermatology,* 109**,** 348-355.
POPOV, L., KOVALSKI, J., GRANDI, G., BAGNOLI, F. & AMIEVA, M. R. 2014. Three-dimensional human skin models to understand Staphylococcus aureus skin colonization and infection. *Frontiers in immunology,* 5**,** 41.
POULIOT, R., LAROUCHE, D., AUGER, F. A., JUHASZ, J., XU, W., LI, H. & GERMAIN, L. 2002. Reconstructed human skin produced in vitro and grafted on athymic mice1, 2. *Transplantation,* 73**,** 1751-1757.
PRUNIÉRAS, M., RÉGNIER, M. & WOODLEY, D. 1983. Methods for cultivation of keratinocytes with an air-liquid interface. *Journal of investigative dermatology,* 81**,** S28-S33.
PULLMANNOVÁ, P., STAŇKOVÁ, K., POSPÍŠILOVÁ, M., ŠKOLOVÁ, B., ZBYTOVSKÁ, J. & VÁVROVÁ, K. 2014. Effects of sphingomyelin/ceramide ratio on the permeability and microstructure of model stratum corneum lipid membranes. *Biochimica et Biophysica Acta (BBA)-Biomembranes,* 1838**,** 2115-2126.
RAFII, S., BUTLER, J. M. & DING, B.-S. 2016. Angiocrine functions of organ-specific endothelial cells. *Nature,* 529**,** 316-325.
RAPOSO, G. & STOORVOGEL, W. 2013. Extracellular vesicles: exosomes, microvesicles, and friends. *Journal of Cell Biology,* 200**,** 373-383.
RATUSHNY, V., GOBER, M. D., HICK, R., RIDKY, T. W. & SEYKORA, J. T. 2012. From keratinocyte to cancer: the pathogenesis and modeling of cutaneous squamous cell carcinoma. *The Journal of clinical investigation,* 122**,** 464-472.
REIJNDERS, C. M., VAN LIER, A., ROFFEL, S., KRAMER, D., SCHEPER, R. J. & GIBBS, S. 2015. Development of a full-thickness human skin equivalent in vitro model derived from TERT-immortalized keratinocytes and fibroblasts. *Tissue Engineering Part A,* 21**,** 2448-2459.
REIS, L., CHIU, L. L., FERIC, N., FU, L. & RADISIC, M. 2014. Injectable biomaterials for cardiac regeneration and repair. *Cardiac Regeneration and Repair.* Elsevier.
RHEINWALD, J. G. & GREEN, H. 1975. Formation of a keratinizing epithelium in culture by a cloned cell line derived from a teratoma. *Cell,* 6**,** 317-330.
RHODES, J. M. & SIMONS, M. 2007. The extracellular matrix and blood vessel formation: not just a scaffold. *Journal of cellular and molecular medicine,* 11**,** 176-205.
ROBINSON, M., COHEN, C., DE FRAISSINETTE, A. D. B., PONEC, M., WHITTLE, E. & FENTEM, J. 2002. Non-animal testing strategies for assessment of the skin corrosion and skin irritation potential of ingredients and finished products. *Food and chemical toxicology,* 40**,** 573-592.
ROCHON, M.-H., FRADETTE, J., FORTIN, V., TOMASETIG, F., ROBERGE, C. J., BAKER, K., BERTHOD, F., AUGER, F. A. & GERMAIN, L. 2010. Normal human epithelial cells regulate the size and morphology of tissue-engineered capillaries. *Tissue Engineering Part A,* 16**,** 1457-1468.
ROGER, M., FULLARD, N., COSTELLO, L., BRADBURY, S., MARKIEWICZ, E., O'REILLY, S., DARLING, N., RITCHIE, P., MÄÄTTÄ, A. & KARAKESISOGLOU, I. 2019. Bioengineering the microanatomy of human skin. *Journal of anatomy,* 234**,** 438-455.
RONFARD, V., RIVES, J.-M., NEVEUX, Y., CARSIN, H. & BARRANDON, Y. 2000. Long-term regeneration of human epidermis on third degree burns transplanted with

autologous cultured epithelium grown on a fibrin matrix1, 2. *Transplantation,* 70**,** 1588-1598.
ROOSTERMAN, D., GOERGE, T., SCHNEIDER, S. W., BUNNETT, N. W. & STEINHOFF, M. 2006. Neuronal control of skin function: the skin as a neuroimmunoendocrine organ. *Physiological reviews,* 86**,** 1309-1379.
RUTTER, B. D. & INNES, R. W. 2017. Extracellular vesicles isolated from the leaf apoplast carry stress-response proteins. *Plant physiology,* 173**,** 728-741.
SABA, I., JAKUBOWSKA, W., BOLDUC, S. & CHABAUD, S. 2018. Engineering tissues without the use of a synthetic scaffold: a twenty-year history of the self-assembly method. *BioMed Research International,* 2018.
SADIK, N., CRUZ, L., GURTNER, A., RODOSTHENOUS, R. S., DUSOSWA, S. A., ZIEGLER, O., VAN SOLINGE, T. S., WEI, Z., SALVADOR-GARICANO, A. M. & GYORGY, B. 2018. Extracellular RNAs: a new awareness of old perspectives. *Extracellular RNA.* Springer.
SAEED, A. I., BHAGABATI, N. K., BRAISTED, J. C., LIANG, W., SHAROV, V., HOWE, E. A., LI, J., THIAGARAJAN, M., WHITE, J. A. & QUACKENBUSH, J. 2006. TM4 microarray software suite. *Methods Enzymol,* 411**,** 134-93.
SAHOTA, P. S., BURN, J. L., HEATON, M., FREEDLANDER, E., SUVARNA, S. K., BROWN, N. J. & MAC NEIL, S. 2003. Development of a reconstructed human skin model for angiogenesis. *Wound repair and regeneration,* 11**,** 275-284.
SASINE, J. P., YEO, K. T. & CHUTE, J. P. 2017. Concise review: paracrine functions of vascular niche cells in regulating hematopoietic stem cell fate. *Stem cells translational medicine,* 6**,** 482-489.
SAVOJI, H., GODAU, B., HASSANI, M. S. & AKBARI, M. 2018. Skin tissue substitutes and biomaterial risk assessment and testing. *Frontiers in bioengineering and biotechnology,* 6**,** 86.
SCHECHNER, J. S., CRANE, S. K., WANG, F., SZEGLIN, A. M., TELLIDES, G., LORBER, M. I., BOTHWELL, A. L. & POBER, J. S. 2003. Engraftment of a vascularized human skin equivalent. *The FASEB journal,* 17**,** 2250-2256.
SCHECHNER, J. S., NATH, A. K., ZHENG, L., KLUGER, M. S., HUGHES, C. C., SIERRA-HONIGMANN, M. R., LORBER, M. I., TELLIDES, G., KASHGARIAN, M. & BOTHWELL, A. L. 2000. In vivo formation of complex microvessels lined by human endothelial cells in an immunodeficient mouse. *Proceedings of the National Academy of Sciences,* 97**,** 9191-9196.
SCHMOOK, F. P., MEINGASSNER, J. G. & BILLICH, A. 2001. Comparison of human skin or epidermis models with human and animal skin in in-vitro percutaneous absorption. *International journal of pharmaceutics,* 215**,** 51-56.
SCHREIBER, S., MAHMOUD, A., VUIA, A., RÜBBELKE, M., SCHMIDT, E., SCHALLER, M., KANDAROVA, H., HABERLAND, A., SCHÄFER, U. & BOCK, U. 2005. Reconstructed epidermis versus human and animal skin in skin absorption studies. *Toxicology in vitro,* 19**,** 813-822.
SEMLIN, L., SCHÄFER-KORTING, M., BORELLI, C. & KORTING, H. C. 2011. In vitro models for human skin disease. *Drug discovery today,* 16**,** 132-139.
SEOK, J., WARREN, H. S., CUENCA, A. G., MINDRINOS, M. N., BAKER, H. V., XU, W., RICHARDS, D. R., MCDONALD-SMITH, G. P., GAO, H. & HENNESSY, L. 2013. Genomic responses in mouse models poorly mimic human inflammatory diseases. *Proceedings of the National Academy of Sciences,* 110**,** 3507-3512.
SERBAN, M. A., LIU, Y. & PRESTWICH, G. D. 2008. Effects of extracellular matrix analogues on primary human fibroblast behavior. *Acta biomaterialia,* 4**,** 67-75.
SHIOHARA, T., HAYAKAWA, J. & MIZUKAWA, Y. 2004. Animal models for atopic dermatitis: are they relevant to human disease? *Journal of dermatological science,* 36**,** 1-9.
SIMON, F., BERGERON, D., LAROCHELLE, S., LOPEZ-VALLÉ, C. A., GENEST, H., ARMOUR, A. & MOULIN, V. J. 2012. Enhanced secretion of TIMP-1 by human hypertrophic scar keratinocytes could contribute to fibrosis. *Burns,* 38**,** 421-427.

SIMPSON, C. L., PATEL, D. M. & GREEN, K. J. 2011. Deconstructing the skin: cytoarchitectural determinants of epidermal morphogenesis. *Nature reviews Molecular cell biology,* 12**,** 565-580.
SKARDAL, A., SHUPE, T. & ATALA, A. 2016. Organoid-on-a-chip and body-on-a-chip systems for drug screening and disease modeling. *Drug discovery today,* 21**,** 1399-1411.
SMOLA, H., STARK, H.-J., THIEKÖTTER, G., MIRANCEA, N., KRIEG, T. & FUSENIG, N. E. 1998. Dynamics of basement membrane formation by keratinocyte–fibroblast interactions in organotypic skin culture. *Experimental cell research,* 239**,** 399-410.
SMOLA, H., THIEKÖTTER, G. & FUSENIG, N. E. 1993. Mutual induction of growth factor gene expression by epidermal-dermal cell interaction. *The Journal of cell biology,* 122**,** 417-429.
SOBRAL, C. S., GRAGNANI, A., CAO, X., MORGAN, J. R. & FERREIRA, L. M. 2007. Human keratinocytes cultured on collagen matrix used as an experimental burn model. *Journal of Burns and Wounds,* 7.
SOCHOROVÁ, M., STAŇKOVÁ, K., PULLMANNOVÁ, P., KOVÁČIK, A., ZBYTOVSKÁ, J. & VÁVROVÁ, K. 2017. Permeability barrier and microstructure of skin lipid membrane models of impaired glucosylceramide processing. *Scientific reports,* 7**,** 1-8.
SORRELL, J. M. & CAPLAN, A. I. 2004. Fibroblast heterogeneity: more than skin deep. *Journal of cell science,* 117**,** 667-675.
SORRELL, J. M. & CAPLAN, A. I. 2009. Fibroblasts—a diverse population at the center of it all. *International review of cell and molecular biology,* 276**,** 161-214.
SOUCY, P. A. & ROMER, L. H. 2009. Endothelial cell adhesion, signaling, and morphogenesis in fibroblast-derived matrix. *Matrix Biology,* 28**,** 273-283.
SPIEKSTRA, S. W., BREETVELD, M., RUSTEMEYER, T., SCHEPER, R. J. & GIBBS, S. 2007. Wound-healing factors secreted by epidermal keratinocytes and dermal fibroblasts in skin substitutes. *Wound Repair and Regeneration,* 15**,** 708-717.
SRIRAM, G., ALBERTI, M., DANCIK, Y., WU, B., WU, R., FENG, Z., RAMASAMY, S., BIGLIARDI, P. L., BIGLIARDI-QI, M. & WANG, Z. 2018. Full-thickness human skin-on-chip with enhanced epidermal morphogenesis and barrier function. *Materials Today,* 21**,** 326-340.
SRIRAM, G., BIGLIARDI, P. L. & BIGLIARDI-QI, M. 2015. Fibroblast heterogeneity and its implications for engineering organotypic skin models in vitro. *European journal of cell biology,* 94**,** 483-512.
STARK, H.-J., BOEHNKE, K., MIRANCEA, N., WILLHAUCK, M. J., PAVESIO, A., FUSENIG, N. E. & BOUKAMP, P. Epidermal homeostasis in long-term scaffold-enforced skin equivalents. Journal of Investigative Dermatology Symposium Proceedings, 2006. Elsevier, 93-105.
STRÜVER, K., FRIESS, W. & HEDTRICH, S. 2017. Development of a perfusion platform for dynamic cultivation of in vitro skin models. *Skin Pharmacology and Physiology,* 30**,** 180-189.
SUHAIL, Y., CAIN, M. P., VANAJA, K., KURYWCHAK, P. A., LEVCHENKO, A. & KALLURI, R. 2019. Systems biology of cancer metastasis. *Cell systems,* 9**,** 109-127.
SUPP, D. M., BELL, S. M., MORGAN, J. R. & BOYCE, S. T. 2000. Genetic modification of cultured skin substitutes by transduction of human keratinocytes and fibroblasts with platelet-derived growth factor-A. *Wound Repair and Regeneration,* 8**,** 26-35.
SUPP, D. M., KARPINSKI, A. C. & BOYCE, S. T. 2004. Vascular endothelial growth factor overexpression increases vascularization by murine but not human endothelial cells in cultured skin substitutes grafted to athymic mice. *The Journal of burn care & rehabilitation,* 25**,** 337-345.
SUPP, D. M., SUPP, A. P., BOYCE, S. T. & BELL, S. M. 2000. Enhanced vascularization of cultured skin substitutes genetically modified to overexpress vascular endothelial growth factor. *Journal of investigative dermatology,* 114**,** 5-13.

SUPP, D. M., WILSON-LANDY, K. & BOYCE, S. T. 2002. Human dermal microvascular endothelial cells form vascular analogs in cultured skin substitutes after grafting to athymic mice. *The FASEB Journal,* 16**,** 797-804.

SWITZER, B. R. & SUMMER, G. K. 1972. Collagen synthesis in human skin fibroblasts: effects of ascorbate, α-ketoglutarate and ferrous ion on proline hydroxylation. *The journal of nutrition,* 102**,** 721-728.

TARABOLETTI, G., D'ASCENZO, S., BORSOTTI, P., GIAVAZZI, R., PAVAN, A. & DOLO, V. 2002. Shedding of the matrix metalloproteinases MMP-2, MMP-9, and MT1-MMP as membrane vesicle-associated components by endothelial cells. *The American journal of pathology,* 160**,** 673-680.

TEIMOURI, A., YEUNG, P. & AGU, R. 2018. 2D vs. 3D cell culture models for in vitro topical (dermatological) medication testing. *Cell Culture.* IntechOpen.

THAKOERSING, V. S., GOORIS, G. S., MULDER, A., RIETVELD, M., EL GHALBZOURI, A. & BOUWSTRA, J. A. 2012. Unraveling barrier properties of three different in-house human skin equivalents. *Tissue Engineering Part C: Methods,* 18**,** 1-11.

THÉRY, C., AMIGORENA, S., RAPOSO, G. & CLAYTON, A. 2006. Isolation and characterization of exosomes from cell culture supernatants and biological fluids. *Current protocols in cell biology,* 30**,** 3.22. 1-3.22. 29.

THÉRY, C., WITWER, K. W., AIKAWA, E., ALCARAZ, M. J., ANDERSON, J. D., ANDRIANTSITOHAINA, R., ANTONIOU, A., ARAB, T., ARCHER, F. & ATKIN-SMITH, G. K. 2018. Minimal information for studies of extracellular vesicles 2018 (MISEV2018): a position statement of the International Society for Extracellular Vesicles and update of the MISEV2014 guidelines. *Journal of extracellular vesicles,* 7**,** 1535750.

TINOIS, E., TIOLLIER, J., GAUCHERAND, M., DUMAS, H., TARDY, M. & THIVOLET, J. 1991. In vitro and post-transplantation differentiation of human keratinocytes grown on the human type IV collagen film of a bilayered dermal substitute. *Experimental cell research,* 193**,** 310-319.

TONELLO, C., VINDIGNI, V., ZAVAN, B., ABATANGELO, S., ABATANGELO, G., BRUN, P. & CORTIVO, R. 2005. In vitro reconstruction of an endothelialized skin substitute provided with a microcapillary network using biopolymer scaffolds. *The FASEB journal,* 19**,** 1546-1548.

TONELLO, C., ZAVAN, B., CORTIVO, R., BRUN, P., PANFILO, S. & ABATANGELO, G. 2003. In vitro reconstruction of human dermal equivalent enriched with endothelial cells. *Biomaterials,* 24**,** 1205-1211.

TRACY, L. E., MINASIAN, R. A. & CATERSON, E. 2016. Extracellular matrix and dermal fibroblast function in the healing wound. *Advances in wound care,* 5**,** 119-136.

TRAMPEZINSKI, S., BERTHIER-VERGNES, O., DENIS, A., SCHMITT, D. & VIAC, J. 2004. Comparative expression of vascular endothelia growth factor family members, VEGF-B,-C, and-D, by normal human keratinocytes and fibroblasts. *Exp. Dermatol,* 13**,** 98-105.

TREINDL, F., RUPRECHT, B., BEITER, Y., SCHULTZ, S., DOTTINGER, A., STAEBLER, A., JOOS, T. O., KLING, S., POETZ, O., FEHM, T., NEUBAUER, H., KUSTER, B. & TEMPLIN, M. F. 2016. A bead-based western for high-throughput cellular signal transduction analyses. *Nat Commun,* 7**,** 12852.

TREMBLAY, P. L., HUDON, V., BERTHOD, F., GERMAIN, L. & AUGER, F. A. 2005. Inosculation of tissue-engineered capillaries with the host's vasculature in a reconstructed skin transplanted on mice. *American journal of transplantation,* 5**,** 1002-1010.

TROTTIER, V., MARCEAU-FORTIER, G., GERMAIN, L., VINCENT, C. & FRADETTE, J. 2008. IFATS collection: Using human adipose-derived stem/stromal cells for the production of new skin substitutes. *Stem cells,* 26**,** 2713-2723.

TURCHINOVICH, A., DRAPKINA, O. & TONEVITSKY, A. 2019. Transcriptome of extracellular vesicles: state-of-the-art. *Frontiers in immunology,* 10**,** 202.

URCIUOLO, F., CASALE, C., IMPARATO, G. & NETTI, P. A. 2019. Bioengineered skin substitutes: the role of extracellular matrix and vascularization in the healing of deep wounds. *Journal of Clinical Medicine,* 8**,** 2083.
URIEL, S., LABAY, E., FRANCIS-SEDLAK, M., MOYA, M. L., WEICHSELBAUM, R. R., ERVIN, N., CANKOVA, Z. & BREY, E. M. 2009. Extraction and assembly of tissue-derived gels for cell culture and tissue engineering. *Tissue Engineering Part C: Methods,* 15**,** 309-321.
VACANTI, C. A. 2006. The history of tissue engineering. *Journal of cellular and molecular medicine*.
VALADI, H., EKSTRÖM, K., BOSSIOS, A., SJÖSTRAND, M., LEE, J. J. & LÖTVALL, J. O. 2007. Exosome-mediated transfer of mRNAs and microRNAs is a novel mechanism of genetic exchange between cells. *Nature cell biology,* 9**,** 654-659.
VAN DEN BOGAARD, E. H., TJABRINGA, G. S., JOOSTEN, I., VONK-BERGERS, M., VAN RIJSSEN, E., TIJSSEN, H. J., ERKENS, M., SCHALKWIJK, J. & KOENEN, H. J. 2014. Crosstalk between keratinocytes and T cells in a 3D microenvironment: a model to study inflammatory skin diseases. *Journal of Investigative Dermatology,* 134**,** 719-727.
VAN DEN BROEK, L. J., NIESSEN, F. B., SCHEPER, R. J. & GIBBS, S. 2012. Development, validation and testing of a human tissue engineered hypertrophic scar model. *Altex,* 29**,** 389-402.
VAN DOREN, S. R. 2015. Matrix metalloproteinase interactions with collagen and elastin. *Matrix Biology,* 44**,** 224-231.
VAN GELE, M., GEUSENS, B., BROCHEZ, L., SPEECKAERT, R. & LAMBERT, J. 2011. Three-dimensional skin models as tools for transdermal drug delivery: challenges and limitations. *Expert opinion on drug delivery,* 8**,** 705-720.
VAN NIEL, G., D'ANGELO, G. & RAPOSO, G. 2018. Shedding light on the cell biology of extracellular vesicles. *Nature reviews Molecular cell biology,* 19**,** 213.
VAN SMEDEN, J., JANSSENS, M., GOORIS, G. & BOUWSTRA, J. 2014. The important role of stratum corneum lipids for the cutaneous barrier function. *Biochimica et Biophysica Acta (BBA)-Molecular and Cell Biology of Lipids,* 1841**,** 295-313.
VARKEY, M., DING, J. & TREDGET, E. E. 2014. Superficial dermal fibroblasts enhance basement membrane and epidermal barrier formation in tissue-engineered skin: implications for treatment of skin basement membrane disorders. *Tissue Engineering Part A,* 20**,** 540-552.
VÁVROVÁ, K., HENKES, D., STRÜVER, K., SOCHOROVÁ, M., ŠKOLOVÁ, B., WITTING, M. Y., FRIESS, W., SCHREML, S., MEIER, R. J. & SCHAEFER-KORTING, M. 2014. Filaggrin deficiency leads to impaired lipid profile and altered acidification pathways in a 3D skin construct. *Journal of Investigative Dermatology,* 134**,** 746-753.
VAVROVA, K., HENKES, D., STRUVER, K., SOCHOROVA, M., SKOLOVA, B., WITTING, M. Y., FRIESS, W., SCHREML, S., MEIER, R. J., SCHAFER-KORTING, M., FLUHR, J. W. & KUCHLER, S. 2014. Filaggrin deficiency leads to impaired lipid profile and altered acidification pathways in a 3D skin construct. *J Invest Dermatol,* 134**,** 746-753.
VEVES, A., FALANGA, V., ARMSTRONG, D. G. & SABOLINSKI, M. L. 2001. Graftskin, a human skin equivalent, is effective in the management of noninfected neuropathic diabetic foot ulcers: a prospective randomized multicenter clinical trial. *Diabetes care,* 24**,** 290-295.
VIDAL, S. E. L., TAMAMOTO, K. A., NGUYEN, H., ABBOTT, R. D., CAIRNS, D. M. & KAPLAN, D. L. 2019. 3D biomaterial matrix to support long term, full thickness, immuno-competent human skin equivalents with nervous system components. *Biomaterials,* 198**,** 194-203.
VIDAL YUCHA, S. E., TAMAMOTO, K. A. & KAPLAN, D. L. 2019. The importance of the neuro-immuno-cutaneous system on human skin equivalent design. *Cell proliferation,* 52**,** e12677.

VLASSOV, A. V., MAGDALENO, S., SETTERQUIST, R. & CONRAD, R. 2012. Exosomes: current knowledge of their composition, biological functions, and diagnostic and therapeutic potentials. *Biochimica et Biophysica Acta (BBA)-General Subjects,* 1820**,** 940-948.

WALLMEYER, L., DIETERT, K., SOCHOROVÁ, M., GRUBER, A. D., KLEUSER, B., VÁVROVÁ, K. & HEDTRICH, S. 2017. TSLP is a direct trigger for T cell migration in filaggrin-deficient skin equivalents. *Scientific reports,* 7**,** 1-12.

WALLMEYER, L., LEHNEN, D., EGER, N., SOCHOROVA, M., OPALKA, L., KOVACIK, A., VAVROVA, K. & HEDTRICH, S. 2015. Stimulation of PPARalpha normalizes the skin lipid ratio and improves the skin barrier of normal and filaggrin deficient reconstructed skin. *J Dermatol Sci,* 80**,** 102-10.

WÄSTER, P., ERIKSSON, I., VAINIKKA, L., ROSDAHL, I. & ÖLLINGER, K. 2016. Extracellular vesicles are transferred from melanocytes to keratinocytes after UVA irradiation. *Scientific reports,* 6**,** 1-13.

WATT, F. M., CELSO, C. L. & SILVA-VARGAS, V. 2006. Epidermal stem cells: an update. *Current opinion in genetics & development,* 16**,** 518-524.

WATT, F. M., ESTRACH, S. & AMBLER, C. A. 2008. Epidermal Notch signalling: differentiation, cancer and adhesion. *Current opinion in cell biology,* 20**,** 171-179.

WEINHART, M., HOCKE, A., HIPPENSTIEL, S., KURRECK, J. & HEDTRICH, S. 2019. 3D organ models—Revolution in pharmacological research? *Pharmacological research,* 139**,** 446-451.

WICKETT, R. R. & VISSCHER, M. O. 2006. Structure and function of the epidermal barrier. *American journal of infection control,* 34**,** S98-S110.

WITJAS, F. M., VAN DEN BERG, B. M., VAN DEN BERG, C. W., ENGELSE, M. A. & RABELINK, T. J. 2019. Concise review: The endothelial cell extracellular matrix regulates tissue homeostasis and repair. *Stem Cells Translational Medicine,* 8**,** 375-382.

WITWER, K. W., BUZÁS, E. I., BEMIS, L. T., BORA, A., LÄSSER, C., LÖTVALL, J., NOLTE-'T HOEN, E. N., PIPER, M. G., SIVARAMAN, S. & SKOG, J. 2013. Standardization of sample collection, isolation and analysis methods in extracellular vesicle research. *Journal of extracellular vesicles,* 2**,** 20360.

WONG, T., MCGRATH, J. & NAVSARIA, H. 2007. The role of fibroblasts in tissue engineering and regeneration. *British Journal of Dermatology,* 156**,** 1149-1155.

WONG, V. W., SORKIN, M., GLOTZBACH, J. P., LONGAKER, M. T. & GURTNER, G. C. 2010. Surgical approaches to create murine models of human wound healing. *Journal of Biomedicine and Biotechnology,* 2011.

WOODLEY, D. T. 2017. Distinct fibroblasts in the papillary and reticular dermis: implications for wound healing. *Dermatologic clinics,* 35**,** 95-100.

WUFUER, M., LEE, G., HUR, W., JEON, B., KIM, B. J., CHOI, T. H. & LEE, S. 2016. Skin-on-a-chip model simulating inflammation, edema and drug-based treatment. *Scientific reports,* 6**,** 37471.

WURM, S., ZHANG, J., GUINEA-VINIEGRA, J., GARCÍA, F., MUÑOZ, J., BAKIRI, L., EZHKOVA, E. & WAGNER, E. F. 2015. Terminal epidermal differentiation is regulated by the interaction of Fra-2/AP-1 with Ezh2 and ERK1/2. *Genes & development,* 29**,** 144-156.

XIE, Y., RIZZI, S. C., DAWSON, R., LYNAM, E., RICHARDS, S., LEAVESLEY, D. I. & UPTON, Z. 2010. Development of a three-dimensional human skin equivalent wound model for investigating novel wound healing therapies. *Tissue Engineering Part C: Methods,* 16**,** 1111-1123.

YAGI, M. & YONEI, Y. 2018. Glycative stress and anti-aging: 7. Glycative stress and skin aging. *Glycative Stress Res,* 5**,** 50-54.

YÁÑEZ-MÓ, M., SILJANDER, P. R.-M., ANDREU, Z., BEDINA ZAVEC, A., BORRÀS, F. E., BUZAS, E. I., BUZAS, K., CASAL, E., CAPPELLO, F. & CARVALHO, J. 2015. Biological properties of extracellular vesicles and their physiological functions. *Journal of extracellular vesicles,* 4**,** 27066.

YOON, T.-J., LEI, T. C., YAMAGUCHI, Y., BATZER, J., WOLBER, R. & HEARING, V. J. 2003. Reconstituted 3-dimensional human skin of various ethnic origins as an in vitro model for studies of pigmentation. *Analytical biochemistry,* 318**,** 260-269.
YOUSEF, H., ALHAJJ, M. & SHARMA, S. 2017. Anatomy, skin (integument), epidermis.
ZHANG, X., YANG, J., LI, Y., LIU, S., LONG, K., ZHAO, Q., ZHANG, Y., DENG, Z. & JIN, Y. 2011. Functional neovascularization in tissue engineering with porcine acellular dermal matrix and human umbilical vein endothelial cells. *Tissue Engineering Part C: Methods,* 17**,** 423-433.
ZHANG, Z. & MICHNIAK-KOHN, B. B. 2012. Tissue engineered human skin equivalents. *Pharmaceutics,* 4**,** 26-41.
ZHONG, W., XING, M. M. & MAIBACH, H. I. 2010. Nanofibrous materials for wound care. *Cutaneous and ocular toxicology,* 29**,** 143-152.

## LIST OF FIGURES IN THE RESULTS

## LIST OF PUBLICATIONS

Löwa, A.*, **Jevtić, M.***, Gorreja, F., Hedtrich, S.: Alternatives to animal testing in basic and preclinical research of atopic dermatitis. Exp Dermatol. 27(5), 476-483 (2018).

* Löwa and Jevtic equally contributed to this study.

**Jevtić M.**, Löwa A., Nováčková A., Kováčik A., Kaessmeyer S., Erdmann G., Vávrová K., Hedtrich S.: Impact of intercellular crosstalk between epidermal keratinocytes and dermal fibroblasts on skin homeostasis. BBA - Mol Cell Res 1867(8):118722 (2020).

**Jevtić M.**, Rieger J., Nováčková A., Kováčik A., Vávrová K.,Hedtrich S., Kaessmeyer S.: Native extracellular matrix significantly improves the differentiation and maturation of three dimensional skin equivalents - Manuscript in preparation

## CONFERENCES PROCEEDINGS

**Jevtić, M.**, Hedtrich, S.: Characterization of small extracellular vesicles secreted by dermal fibroblasts. Poster presentation at the 8th Congress and Annual Meeting of International Society for Extracellular Vesicles (ISEV2019), Kyoto (Japan), 24 – 28 April 2019.

**Jevtić, M.**, Löwa, A., Hedtrich, S.: Intercellular communication between dermal fibroblasts and epidermal keratinocytes in skin models. Poster presented at the 11th Scientific Symposium - Shaping future pharmaceutical research: Junior scientists present (DPhG), Berlin (Germany), July 6, 2018.

**Jevtić, M.**, Löwa, A., Hedtrich, S.: Intercellular crosstalk between fibroblasts and keratinocytes in skin models. Poster presented at the 16th International Perspectives in Percutaneous Penetration Conference, La Grande Motte (France), April 3 – 6, 2018.

**Jevtić, M.**, Löwa, A., Hedtrich, S.: Intercellular crosstalk between fibroblasts and keratinocytes in skin models. Poster presented at the Round table Arbeitsgemeinschaft Dermatologische Forschung e. V., Berlin (Germany), December 8 – 9, 2017.

**Jevtić, M.**, Löwa, A., Hedtrich, S.: Interaction between fibroblasts and keratinocytes in skin equivalents. Poster presented at the Annual Meeting of the German Pharmaceutical Society (DPhG), Saarbrücken (Germany), September 26 – 29, 2017.

## TALKS

**Jevtić, M.**, Löwa, A., Hedtrich, S.: Intercellular crosstalk between fibroblasts and keratinocytes in skin models. The Round table Arbeitsgemeinschaft Dermatologische Forschung e. V., Berlin (Germany), December 8 – 9, 2017.

**Jevtić, M.**, Löwa, A., Hedtrich, S.: Interaction between fibroblasts and keratinocytes in skin equivalents. The Annual Meeting of the German Pharmaceutical Society (DPhG), Saarbrücken (Germany), September 26 – 29, 2017.

## AWARDS

Travel grant by women's representative (Frauenförderung des Fachbereichs BCP) of Freie Universität Berlin, for the conference "PPP: Perspectives in Percutaneous Penetration", April 2018, La Grande Motte (France)

Travel grant by women's representative (Frauenförderung des Fachbereichs BCP) of Freie Universität Berlin, for the 8$^{th}$ Congress Annual Meeting of International Society for Extracellular Vesicles (ISEV2019), April 2019, Kyoto (Japan)

## STATEMENT OF AUTHORSHIP

Hiermit versichere ich, Marijana Jevtić, die vorliegende Arbeit selbstständig verfasst zu haben. Alle verwendeten Hilfsmittel und Hilfen habe ich angegeben. Die Arbeit wurde weder in einem früheren Promotionsverfahren angenommen noch als ungenügend beurteilt.

Berlin,

…….

Marijana Jevtić

## APPENDIX

**Table A1.** List of proteins analyzed DigiWest profiling including the antibody information.

| Analyte | Supplier |
|---|---|
| 14-3-3 epsilon | Cell Signaling |
| 14-3-3 sigma | R&D |
| 14-3-3 zeta delta | Cell Signaling |
| Actin | Santa Cruz |
| Adam9 | Cell Signaling |
| Akt * | Cell Signaling |
| Akt - phospho Ser473 | Cell Signaling |
| Akt1 | Cell Signaling |
| A-Raf | Cell Signaling |
| beta-Catenin | Cell Signaling |
| BMP4 | Epitomics |
| b-Raf | Upstate |
| CASK | Transduction Laboratories |
| Caspase 3 | Cell Signaling |
| CD44 | Epitomics |
| c-Jun | Cell Signaling |
| c-Jun - phospho Ser63 | Cell Signaling |
| Claudin-1 | Invitrogen |
| c-Met (HGF/SF receptor) | Cell Signaling |
| c-myc | Cell Signaling |
| c-myc - phospho Thr58/Ser62 | abcam (Epitomics) |
| CTGF | abcam |
| Cytokeratin 16 * | Epitomics |
| Cytokeratin 17 | Cell Signaling |
| Cytokeratin 19 | Cell Signaling |
| Cytokeratin Pan (4, 5, 6, 8, 10, 13, 18) | Cell Signaling |
| E-Cadherin | R&D |
| EGFR (ErB-1, HER1) | Cell Signaling |
| EphA2 | Cell Signaling |
| EphA2 - phospho Ser897 | Cell Signaling |
| Erk1 (MAPK p44) | Cell Signaling |
| Erk1/2 (MAPK p44/42) | Cell Signaling |
| Erk1/2 (MAPK p44/42) - phospho Thr202/Tyr204 | Cell Signaling |
| Erk2 (MAPK p42) | Cell Signaling |
| Ezh2 | Cell Signaling |
| FGF receptor 1 | Cell Signaling |
| FGF receptor 2 | abcam (Epitomics) |
| FGF-1 | abcam (Epitomics) |
| Filaggrin | abcam |
| GDF3 | Epitomics |
| GLI1 | Cell Signaling |
| gt-blk | |

| | |
|---|---|
| Ha-ras | Upstate |
| Her2 | Dako |
| HES-1 | Epitomics |
| IGF1 receptor beta (Insulin receptor beta, CD221) | Cell Signaling |
| IGF1 receptor beta/Insulin receptor beta (CD221) - phospho Tyr1135/Tyr1136resp.Tyr1150/Tyr1151 | Cell Signaling |
| Involucrin | abcam |
| Jagged1 | Cell Signaling |
| Jagged2 | Cell Signaling |
| JNK/SAPK | Cell Signaling |
| JNK/SAPK - phospho Thr183/Tyr185 | Cell Signaling |
| JNK/SAPK 1/2/3 - phospho Thr183/Tyr185 | Santa Cruz |
| Ki-67 | USBiological |
| KLF4 | Cell Signaling |
| LATS1 | Cell Signaling |
| Loricrin | Invitrogen |
| MEK1 | Cell Signaling |
| ms-blk | |
| Mst1 | Cell Signaling |
| Notch 1 | Cell Signaling |
| Notch 2 | Cell Signaling |
| p21 (Waf1, Cip1, CDKN1A) | Cell Signaling |
| p38 MAPK | Cell Signaling |
| p38 MAPK - phospho Thr180/Tyr182 | Cell Signaling |
| PI3-kinase gamma | Jena Bioscience |
| PIP5K1A | Cell Signaling |
| PPAR alpha | abcam |
| PPAR alpha - phospho Ser12 * | abcam |
| Rac1/cdc42 | Cell Signaling |
| Ras | Cell Signaling |
| RBPSUH | Cell Signaling |
| ROCK1 - cleaved Asp1113 | Calbiochem |
| SHP-2 | Epitomics |
| Slug | Cell Signaling |
| Smad1/5/8 - phospho Ser463/465/467 | Cell Signaling |
| Smad2/3 | Cell Signaling |
| Smad2/3 - phospho Ser465/467/423/425 | Cell Signaling |
| SPRED1 | abcam |
| SPRED2 | abcam |
| SPRY1 (Spry-1, Sprouty 1) | Sigma (aviva systems biology) |
| SPRY2 (Protein sprouty homolog 2) | Millipore |
| Src | Cell Signaling |
| SRC-3 (NCoA3, AIB1, TRAM1) - phospho Thr24 | Cell Signaling |
| SRF | Cell Signaling |
| Stathmin 1 | abcam (Epitomics) |

| | |
|---|---|
| SUFU | Cell Signaling |
| TACE | Cell Signaling |
| TIMP-1 | Epitomics |
| TSG101 | abcam |
| YAP | Cell Signaling |
| YAP/TAZ * | Cell Signaling |
| Yes * | Cell Signaling |
| ZO-1 | Cell Signaling |
| Occludin | Novus |
| Smad4 * | Cell Signaling |